



Universiteit  
Leiden  
The Netherlands

## Mesoporous silica nanoparticle-based protein delivery systems for biomedical applications

Tu, J.

### Citation

Tu, J. (2016, December 21). *Mesoporous silica nanoparticle-based protein delivery systems for biomedical applications*. Retrieved from <https://hdl.handle.net/1887/45230>

Version: Not Applicable (or Unknown)

License: [Licence agreement concerning inclusion of doctoral thesis in the Institutional Repository of the University of Leiden](#)

Downloaded from: <https://hdl.handle.net/1887/45230>

**Note:** To cite this publication please use the final published version (if applicable).

Cover Page



Universiteit Leiden



The handle <http://hdl.handle.net/1887/45230> holds various files of this Leiden University dissertation

**Author:** Jing Tu

**Title:** Mesoporous silica nanoparticle-based protein delivery systems for biomedical applications

**Issue Date:** 2016-12-21

**Mesoporous Silica Nanoparticle-Based Protein  
Delivery Systems for Biomedical Applications**

***JING TU***

Doctoral Thesis, Leiden University, 2016

Cover design: Jing Tu

Printed by GVO drukkers & vormgevers B.V. Ede

ISBN: 978-94-6332-119-8

# **Mesoporous Silica Nanoparticle-based protein delivery systems for biomedical applications**

Proefschrift

ter verkrijging van

de graad van Doctor aan de Universiteit Leiden,

op gezag van Rector Magnificus Prof. mr. C.J.J.M. Stolker,

volgens het besluit van het College voor Promoties

te verdedigen op woensdag 21 december 2016

klokke 10:00 uur

door

**涂晶**

**Jing Tu**

Geboren op 11 Oktober te Wuhan, China in 1985

## **Promotiecomissie**

Promotor: Prof. dr. A. Kros

Overige leden:

Prof. dr. J. Brouwer (voorzitter)

Prof. dr. J. Bouwstra (secretaris)

Prof. dr. J.I. Zink<sup>1</sup>

Dr. S. Bonnet

Dr. C.F. van Nostrum<sup>2</sup>

1 Dept. Chemistry & Biochemistry, UCLA, USA

2 Dept. Pharmaceutics, Utrecht University, the Netherlands

**To my family**





# Table of Contents

## Chapter I

General Introduction 9

## Chapter II

Mesoporous Silica Nanoparticles with Large Pores for the Encapsulation and Release of Proteins 27

## Chapter III

Mesoporous Silica Nanoparticle-Coated Microneedles for Intradermal Delivery of Ovalbumin 49

## Chapter IV

Membrane Fusion Mediated Intracellular Delivery of Lipid Bilayer Coated Mesoporous Silica Nanoparticles 71

## Chapter V

Lipid Bilayer-Coated Mesoporous Silica Nanoparticles Carrying Bovine Hemoglobin as an Erythrocyte Mimic 97

## Chapter VI

Estimation of Single Mesoporous Silica Nanoparticle's Weight 121

## Chapter VII

Summary and Perspectives 129

**Curriculum vitae** 141

**List of publications** 142



# **Chapter I**

## **General Introduction**

## 1.1 Mesoporous silica nanoparticle for protein delivery

The interest in proteins as promising therapeutic agents has increased remarkably in almost every field of medicine, like cancer, inflammatory diseases, vaccines, and also in diagnostics.<sup>1, 2, 3</sup> Human insulin was the first recombinant biopharmaceutical approved by FDA in 1982 and ever since, more than 100 proteins have been approved for clinical use<sup>4</sup> as proteins typically show a high specificity with less interference with normal biological processes.<sup>5, 6</sup> However, proteins used as a therapeutic are usually characterized by their short plasma half-life, high elimination rate, limited ability to cross cell membranes, and poor bioavailability through intestinal administration.<sup>2, 7</sup> Once proteins are present in blood, these biomacromolecules are prone to degradation and cannot be targeted to the desired site of action.<sup>7</sup> In order to improve the therapeutic efficacy of proteins, various nanocarriers are developed to overcome these barriers.

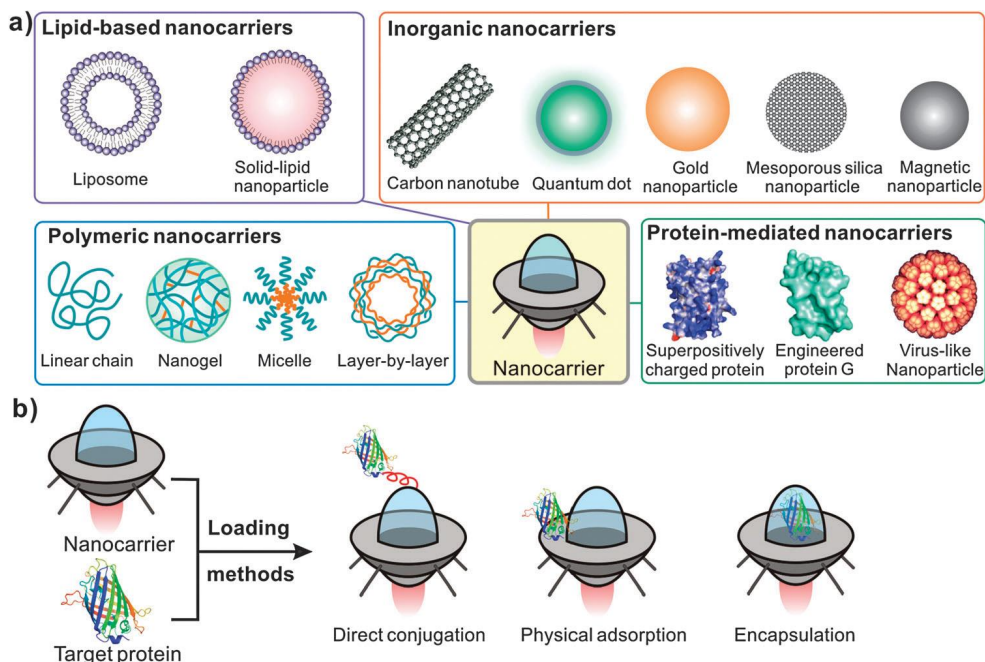


**Figure 1.1** (a) Various types of nanocarriers used for intracellular protein delivery. (b) The three commonly used methods for preparing protein/nanocarrier composites.<sup>3</sup> Figure taken from reference 3.

Delivering therapeutic proteins into cells remains an important challenge<sup>8</sup> and therefore nanocarriers enabling efficient protein delivery are in high demand.<sup>3, 5</sup> Over the last decades,

various nanocarriers (Figure 1.1)<sup>3</sup> such as lipid based assemblies,<sup>4, 9</sup> and polymeric nanoparticles<sup>10, 11</sup> and inorganic nanoparticles have been developed. Loading multiple cargos, for example short peptides and large proteins, within a particulate delivery systems can overcome drawbacks exhibited by conventional free proteins (*e. g.* rapid clearing),<sup>12</sup> retaining pharmacological and enzymatic activity by protecting the cargo against harsh environments.<sup>7, 13</sup> Compared to carbon-based nanomaterials and assemblies, inorganic materials show the unique feature of high thermal/chemical stability and exhibit typically good biocompatibility with relatively low rates of degradation.<sup>14</sup>

Since the M41S family of ordered Mesoporous silica nanoparticles (MSNs) was first reported in the early 1990s,<sup>15</sup> the number of publications on MSNs have increased dramatically.<sup>2, 16 17-20</sup> MSNs have attracted considerable attention for their application in biomedicine because of their fascinating properties.<sup>2, 17, 21, 22</sup> The unique properties of MSNs include the large surface area and pore volume, tunable pore diameter and structure, good chemical and thermal stability and a large variety in chemistry for surface functionalization.<sup>16, 17, 23-26</sup> MSNs contain channels which are able to encapsulate and release therapeutic molecules, including low molecular weight drugs, small interfering RNA,<sup>27</sup> and proteins.<sup>28</sup> Furthermore, MSNs are biocompatible and accepted as “general recognized as safe (GRAS)” by the U. S. Food and Drug Administration (FDA).<sup>18, 29</sup> As a nanomedicine, they possess several requirements to be considered as an ideal biocompatible particle, *i. e.* they are safe to use,<sup>30</sup> are efficiently internalized into cells by phagocytosis or the receptor-mediated endocytosis (Figure 1.2).<sup>22, 31-33</sup> Most importantly, these MSNs can be loaded with drugs, and the drug release can be (externally) triggered and/or controlled.<sup>34</sup>

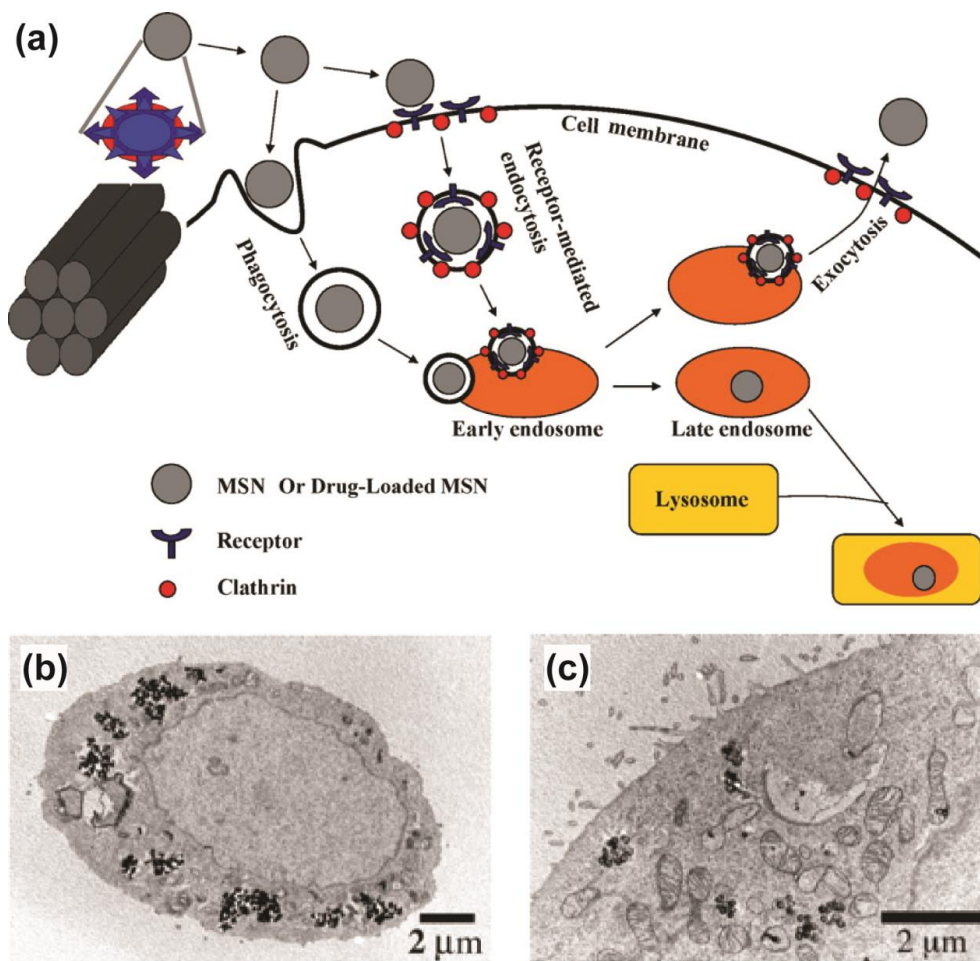


**Figure 1.2** (a) Endocytotic pathway of MSNs in mammalian cells, taken from reference 22. TEM micrographs of PAMAM-MSN (black dots) endocytosed by (b) Chinese hamster ovarian (CHO), taken from reference 32 and (c) human cervical cancer (HeLa) cells, taken from reference 33.

More recently, MSNs with an open-pore structure have emerged as a potential carrier for protein delivery. Due to their structure, MSNs protect proteins from premature degradation in body fluids, thereby increasing the efficiency of protein delivery *in vivo*, thus reducing renal filtration.<sup>3</sup> Furthermore, the silanol-containing surface of MSNs can be easily functionalized,<sup>21, 35</sup> enabling the adsorption of various proteins with different surface properties,<sup>36</sup> or modification with targeting molecules such as folate to enhance cellular uptake.<sup>21, 37</sup> Indeed, several reports have shown that MSNs can facilitate the transport of

protein into the cytosol via an endocytosis pathway and subsequent endosomal escape.<sup>2, 3, 20, 33, 38, 39</sup>

Numerous synthetic protocols for the preparation of MSNs have been developed.<sup>40-45</sup> Encapsulating large biomacromolecules (*e.g.* proteins) in MSNs is still challenging however, because the most commonly used type of MSN have a rather small mesopore diameter (< 3 nm)<sup>44</sup> preventing the effective encapsulation of a broad range of proteins.<sup>46, 47</sup> Therefore MSNs with a large pore size have been synthesized, however in most cases, these particles have a large particle size resulting in decreased cellular uptake efficiency.<sup>44, 48, 49</sup> This is in line with previous studies showing that a particle size between 50 and 200 nm is preferred for endocytic uptake.<sup>33, 48, 50</sup> Therefore, there is still a need for monodisperse MSNs with a particle size in the 50-200 nm range, controllable surface chemistry, and a large pore size (> 5 nm) for applications in the field of drug delivery.<sup>46, 51-53</sup>

## 1.2 Design and synthesis large pore and small diameter of MSNs for protein delivery

In general, MSNs are synthesized using a templating agent,<sup>2</sup> typically a surfactant in aqueous solution which is either neutral or charged.<sup>20</sup> The pH of aqueous solutions used in MSN synthesis controls the hydrolysis and condensation reaction (Figure 1.3).<sup>13, 54</sup> The size, morphology, mesostructures of MSNs can be rationally designed by controlling the reaction parameters (*e.g.* surfactant concentration, pH, temperature, silica source).<sup>17, 18, 43</sup> With the abundant availability of various types of surfactants,<sup>18</sup> numerous synthetic protocols for the preparation of MSNs have been developed.<sup>43, 52</sup>

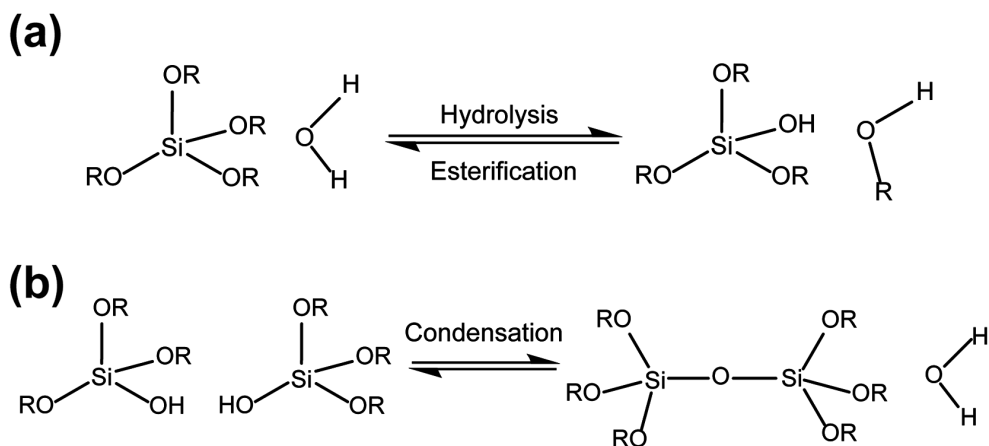


**Figure 1.3** Mechanism of (a) hydrolysis and (b) condensation reactions of alkoxy silanes and organylalkoxy silanes, resulting in a molecular formula of  $\text{Si}(\text{OR})_{4-n}(\text{OH})_n$ .

The two classical examples of MSNs are MCM-41<sup>55</sup> (Mobil Composition of Matter no. 41) and SBA-15<sup>15, 56</sup> (Santa Barbara Amorphous no. 15) which use cetyltrimethylammonium bromide (CTAB) and amphiphilic block copolymers (Pluronic P123, PEO<sub>20</sub>PPO<sub>70</sub>PEO<sub>20</sub>) as a template respectively. MCM-41-type nanoparticles typically have a diameter ranging from 20-500 nm while pore sizes ranges from 2-6 nm (Figure 1.4).<sup>39, 57-59</sup> Therefore, these materials can be used for the encapsulation and release of low to medium molecular weight biomolecules like small proteins (*e. g.* cytochrome, Mw 12384 Da, geometric size  $2.6 \times 3.2 \times 3.3$  nm).<sup>8, 58</sup>



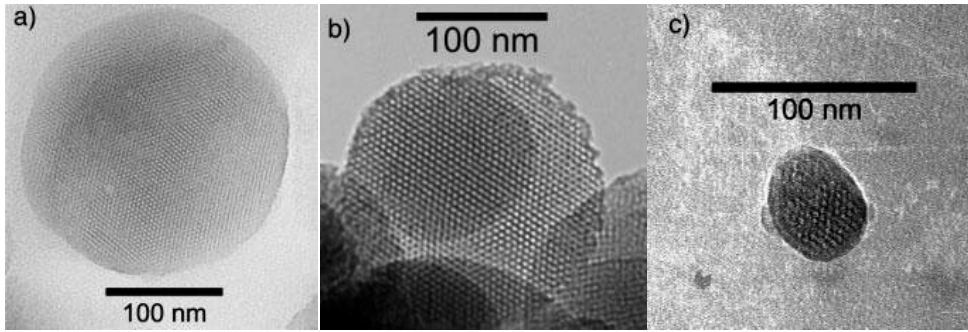


**Figure 1.4** TEM images of three spherical MSNs with different particle and pore diameter: a) particle size ca. 250 nm, pore diameter ca. 2.3 nm.<sup>57</sup> B) particle size ca. 200 nm; pore diameter ca. 6.0 nm.<sup>58</sup> C) particle size ca. 50 nm; pore ca. 2.7 nm.<sup>39</sup> Figure taken from reference 39.

Due to their size, large proteins are predominantly adsorbed onto the external surface of MSNs and do not make use of the protective environment inside MSNs, nor do they utilize the large internal surface area presented by these pores.<sup>16, 60-62</sup> SBA-15 does have large pores (5-30 nm) but the average particle size of these materials is in the range of sub-micrometer to several micrometers rendering these particles less suited for biomedical applications (Figure 1.5).<sup>56, 63</sup>

Therefore several groups have developed methods to control the outer particle diameter and pore-size of MSNs in the nanometer range.<sup>8, 41, 42, 45, 50, 51, 64, 65</sup> Based on geometric considerations, it is expected that MSNs with a large pore-size (> 5 nm) and small diameter (< 200 nm) should facilitate the efficient loading and delivery of biomacromolecules with large molecular sizes.<sup>66</sup> Covalent immobilization of protein into MSNs is one approach to retain their functional characteristics,<sup>47, 67-69</sup> however, irreversible covalent attachment can result in a loss of activity compared to physical adsorption.<sup>70</sup> To avoid complicated chemical reactions, encapsulation of proteins inside MSNs driven by electrostatic interactions (physisorption) will be discussed in this thesis.

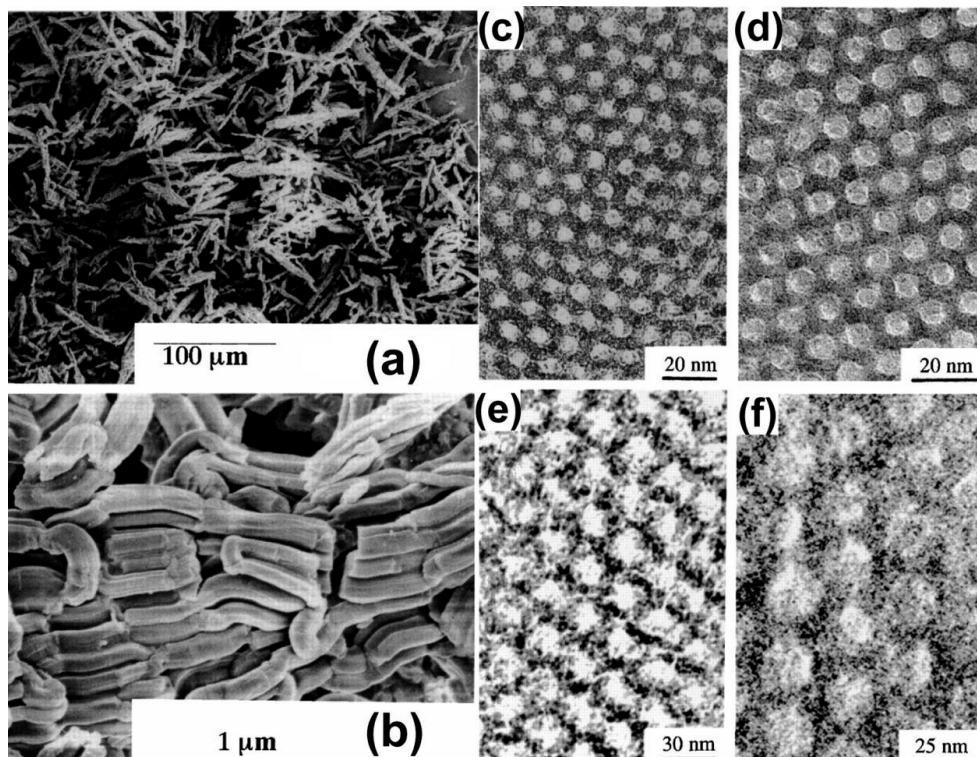


**Figure 1.5** (a) and (b) Scanning electron microscopy and (c-f) transmission electron microscopy images of hexagonal mesoporous silica SBA-15. SBA-15 can be synthesized over a range of reaction mixture compositions and conditions.<sup>56, 63</sup> TEM images show well-ordered hexagonal arrays of mesopores. Figure taken from reference 56.

In this section, a few examples of MSNs with a large pore size and a small particle diameter that previously were used for the intracellular delivery of functional proteins using MSNs are presented.

MCM-41-type MSNs with larger pores (5.4 nm) could be obtained by using mesitylene (TMB) as a pore-expanding agent.<sup>58, 71</sup> Lin and coworkers reported the successful intracellular delivery of the membrane-impermeable protein cytochrome c (molecular weight 12.4 kDa, isoelectric point 11.35) using these MSNs as the nanocarrier and it was shown that the released proteins were still functional and highly active in catalyzing the oxidation of 2,2'-aznio-bis(3-ethylbenzthiazoline-6-sulfonate) (ABTS) by hydrogen peroxide.<sup>58</sup>

Yu and coworkers reported a facile and oil-free approach to synthesize dendritic MSNs with a center-radial pore structure, tunable particle size (79-160 nm) and large pores (22

nm).<sup>64</sup> These MSNs were synthesized in an aqueous phase using sodium trifluoroacetate as an additive to control the growth of MSNs. Antimicrobial lysozyme (molecular weight 14.3 kDa, isoelectric point 10-10.5) was chosen as cargo to study the delivery efficiency of these MSNs.<sup>64, 72</sup> It was found that MSNs with a large pore size and small particle size (MSNs-3) show significantly better antibacterial activity as compared to the particles with small pore sizes (MSNs-1 and MSNs-2, Figure 1. 6).<sup>64</sup>

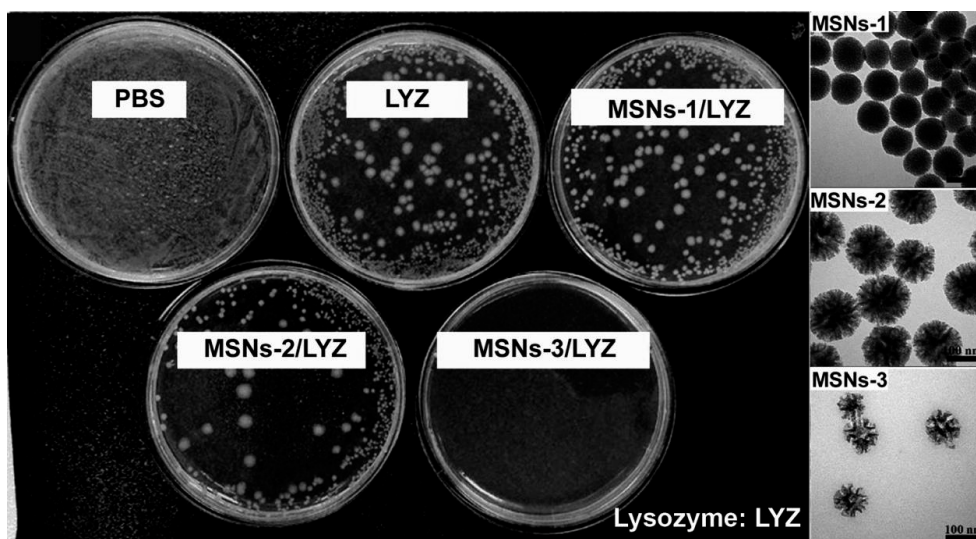


**Figure 1.6** Lysozyme loaded MSNs (500  $\mu\text{g}/\text{mL}$ ) for *Escherichia coli* (*E. coli*) inhibition after 5 days incubation. Figure taken from reference 64.

While some progress has been made with MSNs mediated protein delivery using cytochrome c or lysozyme as model proteins,<sup>44, 73-76</sup> reports on intracellular delivery of large functional proteins (more than 100 kDa) are rare.<sup>8</sup> Yu et al. designed a new type of monodispersed MSNs with a core-cone structure (MSN-CC) with an average pore size of 45 nm (Figure 1.7). These particles were synthesized in a chlorobenzene-water system, using cetyltrimethylammonium chloride (CTAC) as a structure-directing agent and tetraethyl orthosilicate (TEOS) as the silica source. The loading capacity for large molecular weight proteins (*i. e.* IgG, 150 kDa;  $\beta$ -galactosidase, 119 kDa) is 560 mg/g MSNs and 190 mg/g MSNs, respectively. The efficient delivery of active  $\beta$ -galactosidase (119 kDa) into N2a cells (mouse neuroblastoma cells) was quantified by monitoring the enzymatic activity of  $\beta$ -Galactosidase, showing that this core-cone structured MSN is a potential nanocarrier for protein delivery.<sup>8</sup>

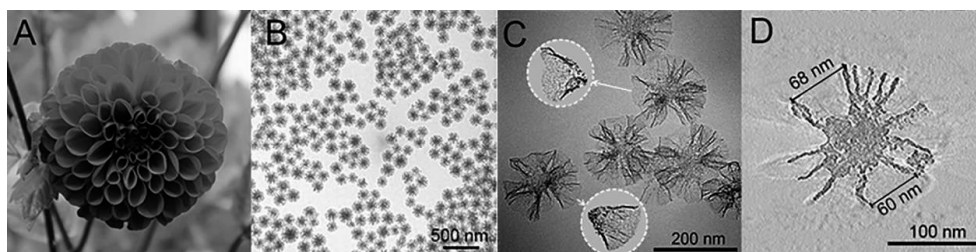


**Figure 1.7** (A) A picture of a dahlia photographed by C. Xu at Tasmania. (B) TEM images at low magnification, (C) high magnification, MSN-CC with uniform diameters of 180 nm, and (D) an electron tomography (ET) slice of MSN-CC. Figure taken from reference 8.

For future *in vivo* applications of these protein-loaded MSNs, there are still some limitations that to be resolved, such as premature protein release and the colloidal instability of MSNs in salt-containing solutions. More specifically, after protein encapsulation the surface properties of MSNs change (e.g. zeta-potential becomes neutral), resulting in aggregation and colloidal instability in physiologic environments.<sup>24</sup> As a result, these aggregated particles are recognized and removed by the mononuclear phagocytical cells in the reticuloendothelial system.<sup>49</sup> As mentioned earlier in this chapter, the efficiency of cellular uptake of MSNs is size-dependent<sup>23</sup> and aggregated particles are therefore less suitable for *in vivo* delivery applications.

### 1.3 A lipid bilayer coated mesoporous silica nanoparticles

Following the pioneering work on supported phospholipid membranes in the 1980s,<sup>77, 78</sup> these reconstituted planar membranes on solid supports (or supported lipid bilayers, SLBs) have become popular as a model system mimicking the membrane of cells, with potential biotechnological applications. For example, as a model of biological membranes to study the transport of ions and molecules (Figure 1.8).<sup>78, 79</sup> Considerable work has been done to investigate the process of bilayer the formation by exposing small lipid vesicles to a hydrophilic support (*e.g.*, silica).<sup>77-81</sup> It was shown that phospholipid membranes are able to assemble into different structures upon contact with a hydrophilic surface,<sup>82</sup> involving vesicle adsorption, rupture and spreading into planar membranes.<sup>79</sup> Cryo-electron microscopy imaging convincingly demonstrated that the lipid bilayers faithfully follow the topology of the silica substrate.<sup>83</sup>

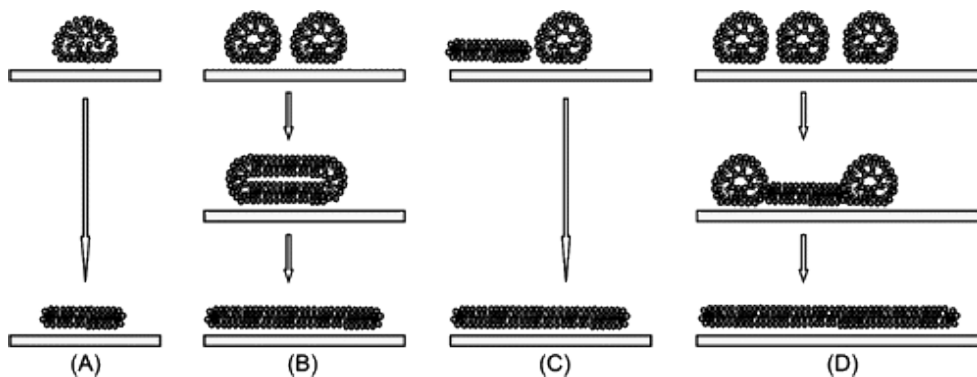


**Figure 1.8** Mechanisms of vesicle rupture: (A) an isolated adsorbed vesicle ruptures spontaneously, driven by its support-induced deformation; (B) neighboring adsorbed vesicles fuse and eventually rupture; (C) the active edge of a supported bilayer patch induces the rupture of a neighboring vesicle; (D) the cooperative action of several neighboring vesicles leads to the rupture of a first vesicle (at the critical vesicular coverage). The active edge thereby exposed triggers the rupture of adjacent vesicles.<sup>79</sup> Figure taken from reference 79.

The long-term colloidal stability of MSNs remains a challenge, especially in *in vivo* experiments. Since the repulsive force between MSNs decreases after protein encapsulation, aggregation readily occurs. Therefore, application of a lipid bilayer on the exterior surface of MSNs could be useful to enhance the colloidal stability. Furthermore, it will also affect the rate of protein release by covering the pores of MSNs.<sup>84, 85</sup> In addition, the composition of supported lipid bilayer, can be modified for specific biological applications, for example by

conjugation of specific molecules in order to achieve cell-specific targeting and controlled intracellular delivery.<sup>27, 86</sup>

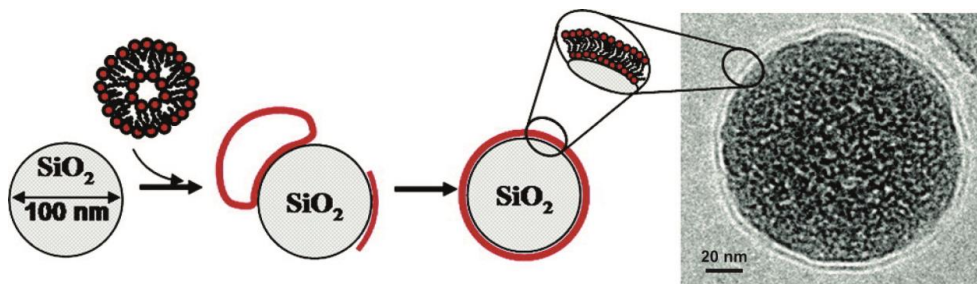


**Figure 1.9** Schematic representation of the elaboration process of silica nanoparticles covered with lipids.<sup>87</sup> Relative cryo-transmission electron microscopy image, the red lines represent lipid patch or a lipid bilayer.<sup>83</sup> Figure taken from reference 83.

The use of supported lipid bilayer coated MSN, sometimes called “protocells” as a new drug delivery tool to ensure efficient cell uptake, was pioneered by Brinker and others.<sup>84, 85 12, 84, 88-91</sup> These protocells can be considered as a mimic of the cellular envelopes and cytoskeleton, combining the favorable properties of MSNs and liposomes.<sup>23</sup> While MSNs possess a high surface area and large accessible pore volumes enabling loading with guest molecules, the lipid bilayer acts as a physical barrier keeping the cargo inside the MSN core and provides colloidal stability.<sup>85, 92, 93</sup> The cargo is therefore protected from the environment and can be transported and released into the cell.<sup>88</sup> MSNs can be coated non-covalent with a physically adsorbed bilayer<sup>23, 83, 86, 87, 92</sup> or modified through covalent bonds with the phospholipids<sup>85, 94</sup> Efforts have been made to develop biocompatible and multifunctional protocells, such as using peptide-modified lipid bilayer coated MSN in order to target a specific tissue or cell type.<sup>12, 27, 86, 95</sup> Furthermore, magnetic field controlled<sup>93</sup> or light-controlled release of cargo,<sup>96</sup> PEGylation lipid composition have been applied to realize effective targeting or extending the circulation time.<sup>25, 88, 94</sup> However, most studies to date with these nanocarriers using lipid bilayer coated MSN mediate the delivery of low molecular weight dyes and drugs only.<sup>84, 85, 90, 97, 98</sup> So far, only a few reports on the delivery of small interfering RNA,<sup>27</sup> DNA<sup>23</sup> and proteins (*i.e.* ricin toxin A-chain, 32 kDa) have been reported.<sup>12, 86</sup>

#### 1.4 Aim and outline of this thesis

In this thesis, we designed a facile synthetic route of a new type of MSNs that are able to effectively encapsulate and release proteins. The delivery of three commonly used proteins (ovalbumin, cytochrome c and hemoglobin) with different surface charges and molecular weight was studied, to investigate the potential biomedical application of large pore MSNs as a vaccine (ovalbumin), in protein therapy (hemoglobin) and in cancer therapy (cytochrome c).

In **Chapter 2**, we present a new type of elongated cuboidal MSNs with average dimensions of  $90 \times 43$  nm that possess disk-shaped cavities, stacked on top of each other, oriented parallel to the short axis of the particle. The MSN surface was modified with amines using 3-aminopropyltriethoxysilane or 3-[2-(2-aminoethylamino)ethylamino]propyltrimethoxysilane (AP-MSNs and AEP-MSNs), in order to obtain a positive surface charge at physiological pH. This unique open mesostructure makes it an ideal scaffold for protein encapsulation and delivery. Seven model proteins ( $\alpha$ -lactalbumin, ovalbumin, bovine serum albumin, catalase, hemoglobin, lysozyme and cytochrome c) were encapsulated and the release was studied. It was found that these large-pore MSNs are suitable protein nanocarriers with favorable physical properties such as rapid encapsulation and with a high loading capacity for a wide range of model proteins. The protein release from these large-pore MSNs was examined showing that the structure of the released proteins remained unaltered. This study proved that these new cuboidal MSNs can be used as an effective platform for therapeutic protein delivery.

To study the scope of potential biomedical applications, a new intradermal delivery system is described in **Chapter 3**, which synergistically integrates the advantages of nanoparticles with microneedle delivery. In this study, ovalbumin-loaded, lipid bilayer-covered MSNs (LB-MSNs) were adsorbed onto pH-sensitive microneedles. The large pores (10 nm) facilitated the rapid encapsulation of ovalbumin (OVA) with a high loading capacity. The introduction of a lipid bilayer significantly improved the colloidal stability of OVA loaded AEP-MSNs and concomitantly reduced the premature release of OVA. In addition, it enables the coating of LB-MSNs on the surface of pH-sensitive microneedle arrays based on electrostatic interactions. Application of LB-MSNs coated microneedle arrays into human skin (*ex vivo*) resulted in the successful delivery of the OVA-loaded nanoparticles into the skin in a pH dependent manner. This microneedle-mediated intradermal delivery system for MSNs can be a promising tool to deliver a wide range of compounds into the skin.

Protein Delivery into the cytoplasm of cells is still a challenging topic in the field of nanomedicine as inefficient cellular uptake and endosomal escape limits potential clinical applications. In **Chapter 4** a complementary pair of coiled-coil lipopeptides (CP<sub>4</sub>E<sub>4</sub> and CP<sub>4</sub>K<sub>4</sub>) was introduced as a way to trigger and control the targeted delivery of lipid bilayer coated MSNs into cells. The positively charged membrane-impermeable protein cytochrome c was used as a model protein in this study. MSNs with large pores rapidly encapsulated cytochrome c and were coated by a phospholipid bilayer containing CP<sub>4</sub>E<sub>4</sub>. These nanoparticles were added to CP<sub>4</sub>K<sub>4</sub> pre-treated HeLa resulting in efficient cell uptake. By applying the fusogenic coiled coil system, cytochrome c was efficiently transported into the cytoplasm of cells within 30 minutes.

The preparation and (bio)physical properties of hemoglobin-based oxygen carrier nanoparticles (Hb-NPs) is described in **Chapter 5**. MSNs with large pores were used to encapsulate bovine hemoglobin (MSNs/Hb) and coated with a lipid bilayer. These large pore MSN act as rigid core to store and provide a protective environment for the encapsulated Hb. The lipid bilayer enhanced the colloidal stability of MSNs/Hb, as well as prevented the premature release of Hb. The *in vivo* circulation was studied in zebrafish embryos, demonstrating the potential for future pharmaceutical applications.

As nanoparticles (NPs) are attractive for pharmaceutical applications due to their unique features, such as its large surface to mass ratio resulting in the ability to encapsulate a wide variety of compounds<sup>99</sup> (e.g. low-molecular weight drugs, proteins, DNA/RNA). For a better characterization of these nanoparticles, it would be helpful to know the mass of a single nanoparticle, and therefore be able to calculate the number of molecules encapsulated per MSN. Nanoparticle Tracking Analysis (NTA) can determine the size distribution, and high sensitively in terms of particle-number concentration.<sup>100</sup> Based on this technique, we developed a simple and low-cost method to estimate the mass of single MSNs (**Chapter 6**).

Finally in **Chapter 7**, the findings and conclusions of this thesis are summarized and further research for potential applications of MSNs are presented.



## 1.5 References

1. T. Vermonden, R. Censi and W. E. Hennink, *Chem. Rev.*, **2012**, 112, 2853-2888.
2. Y. Wang, Q. F. Zhao, N. Han, L. Bai, J. Li, J. Liu, E. X. Che, L. Hu, Q. Zhang, T. Y. Jiang and S. L. Wang, *Nanomedicine*, **2015**, 11, 313-327.
3. Z. Gu, A. Biswas, M. Zhao and Y. Tang, *Chem. Soc. Rev.*, **2011**, 40, 3638-3655.
4. B. Chatin, M. Mevel, J. Devalliere, L. Dallet, T. Haudebourg, P. Peuziat, T. Colombani, M. Berchel, O. Lambert, A. Edelman and B. Pitard, *Mol. Ther.--Nucleic Acids*, **2015**, 4, e244.
5. Y. T. Niu, M. H. Yu, J. Zhang, Y. N. Yang, C. Xu, M. Yeh, E. Taran, J. J. C. Hou, P. P. Gray and C. Z. Yu, *J. Mater. Chem. B*, **2015**, 3, 8477-8485.
6. B. Leader, Q. J. Baca and D. E. Golan, *Nat. Rev. Drug Discovery*, **2008**, 7, 21-39.
7. S. Martins, B. Sarmento, D. C. Ferreira and E. B. Souto, *Int. J. Nanomed.*, **2007**, 2, 595-607.
8. C. Xu, M. H. Yu, O. Noonan, J. Zhang, H. Song, H. W. Zhang, C. Lei, Y. T. Niu, X. D. Huang, Y. N. Yang and C. Z. Yu, *Small*, **2015**, 11, 5949-5955.
9. J. Shi, A. R. Votrubka, O. C. Farokhzad and R. Langer, *Nano Lett.*, **2010**, 10, 3223-3230.
10. R. A. Rosalia, L. J. Cruz, S. van Duikerem, A. T. Tromp, A. L. Silva, W. Jiskoot, T. de Gruijl, C. Lowik, J. Oostendorp, S. H. van der Burg and F. Ossendorp, *Biomaterials*, **2015**, 40, 88-97.
11. K. Y. Lee and S. H. Yuk, *Prog. Polym. Sci.*, **2007**, 32, 669-697.
12. C. E. Ashley, E. C. Carnes, G. K. Phillips, D. Padilla, P. N. Durfee, P. A. Brown, T. N. Hanna, J. Liu, B. Phillips, M. B. Carter, N. J. Carroll, X. Jiang, D. R. Dunphy, C. L. Willman, D. N. Petsev, D. G. Evans, A. N. Parikh, B. Chackerian, W. Wharton, D. S. Peabody and C. J. Brinker, *Nat. Mater.*, **2011**, 10, 389-397.
13. R. Roggers, S. Kanvinde, S. Boonsith and D. Oupicky, *AAPS PharmSciTech*, **2014**, 15, 1163-1171.
14. Y. Chen, H. Chen and J. Shi, *Adv. Mater.*, **2013**, 25, 3144-3176.
15. C. T. Kresge, M. E. Leonowicz, W. J. Roth, J. C. Vartuli and J. S. Beck, *Nature*, **1992**, 359, 710-712.
16. S. Hudson, J. Cooney and E. Magner, *Angew. Chem., Int. Ed.*, **2008**, 47, 8582-8594.
17. C. Argyo, V. Weiss, C. Bräuchle and T. Bein, *Chem. Mater.*, **2014**, 26, 435-451.
18. F. Tang, L. Li and D. Chen, *Adv. Mater.*, **2012**, 24, 1504-1534.
19. V. Mamaeva, C. Sahlgren and M. Linden, *Adv. Drug Delivery Rev.*, **2013**, 65, 689-702.
20. I. I. Slowing, J. L. Vivero-Escoto, B. G. Trewyn and V. S. Y. Lin, *J. Mater. Chem.*, **2010**, 20, 7924-7937.
21. F. Porta, G. E. M. Lamers, J. Morrhayim, A. Chatzopoulou, M. Schaaf, H. den Dulk, C. Backendorf, J. I. Zink and A. Kros, *Adv. Healthcare Mater.*, **2013**, 2, 281-286.
22. T. Asefa and Z. Tao, *Chem. Res. Toxicol.*, **2012**, 25, 2265-2284.
23. E. C. Dengler, J. W. Liu, A. Kerwin, S. Torres, C. M. Olcott, B. N. Bowman, L. Armijo, K. Gentry, J. Wilkerson, J. Wallace, X. M. Jiang, E. C. Carnes, C. J. Brinker and E. D. Milligan, *J. Controlled Release*, **2013**, 168, 209-224.
24. L. S. Wang, L. C. Wu, S. Y. Lu, L. L. Chang, I. T. Teng, C. M. Yang and J. A. A. Ho, *ACS Nano*, **2010**, 4, 4371-4379.
25. J. Liu, X. Jiang, C. Ashley and C. J. Brinker, *J. Am. Chem. Soc.*, **2009**, 131, 7567-7569.
26. S. P. Hudson, R. F. Padera, R. Langer and D. S. Kohane, *Biomaterials*, **2008**, 29, 4045-4055.

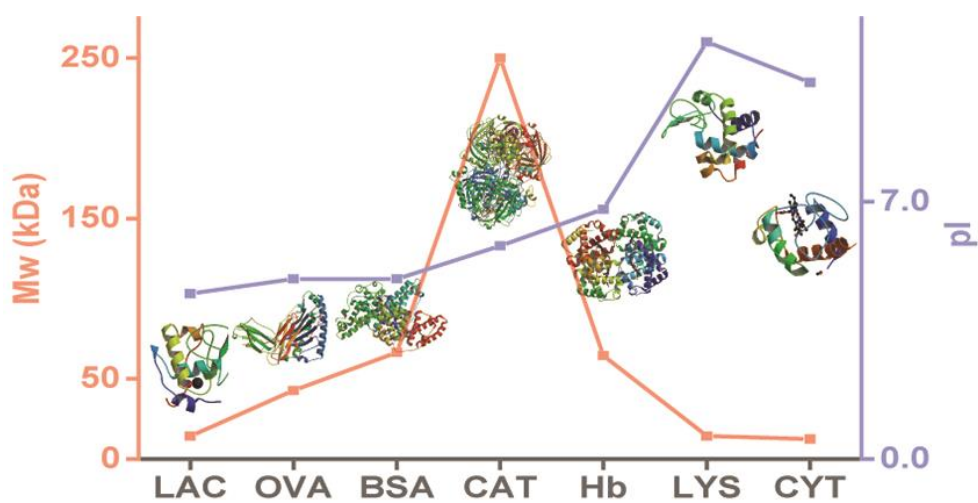
27. C. E. Ashley, E. C. Carnes, K. E. Epler, D. P. Padilla, G. K. Phillips, R. E. Castillo, D. C. Wilkinson, B. S. Wilkinson, C. A. Burgard, R. M. Kalinich, J. L. Townson, B. Chackerian, C. L. Willman, D. S. Peabody, W. Wharton and C. J. Brinker, *ACS Nano*, **2012**, 6, 2174-2188.
28. R. A. Roggers, V. S. Y. Lin and B. G. Trewyn, *Mol. Pharmaceutics*, **2012**, 9, 2770-2777.
29. Y. Piao, A. Burns, J. Kim, U. Wiesner and T. Hyeon, *Adv. Funct. Mater.*, **2008**, 18, 3745-3758.
30. T. A. Xia, M. Kovochich, M. Liong, H. Meng, S. Kabehie, S. George, J. I. Zink and A. E. Nel, *ACS Nano*, **2009**, 3, 3273-3286.
31. W. Y. Zhai, C. L. He, L. Wu, Y. Zhou, H. R. Chen, J. Chang and H. F. Zhang, *J. Biomed. Mater. Res., Part B*, **2012**, 100b, 1397-1403.
32. D. R. Radu, C. Y. Lai, K. Jęftinija, E. W. Rowe, S. Jęftinija and V. S. Y. Lin, *J. Am. Chem. Soc.*, **2004**, 126, 13216-13217.
33. J. L. Vivero-Escoto, Slowing, II, B. G. Trewyn and V. S. Lin, *Small*, **2010**, 6, 1952-1967.
34. L. Maggini, I. Cabrera, A. Ruiz-Carretero, E. A. Prasetyanto, E. Robinet and L. De Cola, *Nanoscale*, **2016**, 8, 7240-7247.
35. P. Yang, S. Gai and J. Lin, *Chem. Soc. Rev.*, **2012**, 41, 3679-3698.
36. C. H. Lei, Y. S. Shin, J. Liu and E. J. Ackerman, *J. Am. Chem. Soc.*, **2002**, 124, 11242-11243.
37. Z. X. Li, J. C. Barnes, A. Bosoy, J. F. Stoddart and J. I. Zink, *Chem. Soc. Rev.*, **2012**, 41, 2590-2605.
38. I. Slowing, B. G. Trewyn and V. S. Lin, *J. Am. Chem. Soc.*, **2006**, 128, 14792-14793.
39. I. I. Slowing, B. G. Trewyn, S. Giri and V. S. Y. Lin, *Adv. Funct. Mater.*, **2007**, 17, 1225-1236.
40. K. Moller, J. Kobler and T. Bein, *Adv. Funct. Mater.*, **2007**, 17, 605-612.
41. Y. Han and J. Y. Ying, *Angew. Chem., Int. Ed.*, **2005**, 44, 288-292.
42. H. Yamada, H. Ujiie, C. Urata, E. Yamamoto, Y. Yamauchi and K. Kuroda, *Nanoscale*, **2015**, 7, 19557-19567.
43. S. H. Wu, C. Y. Mou and H. P. Lin, *Chem. Soc. Rev.*, **2013**, 42, 3862-3875.
44. J. Gu, K. Huang, X. Zhu, Y. Li, J. Wei, W. Zhao, C. Liu and J. Shi, *J. Colloid Interface Sci.*, **2013**, 407, 236-242.
45. A. B. D. Nandiyanto, S.-G. Kim, F. Iskandar and K. Okuyama, *Microporous Mesoporous Mater.*, **2009**, 120, 447-453.
46. J. Sun, H. Zhang, R. Tian, D. Ma, X. Bao, D. S. Su and H. Zou, *Chem. Commun.*, **2006**, 1322-1324.
47. M. Hartmann, *Chem. Mater.*, **2005**, 17, 4577-4593.
48. F. Lu, S. H. Wu, Y. Hung and C. Y. Mou, *Small*, **2009**, 5, 1408-1413.
49. H. Meng, M. Xue, T. Xia, Z. X. Ji, D. Y. Tarn, J. I. Zink and A. E. Nel, *ACS Nano*, **2011**, 5, 4131-4144.
50. I. I. Slowing, J. L. Vivero-Escoto, C. W. Wu and V. S. Y. Lin, *Adv. Drug Delivery Rev.*, **2008**, 60, 1278-1288.
51. Z. Gao and I. Zharov, *Chem. Mater.*, **2014**, 26, 2030-2037.
52. N. Z. Knezevic and J. O. Durand, *Nanoscale*, **2015**, 7, 2199-2209.
53. X. Du, L. Xiong, S. Dai, F. Kleitz and S. Z. Qiao, *Adv. Funct. Mater.*, **2014**, 24, 7627-7637.
54. C. J. Brinker, *J Non-Cryst Solids*, **1988**, 100, 31-50.
55. F. Hoffmann, M. Cornelius, J. Morell and M. Froba, *Angew. Chem., Int. Ed.*, **2006**, 45, 3216-3251.

56. D. Y. Zhao, J. L. Feng, Q. S. Huo, N. Melosh, G. H. Fredrickson, B. F. Chmelka and G. D. Stucky, *Science*, **1998**, 279, 548-552.
57. C. Y. Lai, B. G. Trewyn, D. M. Jeftinija, K. Jeftinija, S. Xu, S. Jeftinija and V. S. Lin, *J. Am. Chem. Soc.*, **2003**, 125, 4451-4459.
58. I. I. Slowing, B. G. Trewyn and V. S. Y. Lin, *J. Am. Chem. Soc.*, **2007**, 129, 8845-8849.
59. K. T. Mody, A. Popat, D. Mahony, A. S. Cavallaro, C. Yu and N. Mitter, *Nanoscale*, **2013**, 5, 5167-5179.
60. C.-H. Lee, T.-S. Lin and C.-Y. Mou, *Nano Today*, **2009**, 4, 165-179.
61. A. Popat, S. B. Hartono, F. Stahr, J. Liu, S. Z. Qiao and G. Q. Lu, *Nanoscale*, **2011**, 3, 2801-2818.
62. D. Mahony, A. S. Cavallaro, F. Stahr, T. J. Mahony, S. Z. Qiao and N. Mitter, *Small*, **2013**, 9, 3138-3146.
63. H. Zhang, J. M. Sun, D. Ma, X. H. Bao, A. Klein-Hoffmann, G. Weinberg, D. S. Su and R. Schlogl, *J. Am. Chem. Soc.*, **2004**, 126, 7440-7441.
64. Y. Wang, Y. A. Nor, H. Song, Y. N. Yang, C. Xu, M. H. Yu and C. Z. Yu, *J. Mater. Chem. B*, **2016**, 4, 2646-2653.
65. K. Zhang, L. L. Xu, J. G. Jiang, N. Calin, K. F. Lam, S. J. Zhang, H. H. Wu, G. D. Wu, B. Albel, L. Bonneviot and P. Wu, *J. Am. Chem. Soc.*, **2013**, 135, 2427-2430.
66. M. Y. Wu, Q. S. Meng, Y. Chen, L. X. Zhang, M. L. Li, X. J. Cai, Y. P. Li, P. C. Yu, L. L. Zhang and J. L. Shi, *Adv. Mater.*, **2016**, 28, 1963-1969.
67. S. B. Hartono, S. Z. Qiao, J. Liu, K. Jack, B. P. Ladewig, Z. P. Hao and G. Q. M. Lu, *J. Phys. Chem. C*, **2010**, 114, 8353-8362.
68. Y. J. Wang and F. Caruso, *Chem. Mater.*, **2005**, 17, 953-961.
69. C. H. Lee, J. Lang, C. W. Yen, P. C. Shih, T. S. Lin and C. Y. Mou, *J. Phys. Chem. B*, **2005**, 109, 12277-12286.
70. S. L. Hirsh, M. M. M. Bilek, N. J. Nosworthy, A. Kondyurin, C. G. dos Remedios and D. R. McKenzie, *Langmuir*, **2010**, 26, 14380-14388.
71. S. Huh, J. W. Wiench, J. C. Yoo, M. Pruski and V. S. Y. Lin, *Chem. Mater.*, **2003**, 15, 4247-4256.
72. L. L. Li and H. Wang, *Adv. Healthcare Mater.*, **2013**, 2, 1351-1360.
73. J. Mendez, M. Morales Cruz, Y. Delgado, C. M. Figueroa, E. A. Orellano, M. Morales, A. Monteagudo and K. Griebenow, *Mol. Pharmaceutics*, **2014**, 11, 102-111.
74. W. Y. Huang, G. L. Davies and J. J. Davis, *Chem. - Eur. J.*, **2013**, 19, 17891-17898.
75. S. K. Kim, M. B. Foote and L. Huang, *Biomaterials*, **2012**, 33, 3959-3966.
76. S. Santra, C. Kaittanis and J. M. Perez, *Mol. Pharmaceutics*, **2010**, 7, 1209-1222.
77. R. Richter, A. Mukhopadhyay and A. Brisson, *Biophys J*, **2003**, 85, 3035-3047.
78. H. M. McConnell, T. H. Watts, R. M. Weis and A. A. Brian, *Biochim. Biophys. Acta*, **1986**, 864, 95-106.
79. R. P. Richter, R. Berat and A. R. Brisson, *Langmuir*, **2006**, 22, 3497-3505.
80. R. Michel, E. Kesselman, T. Plostica, D. Danino and M. Gradzielski, *Angew. Chem., Int. Ed.*, **2014**, 53, 12441-12445.
81. S. Ahmed, S. Savarala, Y. J. Chen, G. Bothun and S. L. Wunder, *Small*, **2012**, 8, 1740-1751.
82. P. Nollert, H. Kiefer and F. Jahnig, *Biophys. J.*, **1995**, 69, 1447-1455.
83. S. Mornet, O. Lambert, E. Duguet and A. Brisson, *Nano Lett.*, **2005**, 5, 281-285.
84. V. Cauda, H. Engelke, A. Sauer, D. Arcizet, C. Brauchle, J. Radler and T. Bein, *Nano Lett.*, **2010**, 10, 2484-2492.
85. J. Zhang, D. Desai and J. M. Rosenholm, *Adv. Funct. Mater.*, **2014**, 24, 2352-2360.

86. K. Epler, D. Padilla, G. Phillips, P. Crowder, R. Castillo, D. Wilkinson, B. Wilkinson, C. Burgard, R. Kalinich, J. Townson, B. Chackerian, C. Willman, D. Peabody, W. Wharton, C. J. Brinker, C. Ashley and E. Carnes, *Adv. Healthcare Mater.*, **2012**, 1, 348-353.
87. A. L. Troutier and C. Ladaviere, *Adv. Colloid Interface Sci.*, **2007**, 133, 1-21.
88. J. W. Liu, A. Stace-Naughton, X. M. Jiang and C. J. Brinker, *J. Am. Chem. Soc.*, **2009**, 131, 1354-1355.
89. J. W. Liu, A. Stace-Naughton and C. J. Brinker, *Chem. Commun.*, **2009**, 5100-5102.
90. X. S. Liu, A. Situ, Y. A. Kang, K. R. Villabroza, Y. P. Liao, C. H. Chang, T. Donahue, A. E. Nel and H. Meng, *ACS Nano*, **2016**, 10, 2702-2715.
91. N. Han, Y. Wang, J. L. Bai, J. J. Liu, Y. Wang, Y. K. Gao, T. Y. Jiang, W. J. Kang and L. L. Wang, *Microporous Mesoporous Mater.*, **2016**, 219, 209-218.
92. R. Veneziano, G. Derrien, S. Tan, A. Brisson, J. M. Devoisselle, J. Chopineau and C. Charnay, *Small*, **2012**, 8, 3674-3682.
93. E. Bringas, O. Koysuren, D. V. Quach, M. Mahmoudi, E. Aznar, J. D. Roehling, M. D. Marcos, R. Martinez-Manez and P. Stroeve, *Chem. Commun.*, **2012**, 48, 5647-5649.
94. M. M. van Schooneveld, E. Vucic, R. Koole, Y. Zhou, J. Stocks, D. P. Cormode, C. Y. Tang, R. E. Gordon, K. Nicolay, A. Meijerink, Z. A. Fayad and W. J. Mulder, *Nano Lett.*, **2008**, 8, 2517-2525.
95. D. Tarn, C. E. Ashley, M. Xue, E. C. Carnes, J. I. Zink and C. J. Brinker, *Acc. Chem. Res.*, **2013**, 46, 792-801.
96. X. Liang, X. Yue, Z. Dai and J. Kikuchi, *Chem. Commun.*, **2011**, 47, 4751-4753.
97. P. N. Durfee, Y. S. Lin, D. R. Dunphy, A. J. Muniz, K. S. Butler, K. R. Humphrey, A. J. Lokke, J. O. Agola, S. S. Chou, I. M. Chen, W. Wharton, J. L. Townson, C. L. Willman and C. J. Brinker, *ACS Nano*, **2016**, 8325-8345.
98. H. Meng, M. Wang, H. Liu, X. Liu, A. Situ, B. Wu, Z. Ji, C. H. Chang and A. E. Nel, *ACS Nano*, **2015**, 3540-3557.
99. W. H. De Jong and P. J. A. Borm, *Int. J. Nanomed.*, **2008**, 3, 133-149.
100. J. A. Gallego-Urrea, J. Tuoriniemi and M. Hasselov, *TrAC, Trends Anal. Chem.*, **2011**, 30, 473-483.

## Chapter II

### Mesoporous Silica Nanoparticles with Large Pores for the Encapsulation and Release of Proteins



Jing Tu, Aimee L. Boyle, Heiner Friedrich, Paul H.H. Bomans, Jeroen Bussmann, Nico A.J.M. Sommerdijk, Wim Jiskoot, and Alexander Kros, *ACS Appl. Mater. Interfaces*, **2016**, DOI: 10.1021/acsami.6b11324

### Abstract

Mesoporous silica nanoparticles (MSNs) have been explored extensively as solid supports for proteins in biological and medical applications. Small (< 200 nm) MSNs with ordered large pores (> 5 nm), capable of encapsulating therapeutic small molecules suitable for delivery applications *in vivo*, are rare however. Here we present small, elongated, cuboidal, MSNs with average dimensions of 90 × 43 nm that possess disk-shaped cavities, stacked on top of each other, which run parallel to the short axis of the particle. Amine-functionalization was achieved by modifying the MSN surface with 3-aminopropyltriethoxysilane or 3-[2-(2-aminoethylamino)ethylamino] propyltrimethoxysilane (AP-MSNs and AEP-MSNs) and were shown to have similar dimensions to the non-functionalized MSNs. The dimensions of these particles, and their large surface areas as measured by nitrogen adsorption-desorption isotherms, make them ideal scaffolds for protein encapsulation and delivery. We therefore investigated the encapsulation and release behavior for seven model proteins ( $\alpha$ -lactalbumin, ovalbumin, bovine serum albumin, catalase, hemoglobin, lysozyme and cytochrome c). It was discovered that all types of MSNs used in this study allow rapid encapsulation, with a high loading capacity, for all proteins studied. Furthermore, the release profiles of the proteins were tunable. The variation in both rate and amount of protein uptake and release was found to be determined by the surface chemistry of the MSNs, together with the isoelectric point (pI), and molecular weight of the proteins, as well as by the ionic strength of the buffer. These MSNs with their large surface area and optimal dimensions, provide a scaffold with a high encapsulation efficiency and controllable release profiles for a variety of proteins, enabling potential applications in fields such as drug delivery and protein therapy.

**Keywords:** mesoporous silica nanoparticles, protein loading, protein release, nanomedicine, sol-gel, drug delivery

## 2.1 Introduction

Proteins participate in a variety of vital processes in the body,<sup>1</sup> and are therefore used as therapeutic agents in a diverse range of biomedical applications,<sup>2</sup> such as cancer therapy,<sup>3, 4</sup> vaccination,<sup>5, 6</sup> and protein therapy.<sup>7, 8</sup> Several barriers have to be overcome for efficient protein delivery however, as most native proteins are membrane impermeable due to electrostatic repulsion, and are prone to degradation or inactivation processes in bodily fluids.<sup>1</sup> Over the last decades, various nanocarriers such as lipid-based assemblies,<sup>9</sup> gold nanoparticles<sup>10</sup> and polymeric nanoparticles,<sup>11</sup> have been developed to overcome these barriers.

Mesoporous silica nanoparticles (MSNs) are a class of molecules that have attracted a lot of attention in the small molecule delivery field, due to their multitude of desirable properties. They possess an open-pore structure; the sizes of the pores and of the MSNs themselves can be controlled synthetically.<sup>12-14</sup> Furthermore, the silanol-containing surface can be readily functionalized,<sup>15-17</sup> enabling modification with targeting molecules such as folate or hyaluronic acid to enhance cellular uptake,<sup>18, 19</sup> and permitting the adsorption of various proteins with different isoelectric points (pI).<sup>16, 20</sup> Due to their structure, MSNs protect proteins from premature degradation in body fluids, thereby increasing the efficiency of protein delivery *in vivo*, thus reducing renal filtration.<sup>1</sup> This combination of properties means MSNs have exhibited potential as a non-invasive and biocompatible platform for protein delivery,<sup>21, 22</sup> especially in the fields of enzyme therapies,<sup>7, 8</sup> vaccination,<sup>5, 6, 23</sup> and imaging.<sup>24</sup> Since MSNs are much smaller than eukaryotic cells, they can facilitate the transport of proteins into the cytosol via an endocytosis pathway and subsequent endosomal escape.<sup>25, 26</sup>

Numerous synthetic protocols for the preparation of MSNs have been developed with the aim of controlling the size and morphology of these nanoparticles.<sup>27-30</sup> Encapsulating proteins in MSNs is still challenging however, and only a few publications concerning the design of MSNs with a morphology that enables the effective encapsulation of a broad range of proteins are available.<sup>31, 32</sup> Typically, proteins are only adsorbed onto the external surface of MSNs due to the small pore diameter (< 3 nm) preventing the proteins from entering the MSNs' interior pores.<sup>5, 33</sup> Proteins adsorbed at the MSNs' outer surface do not make use of the protective environment inside the MSNs, nor do they utilize the large internal surface area presented by the pores.<sup>14, 34</sup> Thus, limitations in generating small (< 200 nm in diameter) MSNs with sufficient pore sizes (> 5 nm) to encapsulate proteins or other biomacromolecules is one of the major hurdles for "comfortably" hosting large molecules.<sup>21, 35-37</sup> In order to solve

this protein inaccessibility issue, MSNs with a large pore size have been synthesized. However, the diameter of the majority of these particles is 1-2  $\mu\text{m}$  and so these are less suited for *in vivo* delivery applications. Studies have shown that particle sizes between 50 and 200 nm are preferred for endocytic uptake.<sup>25, 38, 39</sup> Therefore, monodisperse MSNs with a particle size in the 50-200 nm range, controllable surface chemistry, and a large pore size ( $> 5$  nm) are desired.<sup>31, 36</sup>

Building upon previous methods,<sup>28, 40-42</sup> we designed a facile synthetic route to produce MSNs that are able to effectively encapsulate and release a variety of proteins. To obtain the desired large pores in a sub-200 nm particle, a double-surfactant system consisting of a high molecular weight block copolymer (Pluronic P123),<sup>28, 31, 40</sup> and fluorocarbons,<sup>28, 43</sup> was employed as the structure-directing template. The swelling agent 1,3,5-trimethylbenzene (TMB) was added to expand the diameter of the pores.<sup>28, 40</sup> These MSNs were synthesized as stable colloidal suspensions with a narrow size distribution and channels aligned parallel to the short axis. This mesostructure favors efficient mass transfer,<sup>44</sup> as it possesses a high density of entrances enabling rapid and efficient encapsulation of proteins.<sup>35</sup>

The obtained MSNs bear a net negative charge,<sup>29, 34</sup> at physiological pH. To study the effect of the silica surface charge on protein encapsulation, cationic MSNs were prepared by a post-synthesis grafting method involving the amine-containing silanes (3-aminopropyl)triethoxysilane (APTES) and 3-[2-(2-aminoethylamino)ethylamino] propyltrimethoxysilane (AEPTMS). This modification generated positively charged MSNs at physiological pH, designated as AP-MSNs and AEP-MSNs, respectively.

To illustrate the potential of these new, large-pore MSNs as protein carriers, the encapsulation and release of a range of model proteins<sup>20, 45-48</sup> with different molecular weights (Mw) and isoelectric points (pI) was studied, revealing that the MSNs' surface charge controls the protein encapsulation efficiency. The release profiles of the proteins from these large-pore MSNs were subsequently examined, and it was additionally confirmed that the structure of the released proteins was not altered.

## 2.2 Materials and Methods

### 2.2.1 Materials

Pluronic P123 ( $\text{EO}_{20}\text{PO}_{70}\text{EO}_{20}$ ,  $M_n \sim 5800$  g/mol), tetraethyl orthosilicate (TEOS,  $\geq 98\%$ ), hydrochloric acid (HCl), mesitylene, 3-aminopropyltriethoxysilane (APTES), 3-[2-(2-aminoethylamino)ethylamino] propyltrimethoxysilane (AEPTMS), 1,3,5-trimethylbenzene



(TMB),  $\alpha$ -lactalbumin from bovine milk (LAC), albumin from chicken egg white (OVA), bovine serum albumin (BSA), catalase from bovine liver (CAT), hemoglobin from bovine blood (Hb), cytochrome c from equine heart (CYT) and lysozyme from chicken egg white (LYS) were purchased from Sigma-Aldrich and used as received. Fluorocarbon surfactant FC-4 was purchased from Yick-Vic Chemicals & Pharmaceuticals (HK) Ltd, China. Milli-Q water (18.2 M $\Omega$ /cm, Millipore Co., USA) was used throughout the experiments. The composition of the phosphate buffered saline (PBS) used was: K<sub>2</sub>HPO<sub>4</sub> (14.99 mM), KH<sub>2</sub>PO<sub>4</sub> (5 mM), and NaCl (150.07 mM), with an ionic strength of 270 mM. The phosphate buffer (PB) with an ionic strength of 12 mM was prepared by mixing Na<sub>2</sub>HPO<sub>4</sub> (1 mM) and NaH<sub>2</sub>PO<sub>4</sub> (1 mM) at molar ratio of 5:2. The PB with an ionic strength of 166 mM was prepared by adding 0.9% NaCl into previously described PB with an ionic strength of 12 mM. The pH values were adjusted to 7.4.

### *2.2.2 Preparation of large-pore MSNs and functionalized MSNs*

MSNs were synthesized as follows. 0.5 g of surfactant Pluronic P123 and 1.4 g of FC-4 were dissolved in 80 mL of HCl (0.02 M), followed by the introduction of 0.48 mL of TMB. After stirring for 6 h, 2.14 mL of TEOS was added dropwise. The resulting mixture was stirred at 30 °C for 24 h and transferred to an autoclave at 120 °C for 2 days. Finally, the solid product was isolated by centrifugation, and washed with ethanol and water. The organic template was completely removed by calcination at 550 °C for 5 h.

The MSNs were functionalized with amine-containing groups through a post-modification procedure.<sup>49, 50</sup> For AP-MSNs, 100 mg of MSNs were suspended in 10 mL of ethanol and 0.4 mL of APTES was added. The mixture was refluxed at 77 °C for 10 h with stirring. The resulting particles were collected by centrifugation (13000 rpm, 5 min), washed thoroughly with ethanol and water three times, and freeze-dried. For AEP-MSNs, 100 mg of MSNs were incubated with 4 mL of 20 wt% AEPTMS in ethanol, overnight at room temperature. The AEP-MSNs were purified by centrifugation (13000 rpm, 5 min) and washed with ethanol and water three times to remove unreacted AEPTMS, and freeze-dried.

### *2.2.3 Protein encapsulation studies*

A protein stock solution (0.5 mg/mL) was prepared in phosphate buffer (1 mM, pH 7.4). MSNs, AP-MSNs, and AEP-MSNs (2 mg/mL), were sonicated (10 min) and dispersed in the same buffer. In a typical procedure, 0.5 mL of protein stock solution was mixed with 0.5 mL of MSNs, AP-MSNs or AEP-MSNs suspension and incubated in an Eppendorf mixer (400

rpm, 25 °C). After incubation for 20 min, protein-loaded particles (MSNs, AP-MSNs and AEP-MSNs) were collected by centrifugation (13000 rpm, 5 min) and separated from the non-encapsulated protein, which remained in the supernatant. The encapsulation efficiency (EE%) was determined by measuring the difference in concentration of the protein in the supernatant before and after loading. The concentration of protein was determined using a standard calibration curve of the corresponding protein. The intrinsic fluorescence intensity and absorbance of the proteins were measured using Greiner 96-well flat-bottom black, and Greiner 96-well flat-bottom transparent, microplates respectively in a plate reader (Tecan infinite M1000). For LAC, OVA, BSA, CAT and LYS, the standard curves were based on the intrinsic fluorescence intensity (excitation wavelength = 280 nm and emission wavelength = 320 nm) as a function of concentration (0-500 µg/mL). For Hb and CYT, the calibration curves were based on the absorbance at 405 nm and 412 nm respectively, as a function of concentration (0-500 µg/mL). The EE% and loading capacity (mg/g) were calculated as shown in Equation 2.1 and 2.2.<sup>21, 51</sup>

$$EE\% = \frac{t_{protein} - f_{protein}}{t_{protein}} \times 100\% \quad (2.1)$$

$$\text{Loading capacity (mg/g)} = \frac{t_{protein}(\text{mg}) - f_{protein}(\text{mg})}{\text{amount of MSNs (g)}} \quad (2.2)$$

Where  $t_{protein}$  is the total amount of protein, and  $f_{protein}$  is the amount of free protein.

### 2.2.4 Protein release studies

The *in vitro* release of encapsulated proteins, and the effect of ionic strength on the release profiles, was determined by suspending the protein-loaded MSNs in 1 mL of phosphate buffer of different ionic strengths (12 mM, 166 mM and 270 mM) at a final MSN concentration of 1 mg/mL. All suspensions were placed in an Eppendorf mixer (400 rpm, 37 °C). The amount of released protein was determined by removing the supernatant after centrifugation (13000 rpm, 5 min) and replacing it with clean buffer (1 mL) at specified time points. The amount of protein in the supernatant was measured using a Tecan infinite M1000 plate reader (using the settings described in section 2.3). All measurements were performed in triplicate. CD spectra of the proteins before and after release were measured using a Jasco J-815 spectropolarimeter. Spectra were collected from 260 – 190 nm, at 25 °C to determine whether encapsulation and subsequent release of the proteins had any effect on their secondary structure.

### 2.2.5 Particle analysis

The porous structure of the as-prepared MSNs was characterized using transmission electron microscopy (TEM) operated at 70 kV (TEM, JEOL 1010, USA). (Cryo-) electron tomography was performed in bright-field mode using zero-loss energy filtering with 20 eV energy window on the TU/e cryoTITAN (FEI, FEG, 300 kV, Gatan Energy filter). Images of the tilt-series were collected either dry at room temperature or under cryogenic conditions with the particles suspended in vitrified water over an angular range of  $\pm 65^\circ$  at 2 degree increments and with a nominal underfocus of -200 nm (dry) or -5  $\mu\text{m}$  (cryo). Due to the beam sensitivity of the material, the total accumulated dose over the entire tilt-series was kept below 100  $\text{e}/\text{\AA}^2$ . Alignment by fiducial gold particles, 3D reconstruction and denoising using nonlinear anisotropic diffusion was carried out in IMOD. Visualization was performed in Avizo. Surface analysis of the MSNs was performed by measuring nitrogen-sorption isotherms at 77 K with a Micromeritics TrisStar II 3020 as the analyzer. As a pretreatment, MSNs were outgassed at 300  $^\circ\text{C}$  for 16 h under vacuum (below 0.15 mbar), while the other samples (AP-MSNs, AEP-MSNs, and protein-loaded MSNs) were outgassed at 25  $^\circ\text{C}$  for 16 h. The specific surface areas were calculated using the Brunauer-Emmett-Teller (BET) method. The pore size distribution was calculated from the desorption branch of the isotherm by the Barrett-Joyner-Halenda (BJH) method.<sup>52</sup> The hydrodynamic diameter and zeta-potential of the MSNs were measured with a Malvern Nano-ZS instrument.

## 2.3 Results and discussion

### 2.3.1 Synthesis and characterization of MSNs, AP- and AEP-MSNs

Existing literature details how amphiphilic block copolymers such as Pluronic P123,<sup>31, 40</sup> act as organic structure-directing agents, and co-solvent organic molecules (*e.g.* TMB)<sup>53, 54</sup> can be used as swelling agents to obtain MSNs with large pores. This technique was replicated here and, in addition, the cationic fluorocarbon surfactant FC-4 was utilized to confine the diameter of the MSNs.<sup>28</sup> Additionally, a hydrothermal treatment, similar to the procedure reported by Han,<sup>28, 55</sup> but with a higher temperature (120  $^\circ\text{C}$ ) and a longer reaction time (48 h) was employed to improve mesoscopic regularity and to further extend pore size.<sup>40, 42, 56, 57</sup>

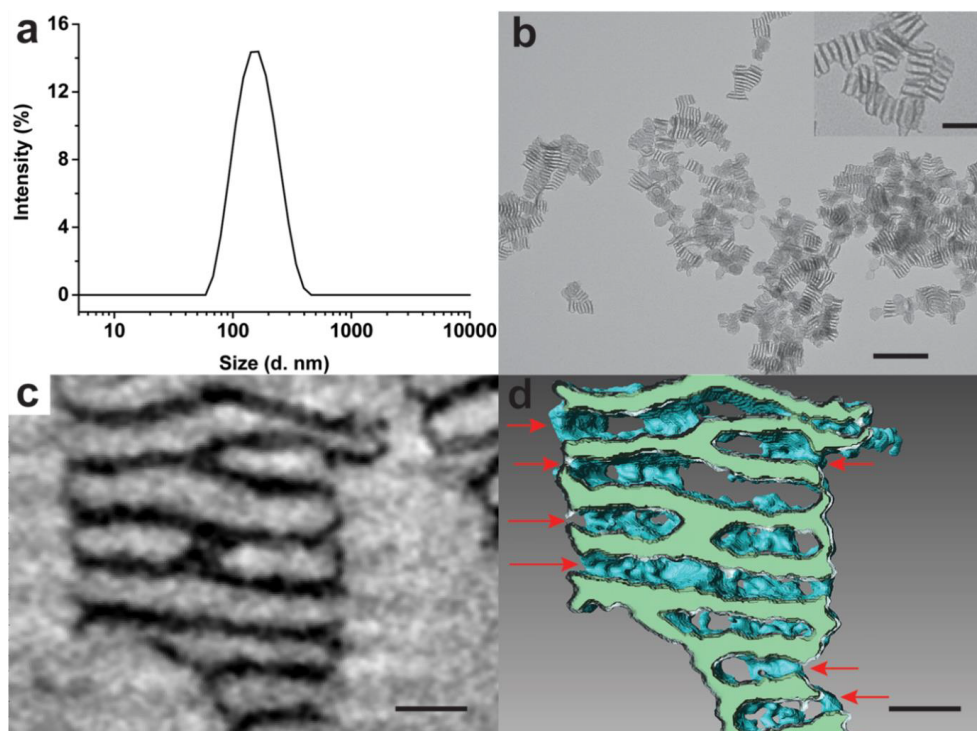


**Figure 2.1** (a) Hydrodynamic diameter by DLS; (b) TEM image of MSNs, scale bar = 200 nm, insert figure with scale bar = 50 nm, (c) and (d) electron tomography results showing cross-section through reconstruction (pores that connect cavities with the environment are indicated by arrows) and 3D rendering of silica surface (cut to expose the interior), scale bar = 25 nm.

Dynamic light scattering (DLS) measurements revealed MSNs with a unimodal distribution that possessed an average hydrodynamic diameter of 146 nm (Figure 2.1a). The morphology and mesoporous structure of the MSNs was visualized by TEM (Figure 2.1b). Analysis of the TEM images revealed the MSNs had lengths of  $90 \pm 20$  nm and widths of  $43 \pm 7$  nm, giving them an elongated cuboidal-like geometry. These sizes were slightly smaller than those determined by DLS, since TEM provides the size distribution of dehydrated particles and DLS measurements yield an average hydrodynamic diameter of the particles in solution.<sup>58</sup> The MSNs were found to possess large channels with an average size of  $10 \pm 1$  nm (measurements from 150 particles). These channels run parallel to the short axis of the MSNs.

Next, a 3D-reconstruction of the MSNs was obtained by (cryo-) electron tomography. This revealed the MSNs possessed disk-shaped cavities, or channels, stacked on top of each

other, which run parallel to the short axis of the particle, consistent with the TEM observations (Figure 2.1c,d).

To further characterize the channels within the MSNs, nitrogen sorption measurements were performed. The MSNs exhibit characteristic type IV isotherms with type-H<sub>1</sub> hysteresis loops<sup>40, 59</sup> in nitrogen sorption measurements, indicative of the presence of channel-like mesopores (Figure 2.2a). The average diameter of the channels inside these MSNs was calculated to be 9-11 nm (Figure 2.2b), consistent with the result obtained by TEM. The MSNs were calculated to have a large specific surface area of 506 m<sup>2</sup>/g (Table 2.1).

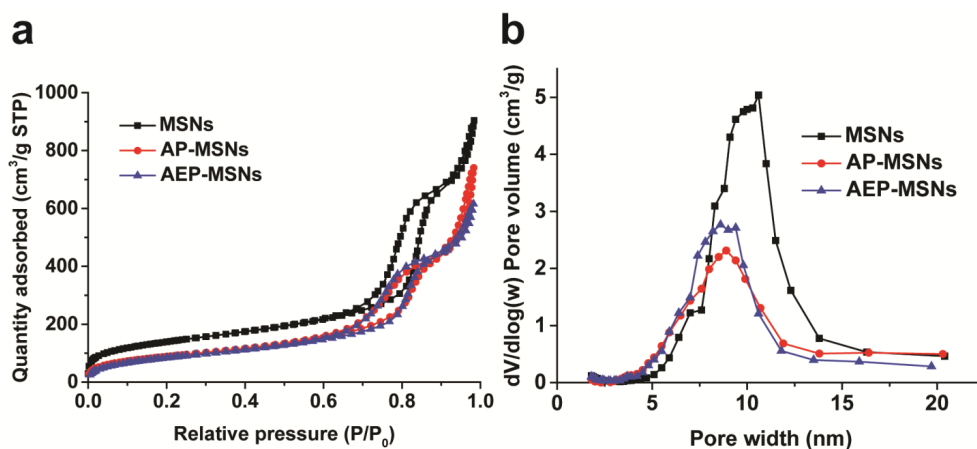


**Figure 2.2** (a) Nitrogen adsorption-desorption isotherms and; (b) corresponding pore size distributions of MSNs, AP-MSNs and AEP-MSNs.

Amino-modified MSNs, termed AP- and AEP-MSNs, were synthesized by reacting the MSNs with APTES, and AEPTMS respectively. These modified MSNs also exhibited type IV isotherms with type-H<sub>1</sub> hysteresis loops (Figure 2.2a), indicating functionalization of the surface of the MSNs with amine groups did not perturb the structure. The presence of amino groups does reduce the specific surface area to 328 m<sup>2</sup>/g and 318 m<sup>2</sup>/g for AP-MSNs and AEP-MSNs respectively (Table 2.1). This is in accordance with the slightly reduced pore diameters of AP- and AEP-MSNs, which are both calculated to be 9 ± 1 nm (Figure 2.2b, Table 2.1), which is still larger than the geometric size of most proteins.

**Table 2.1** Physical characteristics of MSNs, AP-MSNs and AEP-MSNs

Sample	BET specific surface area (m <sup>2</sup> /g)	Specific channel volume (cm <sup>3</sup> /g)	Average channel diameter (nm) <sup>a</sup>
MSNs	506	1.01	10 ± 1
AP-MSNs	328	0.68	9 ± 1
AEP-MSNs	318	0.71	9 ± 1

<sup>a</sup>Calculated from the desorption branch of the N<sub>2</sub> sorption isotherms based on the BJH method.

### 2.3.2 Protein loading studies

To test the potential of these MSNs for protein-based delivery applications we studied the encapsulation and release of seven model proteins with different molecular weights, geometric sizes, shapes, and pI values (Table 2.2). These proteins were selected due to the wide variety of physical properties they collectively presented, (Table 2.2), and because of their biological applications, for example: ovalbumin has been studied for its antigenic properties;<sup>5, 6</sup> catalase is an important antioxidant;<sup>7, 8</sup> hemoglobin is a well-characterised oxygen carrier;<sup>51, 60</sup> and cytochrome c has been known to induce apoptosis.<sup>53, 61</sup>

**Table 2.2** List of encapsulated proteins and their properties

Protein	Classification <sup>a</sup>	Mw/kDa	Size <sup>b</sup> (nm)	pI
LAC	glycoprotein	14.2	2.3 × 2.6 × 4	4.5
OVA	allergen	42.7	4 × 5 × 7	4.9
BSA	transport protein	66.5	5 × 5 × 9	4.9
CAT	oxidoreductase	250	7 × 8 × 10	5.8
Hb	oxygen binding	64.5	5.3 × 5.4 × 6.5	6.8
LYS	hydrolase	14.3	3 × 3 × 4.5	10-10.5
CYT	electron transport	12.4	2.6 × 3.2 × 3.3	11.35

<sup>a</sup>The classification and residue count of these proteins comes from the protein data bank (PDB, [www.rcsb.org](http://www.rcsb.org)). PDB codes: LAC, 1HFX; OVA, 1VAC; BSA, 4F5S; CAT, 1TGU; Hb, 2QSS; LYS, 4YM8; CYT, 2N3B.

<sup>b</sup>Geometric dimensions given by published literature.<sup>34, 62-64</sup>

Proteins were mixed with MSNs, AP- and AEP-MSNs in a 1:4 (protein:MSN) weight ratio. Figure 2.3a shows the encapsulation efficiency (EE%) of these proteins at physiological pH. The encapsulation process was found to be very rapid, with over 95% encapsulation efficiency being achieved within twenty minutes for all proteins.

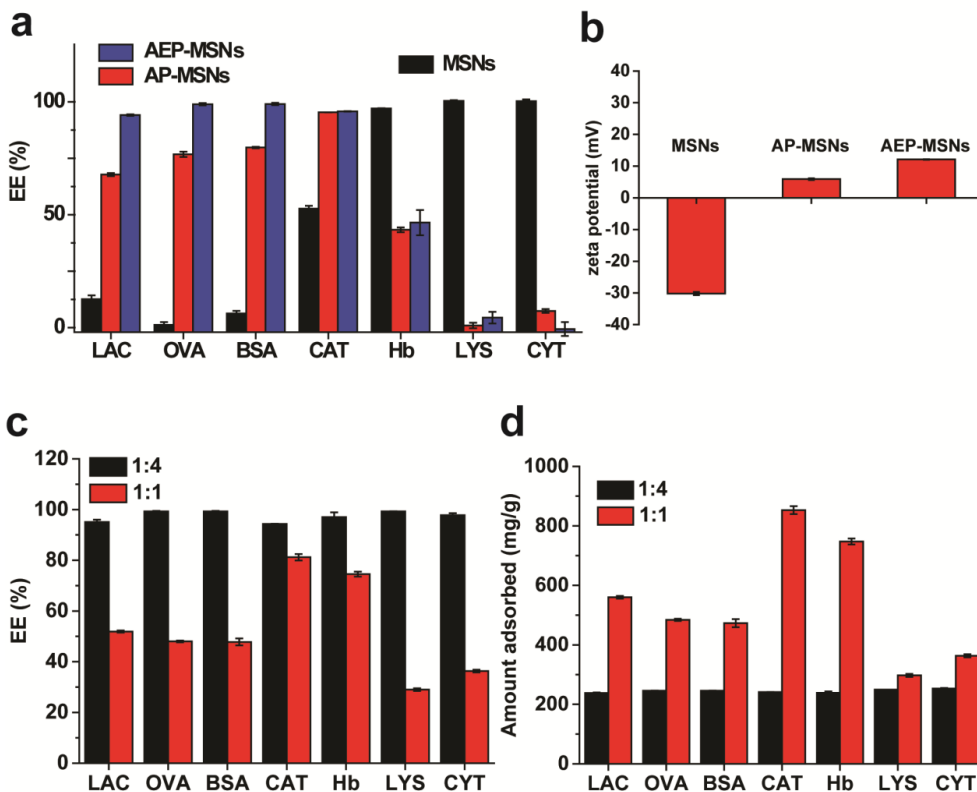


**Figure 2.3** (a) EE% of seven proteins in MSNs (black bars), AP-MSNs (red bars), and AEP-MSNs (blue bars), the initial weight ratio for encapsulation between protein and particles was 1:4 (250 mg of protein/1 g particles); (b) zeta potential of MSNs, AP-MSNs and AEP-MSNs in 1 mM PB, pH 7.4; (c) Encapsulation efficiency (EE%) of seven proteins (LAC, OVA, BSA and CAT in AEP-MSNs, and Hb, LYS and CYT in MSNs), and (d) the corresponding loading capacity (mg/g) for all proteins. The weight ratio for encapsulation between protein and MSNs is 1:4 (black bars) and 1:1 (red bars). Conditions for encapsulation of all proteins: 1 mM PB, ionic strength 12 mM, 25 °C, 20 min.

The charges of the MSNs, AP-MSNs and AEP-MSNs vary due to the surface chemistry of the particles. Zeta-potential analysis (Figure 2.3b), revealed a negative surface charge for MSNs (-30.2 mV), but a positive charge for both AP- and AEP-MSNs (+5.9 mV and +12.1 mV, respectively). This charge affects the extent of protein encapsulation; for proteins with a negative surface charge (LAC, OVA, BSA and CAT), encapsulation in positively charged AP- and AEP-MSNs was more efficient when compared to encapsulation in unmodified

MSNs. This was especially relevant with AEP-MSNs, where the encapsulation efficiency for all four of these proteins reached more than 95%. It is therefore evident that the amount of LAC, OVA, BSA and CAT encapsulated can be increased by the introduction of positively charged amine moieties onto the MSNs surface. Conversely, for the positively charged proteins LYS and CYT the amount encapsulated decreases when AP- or AEP-MSNs are employed. The observed results indicate that electrostatic interactions are likely to be the main driving force for protein encapsulation.<sup>45, 65, 66</sup> It is also interesting to note that CAT (250 kDa, *ca.* 10 nm diameter)<sup>46</sup> can be encapsulated into the mesopore network despite the fact that the pore size is similar to that of protein.<sup>67</sup> Interestingly, Hb (pI = 6.8) is still negatively charged when dissolved in phosphate buffer at pH 7.4. Still, the EE% of Hb reached 97%, while for AP-MSNs the EE% was 43% and for AEP-MSNs, 47%. For positively charged proteins (LYS and CYT), a high encapsulation efficiency (97% and 98% respectively), was obtained with unmodified MSNs while the encapsulation in AP-MSNs and AEP-MSNs was limited due to electrostatic repulsion.

Considering the initial weight ratio between the proteins and MSNs (1:4), and the EE%, these results clearly showed that MSNs (with an appropriate surface charge) can act as nanocarriers to efficiently encapsulate a wide variety of proteins (Mw 12.3-250 kDa, pI 4.5-11.3) with a loading capacity of at least 25 wt% (250 mg/g). When the initial weight ratio between the proteins and MSNs was increased (1:1), the EE% decreased but the total amount of protein encapsulated increased. For example, the loading capacity of CAT into AEP-MSNs increased from  $241.7 \pm 0.4$  mg/g to  $852.9 \pm 13.2$  mg/g, while for Hb  $239.1 \pm 4.6$  mg/g was encapsulated at the 1:4 ratio, but this rose to  $747.5 \pm 10.0$  mg/g when a 1:1 ratio was used. For LAC an increase from  $238.0 \pm 2.3$  mg/g to  $560.0 \pm 4.4$  mg/g was observed (Figure 2.3c,d). The large pore size is advantageous, especially for proteins with a high molecular weight and hence a large size. Upon protein encapsulation, both the surface area and pore diameter of the MSNs decreased, showing that the protein molecules had been encapsulated within the channels of the MSNs (Figure 2.4 and Table 2.S1).<sup>31</sup>



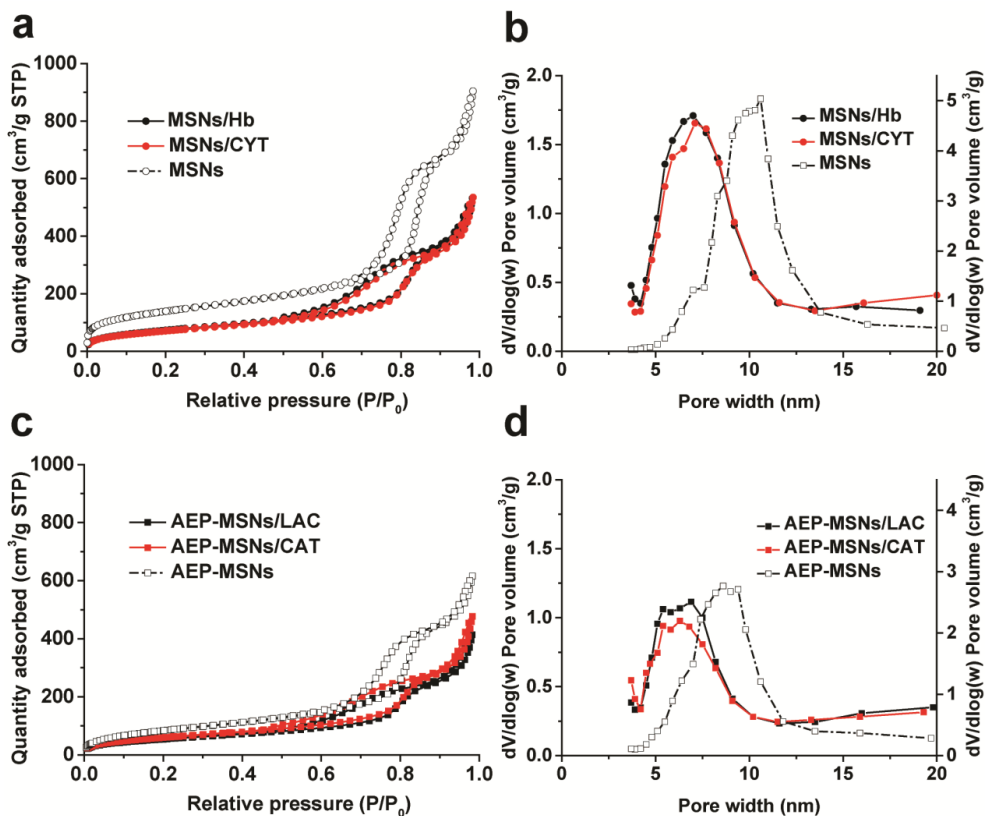


**Figure 2.4** (a) Nitrogen adsorption-desorption isotherms of MSNs/proteins (Hb and CYT), and (b) corresponding pore size distributions, with MSNs as a control; (c) nitrogen adsorption-desorption isotherms of AEP-MSNs/proteins (LAC and CAT), and corresponding (d) pore size distributions, with AEP-MSNs as a control.

### 2.3.3 Protein release studies

The *in vitro* release of proteins from MSNs or AEP-MSNs was investigated using a high ionic strength (270 mM) PBS buffer. For this study MSNs containing Hb, LYS and CYT, and AEP-MSNs loaded with LAC, OVA, BSA and CAT were tested. All the profiles showed a rapid burst release (Figure 2.5),<sup>68</sup> and a direct correlation between the final released percentage and the molecular weight of the protein was observed.

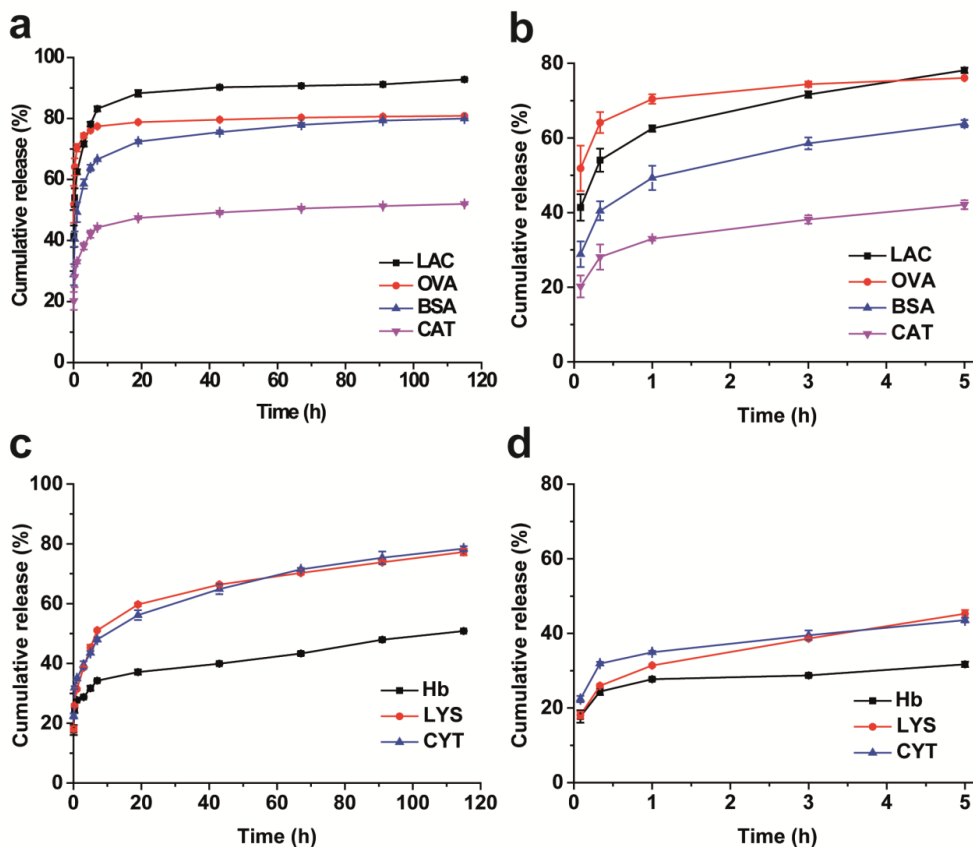


**Figure 2.5** (a) and (b) LAC, OVA, BSA and CAT release profiles from AEP-MSNs and; (c) and (d) Hb, LYS and CYT release profiles from MSNs. Conditions for release of all proteins: PBS, (ionic strength 270 mM), 37 °C.

A large amount of the encapsulated LAC (93%) was released from AEP-MSNs. This was the smallest protein to be encapsulated into these MSNs, so it is rational that this shows the highest released percentage as its small size makes ‘escape’ from the pores easier. OVA and BSA showed comparable release percentages (81 and 80%, respectively). These proteins are similar in size, therefore it is unsurprising that the amounts released are similar. They are significantly larger than LAC however, and the high release percentages are encouraging as these reveal that reasonably large proteins can escape from the MSN channels. Only 52% of CAT, the largest protein to be encapsulated in the AEP-MSNs was released however. The dimensions of CAT are  $7 \times 8 \times 10$  nm, this is close to the diameter of the pores and so it is possible that this protein gets trapped inside the pores resulting in a lower released percentage.

For the proteins encapsulated in the unmodified MSNs, a similar trend was seen. The two smallest proteins, CYT and LYS, exhibited similar release percentages (78 and 77% respectively). For Hb, the largest protein encapsulated into these MSNs, only 41% was released over the time frame studied, indicating that size plays an important role in release dynamics in these MSNs as well.

The effect of the ionic strength of the buffer on the proteins' release kinetics was also investigated (Figure 2.S1). Comparison of Figure 2.5a,b with Figure 2.S1a,b clearly shows the effect of ionic strength on the AEP-MSNs encapsulated proteins' release. When a low ionic strength buffer was used, the amount of protein released decreased for all the proteins investigated. The largest decrease was seen for LAC; 93% of the encapsulated protein was released when PBS with an ionic strength of 270 mM was used, this decreased to 69% for 166 mM PB buffer and a further decrease to 21% was observed when PB buffer with 12 mM ionic strength was employed, with the other proteins following a similar trend. These results indicate that a higher ionic strength of the buffer and a smaller molecular weight of the protein results in a larger percentage of released protein. This is likely to be because a smaller protein can escape the channels more easily, and a higher ionic strength buffer,<sup>16</sup> screens electrostatic interactions more effectively, meaning the electrostatic interactions that are holding the proteins in place in the MSNs are diminished.

The release of the MSN-encapsulated proteins did not follow such a clear trend when the ionic strength of the buffer was changed; compare Figure 2.5c,d and 2.S1c,d. At low ionic strength, the initial release rate of LYS was very low; this increased with an increasing buffer strength, as did the total amount of protein released. Hb and CYT exhibited different properties however. Both proteins showed burst release kinetics at high ionic strengths, whereas at low ionic strength the release was more sustained. The total amount released did not change as much for these proteins upon altering the ionic strength of the buffer (24, 27%, and 51% for Hb and 54, 69%, and 78% for CYT at 12 mM, 166 mM, and 270 mM ionic strength respectively) as it did for others. This suggests the factors controlling the release from the negatively-charged MSNs are more subtle than from the AEP-MSNs. Both protein size and charge (distribution) have an effect, but the effects of these are not easily separated. It would be interesting for future work to study the release of more proteins with MSNs to disentangle these effects and to determine which is more important – molecular weight or charge of the protein.

Finally, for any application, it is important that the released proteins are not misfolded, for example, due to strong MSN-protein interactions. Therefore the secondary structure of the

released proteins was compared to that of non-encapsulated proteins. The structures were measured using circular dichroism (CD) spectroscopy and no change was seen in any of the protein's secondary structure after encapsulation and release (Figure 2.S2).

## **2.4 Conclusion**

Here we have described a method to synthesize sub-200 nm MSNs with large (10 nm) channels perpendicular to the long axis of the particles. As a result, the MSNs (or the facilely modified AP- and AEP-MSNs) have a rapid, high encapsulation efficiency of a wide range of proteins with vastly different properties. Encapsulation was found to be dependent on the surface chemistry within the channels, and was directly related to the surface charge of the protein. The release of such proteins is tunable, and is dependent on the ionic strength of the release medium and the MSN surface chemistry. Protein properties such as molecular weight and charge also play a role in the release kinetics, with the parameters governing release being more subtle and involved than those controlling encapsulation.

This novel type of MSN with large channels and therefore a high surface area, resulting in a high encapsulation efficiency and controllable release profiles of proteins enables potential applications in fields such as protein therapy and drug delivery.

Supporting Information

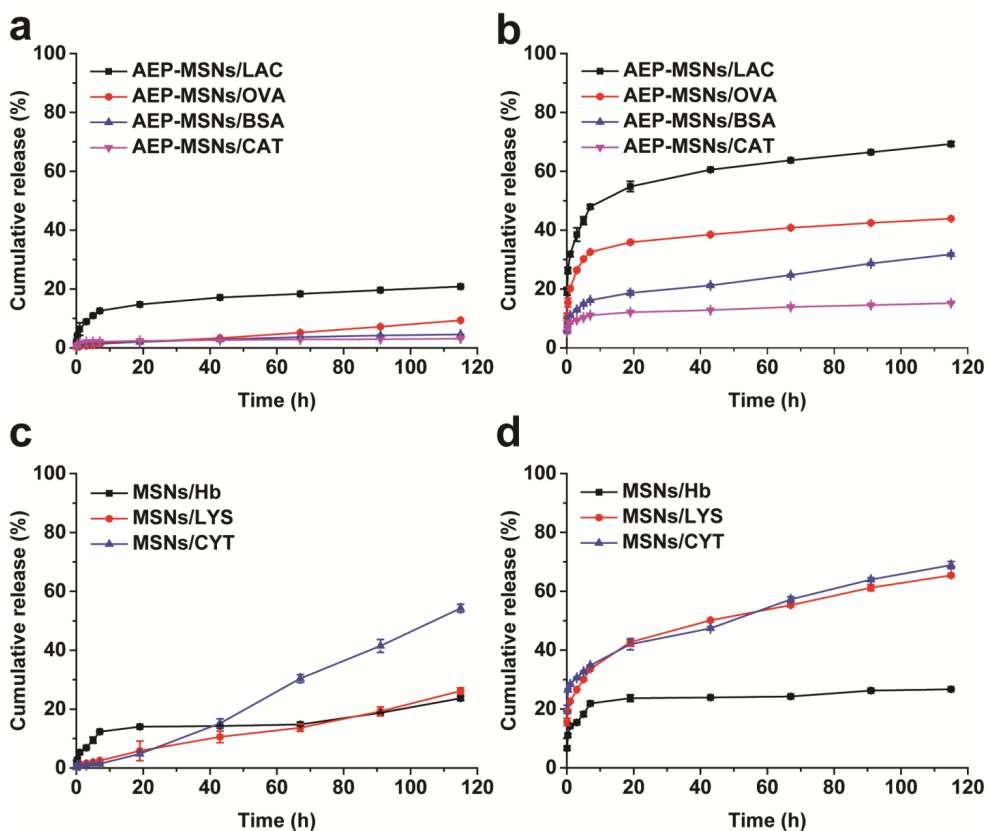


**Figure 2.S1** LAC, OVA, BSA and CAT release profiles from AEP-MSNs in (a) 1 mM PB (ionic strength 12 mM), and (b) 1 mM PB with 0.9% NaCl at 37 °C (ionic strength 166 mM); Hb, LYS and CYT release profiles from MSNs in (c) 1 mM PB (ionic strength 12 mM), and (d) 1 mM PB with 0.9% NaCl at 37 °C (ionic strength 166 mM).

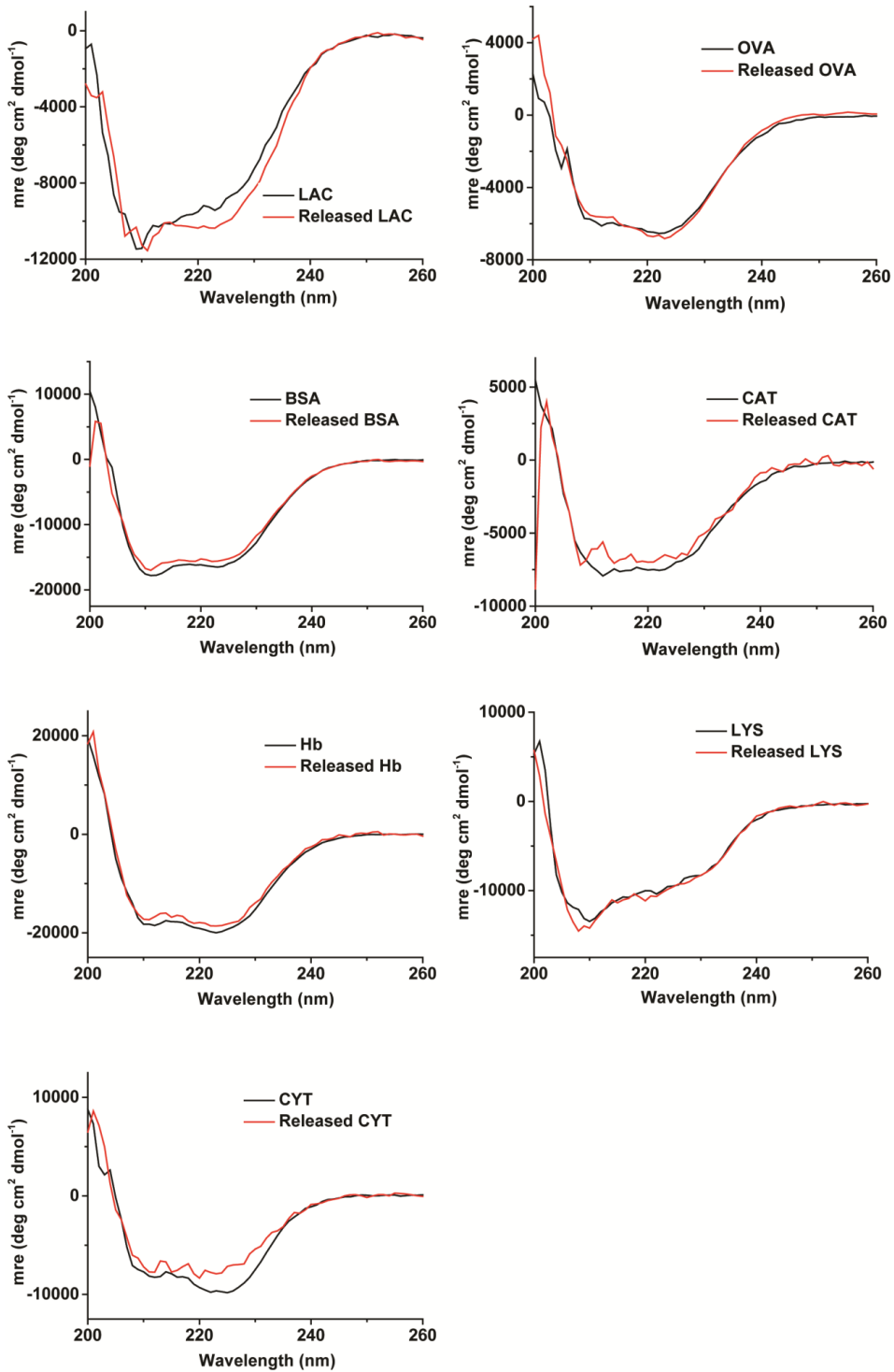


**Figure 2.S2** CD spectra of free proteins (black) and the released proteins from MSNs (or AEP-MSNs) (red) in PBS, pH 7.4, 25 °C. Concentration of non-encapsulated and encapsulated proteins were matched to provide accurate comparisons.

**Table 2.S1** Physical characteristics of MSNs and AEP-MSNs

Sample	BET surface area (m <sup>2</sup> /g)	Channel volume (cm <sup>3</sup> /g)	Channel diameter (nm) <sup>a</sup>
MSNs	506	1.01	10 ± 1
MSNs/CYT	263	0.56	7.5 ± 1.5
MSNs/Hb	275	0.58	7.5 ± 1.5
AEP-MSNs	318	0.71	9 ± 1
AEP-MSNs/LAC	203	0.42	6.5 ± 1.5
AEP-MSNs/CAT	223	0.46	6.5 ± 1.5

<sup>a</sup>Calculated from the desorption branch of the N<sub>2</sub> sorption isotherms based on the BJH method.

### 2.5 References

1. Z. Gu, A. Biswas, M. Zhao and Y. Tang, *Chem. Soc. Rev.*, **2011**, 40, 3638-3655.
2. B. Leader, Q. J. Baca and D. E. Golan, *Nat. Rev. Drug Discovery*, **2008**, 7, 21-39.
3. K. Epler, D. Padilla, G. Phillips, P. Crowder, R. Castillo, D. Wilkinson, B. Wilkinson, C. Burgard, R. Kalinich, J. Townson, B. Chackerian, C. Willman, D. Peabody, W. Wharton, C. J. Brinker, C. Ashley and E. Carnes, *Adv. Healthcare Mater.*, **2012**, 1, 348-353.
4. M. X. Zhao, B. L. Hu, Z. Gu, K. I. Joo, P. Wang and Y. Tang, *Nano Today*, **2013**, 8, 11-20.
5. D. Mahony, A. S. Cavallaro, F. Stahr, T. J. Mahony, S. Z. Qiao and N. Mitter, *Small*, **2013**, 9, 3138-3146.
6. D. D. Li, N. Kordalivand, M. F. Fransen, F. Ossendorp, K. Raemdonck, T. Vermonden, W. E. Hennink and C. F. van Nostrum, *Adv. Funct. Mater.*, **2015**, 25, 2993-3003.
7. F. P. Chang, Y. P. Chen and C. Y. Mou, *Small*, **2014**, 10, 4785-4795.
8. V. V. Shuvaev and V. R. Muzykantov, *J. Controlled Release*, **2011**, 153, 56-63.
9. M. Wang, J. A. Zuris, F. T. Meng, H. Rees, S. Sun, P. Deng, Y. Han, X. Gao, D. Pouli, Q. Wu, I. Georgakoudi, D. R. Liu and Q. B. Xu, *Proc. Natl. Acad. Sci. U. S. A.*, **2016**, 113, 2868-2873.
10. P. Ghosh, X. C. Yang, R. Arvizo, Z. J. Zhu, S. S. Agasti, Z. H. Mo and V. M. Rotello, *J. Am. Chem. Soc.*, **2010**, 132, 2642-2645.
11. T. Vermonden, R. Censi and W. E. Hennink, *Chem. Rev.*, **2012**, 112, 2853-2888.
12. D. Tarn, C. E. Ashley, M. Xue, E. C. Carnes, J. I. Zink and C. J. Brinker, *Acc. Chem. Res.*, **2013**, 46, 792-801.
13. C. Argyo, V. Weiss, C. Bräuchle and T. Bein, *Chem. Mater.*, **2014**, 26, 435-451.
14. C.-H. Lee, T.-S. Lin and C.-Y. Mou, *Nano Today*, **2009**, 4, 165-179.
15. P. Yang, S. Gai and J. Lin, *Chem. Soc. Rev.*, **2012**, 41, 3679-3698.
16. Y.-J. Han, G. D. Stucky and A. Butler, *J. Am. Chem. Soc.*, **1999**, 121, 9897-9898.
17. J. F. Diaz and K. J. Balkus, *J. Mol. Catal. B: Enzym.*, **1996**, 2, 115-126.
18. N. Z. Knezevic and J. O. Durand, *Chempluschem*, **2015**, 80, 26-36.
19. M. Ma, H. R. Chen, Y. Chen, K. Zhang, X. Wang, X. Z. Cui and J. L. Shi, *J. Mater. Chem.*, **2012**, 22, 5615-5621.
20. L. C. Sang, A. Vinu and M. O. Coppens, *Langmuir*, **2011**, 27, 13828-13837.
21. C. Xu, M. H. Yu, O. Noonan, J. Zhang, H. Song, H. W. Zhang, C. Lei, Y. T. Niu, X. D. Huang, Y. N. Yang and C. Z. Yu, *Small*, **2015**, 11, 5949-5955.
22. Y. P. Chen, C. T. Chen, Y. Hung, C. M. Chou, T. P. Liu, M. R. Liang, C. T. Chen and C. Y. Mou, *J. Am. Chem. Soc.*, **2013**, 135, 1516-1523.
23. K. T. Mody, A. Popat, D. Mahony, A. S. Cavallaro, C. Yu and N. Mitter, *Nanoscale*, **2013**, 5, 5167-5179.
24. Z. W. Cai, Z. M. Ye, X. W. Yang, Y. L. Chang, H. F. Wang, Y. F. Liu and A. N. Cao, *Nanoscale*, **2011**, 3, 1974-1976.
25. I. I. Slowing, J. L. Vivero-Escoto, C. W. Wu and V. S. Y. Lin, *Adv. Drug Delivery Rev.*, **2008**, 60, 1278-1288.
26. T. F. Martens, K. Remaut, J. Demeester, S. C. De Smedt and K. Braeckmans, *Nano Today*, **2014**, 9, 344-364.
27. K. Moller, J. Kobler and T. Bein, *Adv. Funct. Mater.*, **2007**, 17, 605-612.
28. Y. Han and J. Y. Ying, *Angew. Chem., Int. Ed.*, **2005**, 44, 288-292.
29. S. H. Wu, C. Y. Mou and H. P. Lin, *Chem. Soc. Rev.*, **2013**, 42, 3862-3875.
30. A. B. D. Nandiyanto, S.-G. Kim, F. Iskandar and K. Okuyama, *Microporous Mesoporous Mater.*, **2009**, 120, 447-453.
31. J. Sun, H. Zhang, R. Tian, D. Ma, X. Bao, D. S. Su and H. Zou, *Chem. Commun.*, **2006**, 1322-1324.
32. M. Hartmann, *Chem. Mater.*, **2005**, 17, 4577-4593.
33. A. Katiyar, L. Ji, P. G. Smirniotis and N. G. Pinto, *Microporous Mesoporous Mater.*, **2005**, 80, 311-320.
34. S. Hudson, J. Cooney and E. Magner, *Angew. Chem., Int. Ed.*, **2008**, 47, 8582-8594.
35. J. Fan, J. Lei, L. Wang, C. Yu, B. Tu and D. Zhao, *Chem. Commun.*, **2003**, 2140-2141.

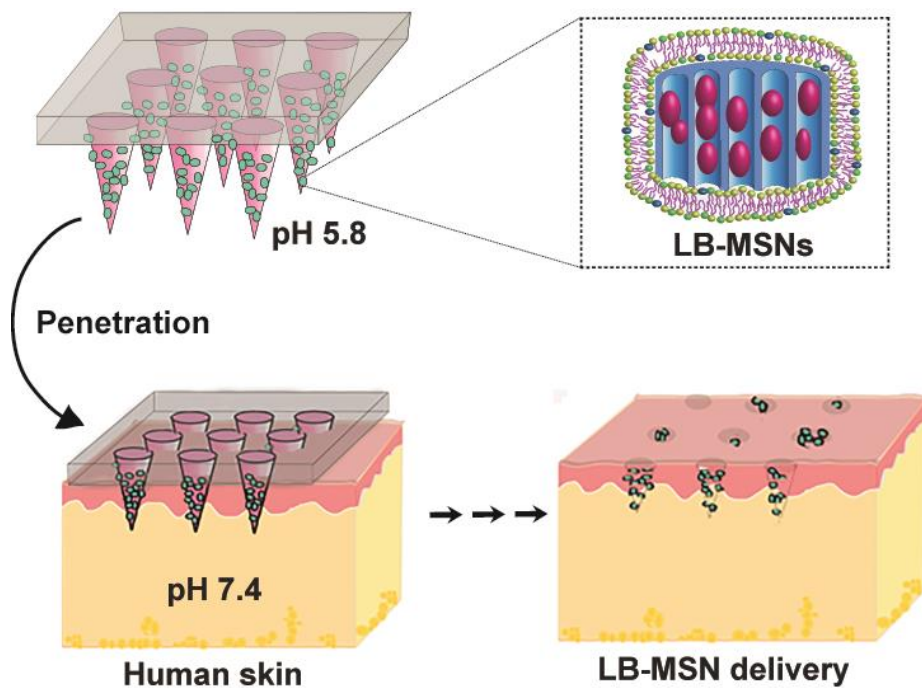


36. N. Z. Knezevic and J. O. Durand, *Nanoscale*, **2015**, 7, 2199-2209.
37. H. S. Shin, Y. K. Hwang and S. Huh, *ACS Appl. Mater. Interfaces*, **2014**, 6, 1740-1746.
38. F. Lu, S. H. Wu, Y. Hung and C. Y. Mou, *Small*, **2009**, 5, 1408-1413.
39. J. L. Vivero-Escoto, Slowing, II, B. G. Trewyn and V. S. Lin, *Small*, **2010**, 6, 1952-1967.
40. D. Y. Zhao, J. L. Feng, Q. S. Huo, N. Melosh, G. H. Fredrickson, B. F. Chmelka and G. D. Stucky, *Science*, **1998**, 279, 548-552.
41. Y. Han, D. F. Li, L. Zhao, J. W. Song, X. Y. Yang, N. Li, Y. Di, C. J. Li, S. Wu, X. Z. Xu, X. J. Meng, K. F. Lin and F. S. Xiao, *Angew. Chem., Int. Ed.*, **2003**, 42, 3633-3637.
42. Q. Y. Yu, J. F. Hui, P. P. Wang, B. Xu, J. Zhuang and X. Wang, *Nanoscale*, **2012**, 4, 7114-7120.
43. S. B. Hartono, N. T. Phuoc, M. H. Yu, Z. F. Jia, M. J. Monteiro, S. H. Qiao and C. Z. Yu, *J. Mater. Chem. B*, **2014**, 2, 718-726.
44. H. Zhang, J. M. Sun, D. Ma, X. H. Bao, A. Klein-Hoffmann, G. Weinberg, D. S. Su and R. Schlögl, *J. Am. Chem. Soc.*, **2004**, 126, 7440-7441.
45. A. Vinu, V. Murugesan, O. Tangermann and M. Hartmann, *Chem. Mater.*, **2004**, 16, 3056-3065.
46. Y. Wang and F. Caruso, *Chem. Commun.*, **2004**, 1528-1529.
47. Y. Urabe, T. Shiomi, T. Itoh, A. Kawai, T. Tsunoda, F. Mizukami and K. Sakaguchi, *Chembiochem*, **2007**, 8, 668-674.
48. Y. J. Wang and F. Caruso, *Chem. Mater.*, **2005**, 17, 953-961.
49. Y. Zhang, Z. Zhi, T. Jiang, J. Zhang, Z. Wang and S. Wang, *J. Controlled Release*, **2010**, 145, 257-263.
50. C. E. Ashley, E. C. Carnes, G. K. Phillips, D. Padilla, P. N. Durfee, P. A. Brown, T. N. Hanna, J. Liu, B. Phillips, M. B. Carter, N. J. Carroll, X. Jiang, D. R. Dunphy, C. L. Willman, D. N. Petsev, D. G. Evans, A. N. Parikh, B. Chackerian, W. Wharton, D. S. Peabody and C. J. Brinker, *Nat. Mater.*, **2011**, 10, 389-397.
51. W. Gao, B. Y. Sha, W. Zou, X. Liang, X. Z. Meng, H. Xu, J. Tang, D. C. Wu, L. X. Xu and H. Zhang, *Biomaterials*, **2011**, 32, 9425-9433.
52. E. P. J. Barrett, L. E.; HALENDA, P., *J. Am. Chem. Soc.*, **1951**, 73, 373-380.
53. I. I. Slowing, B. G. Trewyn and V. S. Y. Lin, *J. Am. Chem. Soc.*, **2007**, 129, 8845-8849.
54. C. T. Kresge, M. E. Leonowicz, W. J. Roth, J. C. Vartuli and J. S. Beck, *Nature*, **1992**, 359, 710-712.
55. S. Areva, C. Boissiere, D. Grosso, T. Asakawa, C. Sanchez and M. Linden, *Chem. Commun.*, **2004**, 1630-1631.
56. J. R. Matos, M. Kruk, L. P. Mercuri, M. Jaroniec, L. Zhao, T. Kamiyama, O. Terasaki, T. J. Pinnavaia and Y. Liu, *J. Am. Chem. Soc.*, **2003**, 125, 821-829.
57. D. H. Pan, P. Yuan, L. Z. Zhao, N. A. Liu, L. Zhou, G. F. Wei, J. Zhang, Y. C. Ling, Y. Fan, B. Y. Wei, H. Y. Liu, C. Z. Yu and X. J. Bao, *Chem. Mater.*, **2009**, 21, 5413-5425.
58. T. Ito, L. Sun, M. A. Bevan and R. M. Crooks, *Langmuir*, **2004**, 20, 6940-6945.
59. R. Schmidt, E. W. Hansen, M. Stocker, D. Akporiaye and O. H. Ellestad, *J. Am. Chem. Soc.*, **1995**, 117, 4049-4056.
60. L. Duan, X. H. Yan, A. H. Wang, Y. Jia and J. B. Li, *ACS Nano*, **2012**, 6, 6897-6904.
61. J. Mendez, M. Morales Cruz, Y. Delgado, C. M. Figueroa, E. A. Orellano, M. Morales, A. Monteagudo and K. Griebenow, *Mol. Pharmaceutics*, **2014**, 11, 102-111.
62. M. Hamborg, F. Rose, L. Jorgensen, K. Bjorklund, H. B. Pedersen, D. Christensen and C. Foged, *Biochim. Biophys. Acta*, **2014**, 1838, 2001-2010.
63. F. Meder, C. Brandes, L. Treccani and K. Rezwani, *Acta Biomater*, **2013**, 9, 5780-5787.
64. J. Ambati, A. M. Lopez, D. Cochran, P. Wattamwar, K. Bean, T. D. Dziubla and S. E. Rankin, *Acta Biomater.*, **2012**, 8, 2096-2103.
65. J. Wu, X. Li, Y. Yan, Y. Hu, Y. Zhang and Y. Tang, *J. Colloid Interface Sci.*, **2013**, 406, 130-138.
66. S. B. Hartono, S. Z. Qiao, K. Jack, B. P. Ladewig, Z. P. Hao and G. Q. Lu, *Langmuir*, **2009**, 25, 6413-6424.
67. R. Ravindra, Z. Shuang, H. Gies and R. Winter, *J. Am. Chem. Soc.*, **2004**, 126, 12224-12225.
68. E. Chiavazzo, M. Fasano, P. Asinari and P. Decuzzi, *Nat. Commun.*, **2014**, 5.



## Chapter III

### Mesoporous Silica Nanoparticle-Coated Microneedles for Intradermal Delivery of Ovalbumin



Jing Tu, Guangsheng Du, M. Reza Nejadnik, Juha Mönkäre, Koen van der Maaden, Paul H. H. Bomans, Nico A. J. M. Sommerdijk, Wim Jiskoot, Joke A. Bouwstra, and Alexander Kros

**Abstract**

Herein we report a new intradermal delivery system by coating pH-sensitive microneedles with antigen-loaded, lipid bilayer-covered MSNs. A novel type of ultrafine MSNs with large pores (~10 nm in diameter) was synthesized with a positive surface charge, resulting in efficient loading of ovalbumin (OVA) in the MSN pores (AEP-MSNs). A lipid bilayer (LB) was assembled at the MSN surface to enhance the colloidal stability (LB-MSNs). The designed LB-MSNs were coated onto pH-sensitive pyridine modified microneedles by electrostatic interactions between the modified silicon surface and the LB-MSNs at low ionic strength. The presence of LB-MSNs on the surface of pyridine modified microneedles was confirmed by both scanning electron microscopy (SEM) and confocal laser scanning microscope (CLSM). The delivery of LB-MSNs into *ex vivo* human skin was studied. This designed microneedle-mediated intradermal delivery system for mesoporous nanoparticles could be a promising tool to deliver a wide range of compounds into the skin. The method is not restricted to the delivery of antigens, but can also be used to deliver any compound that can be encapsulated in MSNs like (low-molecular-weight) drugs, RNA/DNA and proteins.

**Keywords:** Intradermal antigen delivery, lipid bilayer, mesoporous silica nanoparticles, pH-sensitive microneedles

### 3.1 Introduction

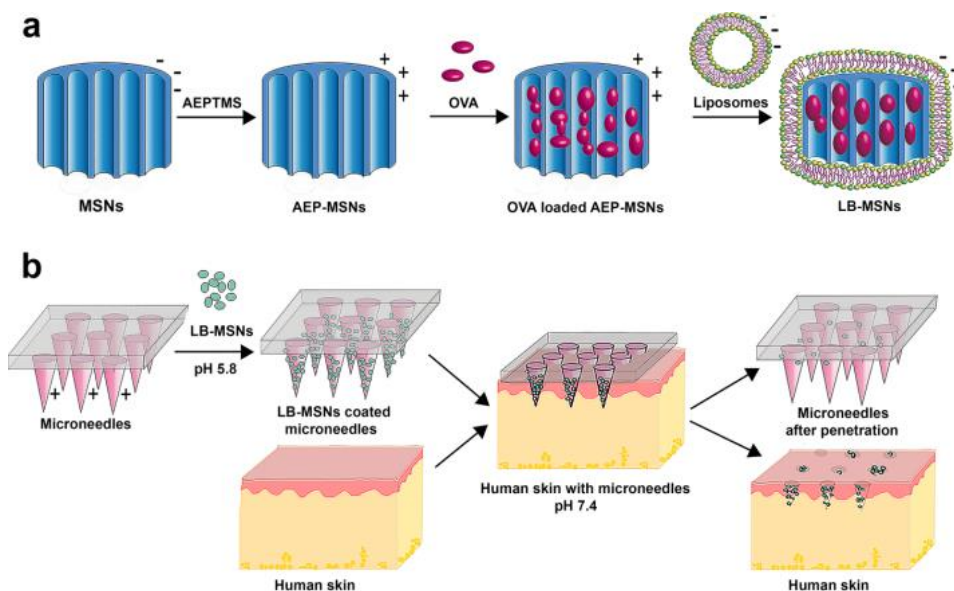
Vaccination is regarded as one of the most promising strategies for reducing mortality and improving human health.<sup>1,2</sup> Most of the current vaccines are delivered by intramuscular or subcutaneous injection, but the inherent limitations are obvious, such as the risk of the needle-related disease induced by reusing needles and syringes, the needle fear by children and patients, and the need for maintaining a proper cold chain during storage and transport.<sup>1,2</sup> Therefore, new needle-free, easy to use and effective vaccination methods are urgently needed. One of these potential methods is microneedle-mediated intradermal vaccination.<sup>3</sup>

Intradermal vaccination is attractive because the skin is easily accessible and the large number of immune cells inside the skin, such as dendritic cells (DCs), make the skin promising for vaccination.<sup>1,4-6</sup> Microneedles are micron-sized structures with a length of less than 1 mm which can be used to overcome the skin barrier located in the top layer of the skin. Microneedles enable minimally-invasive and potentially pain free delivery of vaccine into skin.<sup>5-8,9,10</sup> Previously, in our lab we designed pH-sensitive pyridine modified microneedles with a surface  $pK_a$  below physiological pH, which allows the adsorption of negatively-charged proteins at slightly acidic conditions (pH 5.8) and the release at neutral pH (pH 7.4). We studied the immunization of mice by using ovalbumin (OVA) coated pH-sensitive microneedles.<sup>8,11</sup> It was found that microneedle-mediated immunization led to comparable T-cell responses but lower IgG responses as conventional subcutaneous or intradermal immunization. Possible strategies to further improve the immunogenicity of vaccines by the intradermal route could be adding an adjuvant or using nanoparticles to deliver the antigens.<sup>2,8,12-17</sup>

To improve the uptake of antigens by DCs and elicit a more potent immune response, antigens can be formulated into nanoparticles.<sup>13,18</sup> The adjuvanticity of nanoparticles is attributed to their capability of protecting antigen from degradation, forming a depot at the site of injection, and facilitating antigen uptake by DCs.<sup>19</sup> A variety of nanosized vaccine delivery systems have been developed, such as polymeric nanoparticles,<sup>20</sup> emulsions,<sup>21</sup> and lipid-based nanoparticles.<sup>19,20,22</sup> Recently mesoporous silica nanoparticles (MSNs) have gained significant attention as drug delivery vehicles because of their large surface area and large pore volume for the loading of active small molecules or proteins, controlled size and mesostructure, and excellent *in vivo* biocompatibility.<sup>2,23-32</sup>

Herein, we report a new intradermal delivery system, which synergistically integrates the advantages of nanoparticles and microneedles, by coating pH-sensitive microneedles with

antigen-loaded, lipid bilayer-covered MSNs. OVA was used as model antigen that is negatively charged (pI of 4.9)<sup>33</sup> at pH 7.4. For the delivery of proteins, a novel type of ultrafine MSNs with large pores (~10 nm in diameter) was synthesized with a positive surface charge, resulting in efficient loading of OVA in the MSN pores (AEP-MSNs). To enhance the colloidal stability of OVA loaded AEP-MSNs, a lipid bilayer (LB) was assembled at the MSN surface and the lipid-coated MSNs are referred to as LB-MSNs.<sup>34-37</sup> This method synergistically combines features of liposomes and MSNs and has been reported to address the multiple challenges, like stability, targeting and multicomponent delivery.<sup>35-37</sup> The designed LB-MSNs were coated onto pH-sensitive pyridine modified microneedles by the electrostatic interactions between the modified silicon surface and the LB-MSNs at low ionic strength. Piercing the LB-MSNs coated microneedles into *ex vivo* human skin resulted in the successful release of the nanoparticles due to a shift in pH from 5.8 to 7.4 (Scheme 3.1).



**Scheme 3.1** Preparation and application of pH-sensitive microneedle arrays coated with LB-MSNs. (a) Encapsulation of OVA into AEP-MSNs, followed by fusion of liposomes (composed of DOPC/DOPS/cholesterol), resulting in LB-MSNs. (b) Adsorption of LB-MSNs onto pH-sensitive microneedles and penetration of microneedles into human skin, resulting in a pH shift and delivery of LB-MSNs into the viable epidermis and dermis.

## **3.2 Materials and Methods**

### *3.2.1 Materials*

Tetraethyl orthosilicate (TEOS), ethanol, acetone, methanol, isopropanol, sulfuric acid (96-98%), acetic acid, hydrochloric acid (36%-38%), (3-aminopropyl)triethoxysilane (APTES), 4-pyridinecarboxaldehyde, sodium cyanoborohydride, 3-[2-(2-aminoethylamino)ethylamino] propyltrimethoxysilane (AEPTMS), Ovalbumin (OVA), 1,3,5-trimethylbenzene (TMB), Pluronic P123 and cholesterol were purchased from Sigma-Aldrich. Fluorocarbon surfactant FC-4 was purchased from Yick-Vic Chemicals & Pharmaceuticals (HK) Ltd. 1,2-dioleoyl-sn-glycero-3-phosphocholine (DOPC), 1,2-dioleoyl-sn-glycero-3-[phosphor-L-serine](sodium salt) (DOPS), and 1,2-dioleoyl-sn-glycero-3-phosphoethanolamine-N-(lissamine rhodamine B sulfonyl) (ammonium salt) (DOPE-LR) were purchased from Avanti Polar Lipids Inc. Hydrogen peroxide (30%) and ethylenediaminetetraacetic acid (EDTA) were purchased from Fluka. Toluene was purchased from Biosolve. Alexa Fluor<sup>®</sup>488 ovalbumin conjugates (OVA-AF488) was purchased from Thermo Fisher Scientific. Sterile phosphate buffered saline (PBS, 163.9 mM Na<sup>+</sup>, 140.3 mM Cl<sup>-</sup>, 8.7 mM HPO<sub>4</sub><sup>2-</sup>, 1.8 mM H<sub>2</sub>PO<sub>4</sub><sup>-</sup>, pH 7.4) was obtained from Braun. All reagents were used without further purification. Milli-Q water (18.2 MΩ/cm, Millipore Co., USA) was used for the preparation of solutions. 1 mM phosphate buffer (PB) with a pH of 7.4 was prepared in the lab. Silicon microneedle arrays with 576 microneedles per array on a back plate of 5 × 5 mm<sup>2</sup> and a length of 200 μm per microneedle were kindly provided by Bosch.

### *3.2.2 Preparation of mesoporous silica nanoparticles (MSNs) with large ordered mesochannels*

MSNs were synthesized according to a published procedure<sup>38</sup> with modifications.<sup>39</sup> Briefly, surfactant Pluronic P123 (0.5 g) and FC-4 (1.4 g) were dissolved in HCl (80 mL, 0.02 M), followed by the introduction of TMB (0.48 mL). After stirring for 6 h, TEOS (2.14 mL) was added dropwise. The resulting mixture was stirred at 30 °C for 24 h and transferred to an autoclave at 120 °C for 2 days. Finally, the solid product was isolated by centrifugation, and washed with ethanol and Milli-Q water. The organic template was completely removed by calcination at 550 °C for 5 h.

### *3.2.3 Synthesis of amino-functionalized MSNs (AEP-MSNs)*

To prepare cationic MSNs, AEPTMS in absolute ethanol (4 mL, 20 wt%) was incubated with MSNs (100 mg) overnight at room temperature. The desired AEP-MSNs were collected by centrifugation and washed with ethanol to remove unreacted AEPTMS.

#### 3.2.4 Encapsulation of OVA in AEP-MSNs

To determine the encapsulation kinetics of OVA in AEP-MSNs, AEP-MSNs (0.5 mL, 2 mg/mL) and OVA (0.5 mL, 0.5 mg/mL) were mixed and incubated in Eppendorf mixer (400 rpm, 25 °C) for different time period (0, 0.5, 1, 2, 4, 8 and 24 h). After incubation, the suspensions were centrifuged and the encapsulation efficiency (EE%) of OVA was determined by measuring the difference in its intrinsic fluorescence intensity with a plate reader (Tecan M1000) (excitation wavelength = 280 nm and emission wavelength = 320 nm) in the supernatant before and after the encapsulation.

To determine the maximum loading capacity (LC%) of OVA in AEP-MSNs, AEP-MSNs (2 mg/mL) were mixed with different initial concentrations of OVA (ranging from 0.25, 0.5, 1, 1.5, 2 to 3 mg/mL) and incubated in an Eppendorf mixer (400 rpm, 25 °C) for 0.5 h. Next, the suspensions were centrifuged at 9000 g for 5 min. The EE% of OVA was determined by measuring the difference in their intrinsic fluorescence intensity in the supernatant before and after the encapsulation with a plate reader (Tecan M1000). The EE% and LC% were calculated as below:<sup>19, 40</sup>

$$EE \% = \frac{t_{ova} - f_{ova}}{t_{ova}} \times 100 \% \quad (3.1)$$

$$LC \% = \frac{t_{ova} - f_{ova}}{OVA \text{ loaded AEP-MSNs}} \times 100 \% \quad (3.2)$$

Where  $t_{ova}$  represents the total content of OVA, and  $f_{ova}$  is the content of free OVA (OVA in the supernatant).

#### 3.2.5 Preparation of liposomes

Liposomes were prepared by dispensing stock solutions of DOPC (70  $\mu$ l, 25 mg/mL), DOPS (20  $\mu$ l, 12.5 mg/mL) and cholesterol (10  $\mu$ l, 25 mg/mL) into scintillation vials. All lipids were dissolved in chloroform. A lipid film was created by slow evaporation of chloroform in the vial under a nitrogen flow and dried in vacuum overnight. The lipid film was rehydrated by the addition of PB (1 mL, 1 mM, pH 7.4) and the mixture was vortexed for 10 seconds to form a cloudy lipid suspension. The obtained suspension was sonicated in a water bath for 10 min. The resulting clear liposomes dispersions were stored at 4 °C. To



obtain fluorescent liposomes, a fluorescently labeled lipid (DOPE-LR) was incorporated into the liposomes by adding the lipids at 1 wt% DOPE-LR to make to the lipid solution prior to liposome formation.

### *3.2.6 Preparation of LB-MSNs*

To prepare LB-MSNs, OVA (0.5 mL, 0.25 mg/mL) solution in PB (1 mM, pH 7.4) was first transferred into a 2-mL Eppendorf tube, followed by the addition of AEP-MSNs suspension (0.5 mL, 1 mg/mL) and liposome solution (0.5 mL, 2 mg/mL). The resulting mixture was incubated in the Eppendorf mixer for 1.5 h (400 rpm, 25 °C). The particles were collected and excess liposomes and OVA were removed by centrifugation (9000 g, 5 min). The encapsulation of OVA was determined by measuring the difference in their intrinsic fluorescence intensity in the supernatant before and after the encapsulation on a Tecan M1000 plate reader. All experiments were performed in triplicate.

### *3.2.7 Characterization of MSNs, AEP-MSNs and LB-MSNs*

Transmission electron microscopy (TEM) images were collected by using a JEOL 1010 instrument with an accelerating voltage of 70 kV. Nitrogen adsorption-desorption isotherms were obtained with a Micromeritics TriStar II 3020 surface area analyzer. Before each measurement, MSNs were outgassed in the vacuum (below 0.15 mbar) at 300 °C for 16 h, while AEP-MSNs were outgassed at room temperature. The specific surface areas were calculated from the adsorption data in the low pressure range using the Brunauer-Emmett-Teller (BET) model.<sup>41</sup> The pore size distribution was determined following the Barrett-Joyner-Halenda (BJH) model.<sup>42</sup> The hydrodynamic size distribution and zeta-potential of the samples were measured with a Malvern Nano-zs instrument. Nanoparticle tracking analysis (NTA) measurement was performed by using a NanoSight LM20 (NanoSight, Amesbury, United Kingdom). The software used for capturing and analyzing the data was the NTA 2.0 Build 127. Thermogravimetric analysis (TGA) was conducted with a Perkin Elmer TGA7. All the samples were tested under an air atmosphere from 25 °C to 800 °C at a heating rate of 10 °C/min.

Sample vitrification for Cryo-TEM was carried out using an automated vitrification robot (FEI Vitrobot™ Mark III). Sample supports, type R2/2 Quantifoil Jena, were purchased from Quantifoil Micro Tools GmbH and contained a carbon support film on a copper grid. Prior to use the TEM grids were glow discharged by a Cressington 208 carbon coater to render them hydrophilic. Cryo-samples were prepared from a 3 µL droplet of sample solution placed on

the grid inside the Vitrobot™ chamber at 100% relative humidity and temperature of 20 °C, after which it was blotted to remove excess solution and subsequently plunged into liquid ethane for vitrification. Imaging performed using a FEI CryoTitan operating at 300 kV and equipped with a field emission gun (FEG) using low dose procedures.<sup>43</sup>

#### 3.2.8 OVA release studies from AEP-MSNs and LB-MSNs

To study the influence of ionic strength on the release of OVA from AEP-MSNs, Phosphate buffer (PB, 1 mM Na<sub>2</sub>HPO<sub>4</sub> and 1 mM NaH<sub>2</sub>PO<sub>4</sub> were mixed at molar ratio of 5:2, pH 7.4) with various concentrations of NaCl (0, 0.9, 1.8, 3.6, 7.2, 14.4 and 28.8%, m/v) were prepared. OVA loaded AEP-MSNs (1 mg, based on the mass of AEP-MSNs) were dispersed in one of the buffers (1 mL) mentioned above. The suspensions were kept in the Eppendorf mixer for 0.5 h (400 rpm, 37 °C) and followed by centrifugation (9000 g, 5 min) to collect the supernatant. The amount of released OVA in the buffer was quantified by measuring the intrinsic fluorescence intensity of OVA with a Tecan M1000 plate reader. The released OVA in PB with 0.9, 1.8 and 3.6% NaCl was also tested by high pressure size-exclusion chromatography (HP-SEC). Far-UV circular dichroism (CD) spectra of OVA before and after release were measured by using a Jasco J-815 spectropolarimeter. Spectra were collected from 260 – 190 nm, at 25 °C.

To compare the *in vitro* release of OVA from AEP-MSNs and LB-MSNs, OVA loaded AEP-MSNs and LB-MSNs were dispersed in PBS (pH 7.4) and incubated in the Eppendorf mixer (400 rpm, 37 °C). At various time points, the suspensions were centrifuged and the supernatants were replaced with fresh PBS. The amount of OVA released into the supernatant was determined by measuring the intrinsic fluorescence intensity of OVA on a Tecan M1000 plate reader.

#### 3.2.9 Modification of silicon microneedle arrays to obtain pH-sensitive surface

To coat negatively charged particles onto silicon microneedle arrays, the microneedles were chemically modified to obtain a pH sensitive surface (positively charged at pH 5.8) by using pyridine groups, as described previously.<sup>44</sup> The surface of silicon was first cleaned by acetone and methanol. Next the surfaces were hydroxylated by a fresh piranha mixture consisting of 30 % (v/v) H<sub>2</sub>O<sub>2</sub> and 70 % (v/v) H<sub>2</sub>SO<sub>4</sub>. Then the surface was incubated with 2 % (v/v) APTES in toluene overnight at room temperature to obtain the amine modified silicon surface.

The amine modified surface was modified with 4-pyridinecarboxaldehyde (100 mM) in anhydrous isopropanol with acetic acid (1%, v/v) at room temperature. The obtained imine bonds on pyridine-modified surface were reduced to a secondary amine by incubating in NaBH<sub>3</sub>CN (50 mM) in isopropanol for 2 h. Finally the modified surface was cleaned with isopropanol and methanol and dried in a vacuum oven at 50 °C for 0.5 h.

### *3.2.10 Coating of LB-MSNs on pH-sensitive microneedle arrays*

To determine the level of binding of LB-MSNs on the microneedle arrays, DOPE-LR was added to the lipids when the LB-MSNs were prepared. The top of the microneedle arrays was incubated with LB-MSNs (50 µl) with a concentration of 0.1, 0.5 and 1 mg/mL in EDTA buffer (1 mM, pH 5.8) for 2 h at room temperature. The microneedles were then washed with coating buffer (450 µl) and the solution was kept for measurement. The binding efficiency of LB-MSNs was determined by comparing the DOPE-LR concentration in the coating solution before and after coating by using a Tecan M1000 plate reader (Excitation wavelength = 575 nm and Emission wavelength = 590 nm). The structure, geometry and the surface morphology of the LB-MSNs coated pH-sensitive microneedle arrays were examined by scanning electron microscopy (SEM) in a FEI NOVA nanoSEM 200. The LB-MSNs coated on microneedle arrays were also visualized by Nikon D-Eclipse C1 confocal laser scanning microscope (CLSM) with a depth resolution of 5 µm/step, equipped with a 10 × Plan Apo objective. The x and y resolution was 2.5 µm. An argon laser (488 nm) was used to visualize OVA-AF488 with a 530/55 emission filter and a diode-pumped solid-state laser (561 nm) with a 590/55 emission filter was used to visualize DOPE-LR.

### *3.2.11 Delivery of LB-MSNs from microneedles into ex vivo human skin*

After coated with LB-MSNs, the pH-sensitive microneedles were pierced into abdomen human skin, which was used within 24 h after cosmetic surgery from a local hospital. The microneedles were applied into the skin by an impact-insertion applicator with a velocity of 54.8 cm/sec as described previously.<sup>8</sup> After 1 second, the applicator was removed and the microneedles were kept inside the skin for 30 min. Then the microneedles were removed and the skin was visualized by Nikon D-Eclipse C1 CLSM with a depth resolution of 5 µm/step, equipped with a 4 × Plan Apo objective. The x and y resolution was 6.3 µm. An argon laser (488 nm) was used to visualize OVA-AF488 with a 530/55 emission filter and a diode-pumped solid-state laser (561 nm) with a 590/55 emission filter was used to visualize DOPE-LR.

## 3.2.12 Statistical analysis

All data shown are mean corrected values  $\pm$  SD of at least three experiments.

## 3.3 Results and discussion

For the efficient dermal delivery of proteins, nanoparticles are required that are small (diameter < 200 nm) and with large pores (inner diameter > 5 nm) in order to encapsulate large amounts of proteins. Most nanosized mesoporous silica nanoparticles do not fit these criteria and only recently some examples have emerged, mainly for the delivery of DNA/RNA.<sup>35, 45-50</sup> Therefore we synthesized a new type of large pore MSNs in order to encapsulate proteins with high efficiency. The MSNs were synthesized from the silica precursor tetraethoxy silane (TEOS) by using a mixture of a nonionic triblock copolymer (Pluronic P-123) and the cationic fluorocarbon surfactant (FC-4) as organic templates. Furthermore the swelling agent 1,3,5-trimethylbenzene (TMB) was added to induce the formation of large-pore MSNs.<sup>38</sup> The obtained pristine MSNs were modified with 3-[2-(2-aminoethylamino)ethylamino] propyltrimethoxysilane (AEPTMS) in order to create a positively charged surface (AEP-MSNs). Inspection with transmission electron microscopy (TEM) revealed that the prepared negatively charged MSNs were rectangular in shape with mesochannels along the short axis (Figure 3.1a). Modification with AEPTMS did not alter the morphology and mesostructure (Figure 3.1b), as compared to pristine MSNs. Furthermore, characterization with N<sub>2</sub> adsorption-desorption isotherms of both MSNs and AEP-MSNs showed that these nanoparticles have typical IV isotherms according to International Union of Pure and Applied Chemistry (IUPAC) classification (Figure 3.1c).<sup>51</sup> The existence of channel-type of mesopores was confirmed by the observed existence of a type-H<sub>1</sub> hysteresis loop (Figure 3.1c).<sup>52</sup> The values for Brunauer-Emmett-Teller (BET) specific surface area ( $S_{\text{BET}}$ ), the total pore volume ( $V_t$ ), Barrett-Joyner-Halenda (BJH) pore diameter ( $W_{\text{BJH}}$ ) and surface charge of MSNs and AEP-MSNs are summarized in Table 3.1.

**Table 3.1** Physical characteristics of MSNs and AEP-MSNs

Sample	BET surface area (m <sup>2</sup> /g)	Pore volume (cm <sup>3</sup> /g)	Pore diameter (nm) <sup>a</sup>	Zeta-potential (mV) <sup>b</sup>
MSNs	506	1.01	10 $\pm$ 1	-27.8 $\pm$ 0.4
AEP-MSNs	318	0.71	9 $\pm$ 1	10.9 $\pm$ 0.5

<sup>a</sup>Calculated from desorption branch of the N<sub>2</sub> sorption isotherms based on the BJH method.

<sup>b</sup>Zeta-potential was measured in 1 mM PB at pH 7.4.

It can be seen that after modification with AEPTMS,  $S_{\text{BET}}$ ,  $V_t$  and  $W_{\text{BJH}}$  were slightly reduced because of the attachment of the functionalized silanes on the pore surface. The pore diameter of the AEP-MSNs was 1-2 nm smaller than that of MSNs (Figure 3.1c inset), but still sufficiently large to accommodate OVA ( $4 \times 5 \times 7$  nm).<sup>33</sup> Dynamic light scattering (DLS) measurements showed that the hydrodynamic diameter of MSNs and AEP-MSNs was  $146.3 \pm 0.3$  nm and  $213.7 \pm 0.8$  nm with a low polydispersity index (PDI), respectively (Figure 3.1d). The observed increase in Z-average size for AEP-MSNs may be attributed to some particle aggregation, which is probably due to the decreased charge repulsion among AEP-MSNs compared to MSNs (Table 3.1).

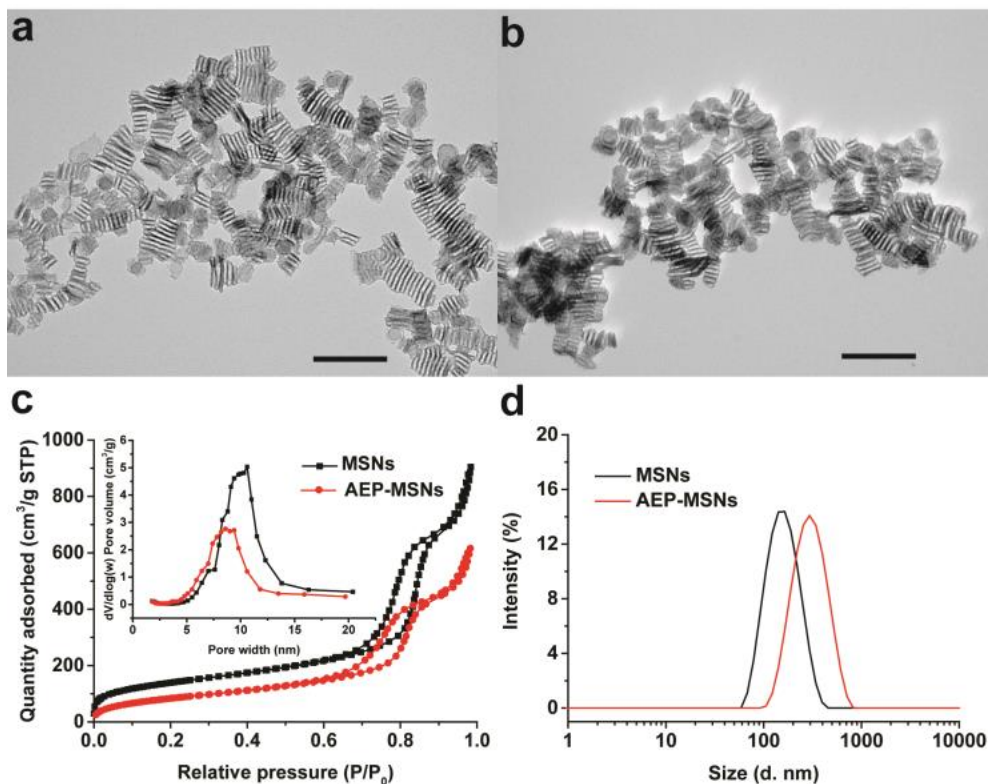


**Figure 3.1** Characterization of the MSNs and AEP-MSNs. TEM images of (a) MSNs and (b) AEP-MSNs. Scale bar = 200 nm. (c) Nitrogen adsorption-desorption isotherms and plots of pore diameter vs. pore volume (inset), calculated from the desorption isotherms using BJH model, show that the MSNs and AEP-MSNs have an average pore diameter of 10 nm and 9 nm, respectively. (d) Hydrodynamic diameter of MSNs and AEP-MSNs according to DLS.

The percentage of graft amine-containing groups on the surface of AEP-MSNs was 6.9%, as determined by thermogravimetric analysis (TGA, see Figure 3.2a). The encapsulation efficiency (EE%), defined as the percentage of the protein OVA which is adsorbed in the MSNs or AEP-MSNs was determined as a function of incubation time (Figure 3.2b). This study revealed that the OVA encapsulation within AEP-MSNs was very efficient, as  $94.83 \pm 0.38\%$  (mean  $\pm$  SD,  $n = 3$ ) of the protein was encapsulated in the AEP-MSNs. Furthermore, equilibrium of OVA encapsulation was reached in less than 5 min. In comparison, only  $11.70 \pm 2.23\%$  (mean  $\pm$  SD,  $n = 3$ ) of OVA was encapsulated in negatively charged MSNs after 24 h. The loading capacity (LC%) of OVA was calculated from the amount of OVA encapsulated in AEP-MSNs and expressed as the percentage of the total weight of OVA loaded AEP-MSNs. The LC% of OVA in AEP-MSNs was dependent on the initial concentration of OVA (Figure 3.2c). The maximum LC% was about  $33.94 \pm 3.64\%$  (mean  $\pm$  SD,  $n = 3$ ) by increasing the initial concentration of OVA, indicating a diffusion-driven encapsulation process.<sup>53</sup>

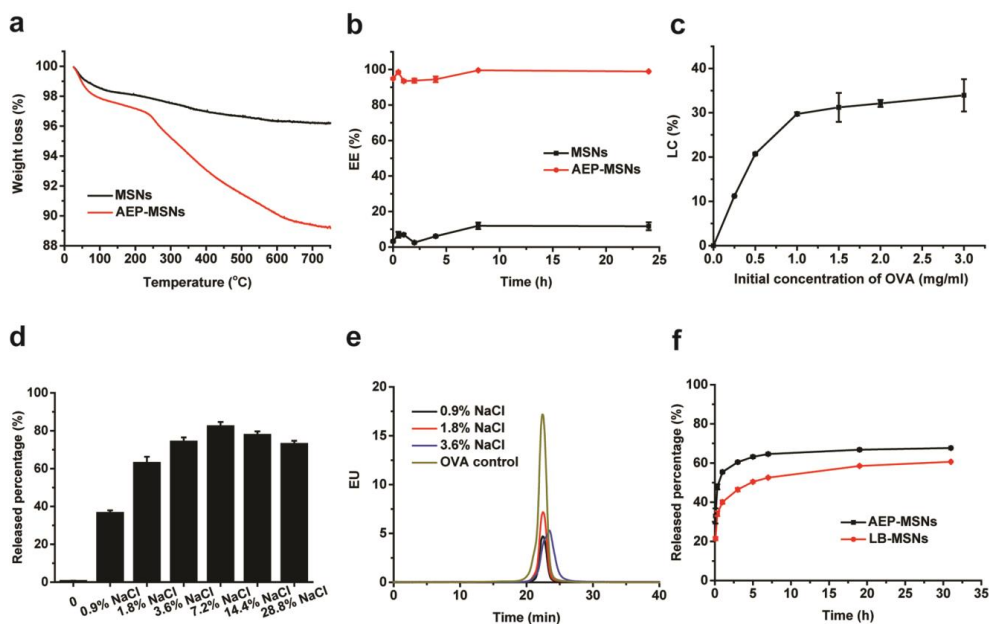


**Figure 3.2** (a) Thermogravimetric analysis (TGA) curves of MSNs and AEP-MSNs. (b) Encapsulation kinetics of OVA into MSNs and AEP-MSNs, concentration of OVA is 0.5 mg/mL and MSNs (AEP-MSNs) is 2 mg/mL. (c) Loading capacity (LC%) of OVA into AEP-MSNs at different initial concentration of OVA. (d) Influence of ionic strength on OVA release

from AEP-MSNs. (e) HP-SEC chromatograms of the released OVA from AEP-MSNs. (f) OVA release profiles of OVA from AEP-MSNs and LB-MSNs in PBS (pH 7.4).

To examine the influence of ionic strength of the medium on the release profile of OVA from the AEP-MSNs, the concentration of NaCl in the buffer was varied. The release percentage of OVA (defined as the percentage of OVA released from total encapsulated OVA in AEP-MSNs) increased from  $0.64 \pm 0.16\%$  (mean  $\pm$  SD,  $n=3$ ) in NaCl-free buffer to  $82.40 \pm 1.84\%$  (mean  $\pm$  SD,  $n = 3$ ) in the buffer containing 7.2% NaCl (Figure 3.2d). These results demonstrate that the ionic strength of the medium plays an important role in the release of OVA, indicating that the interaction between OVA and AEP-MSNs is mainly of electrostatic nature. The structural integrity of the released OVA was examined by high pressure size-exclusion chromatography (HP-SEC), showing that the released OVA was mainly monomeric (Figure 3.2e), and far-UV circular dichroism (CD) spectroscopy, indicating that the secondary structure of released protein was similar to that of native OVA (Figure 3.S1). These results strongly indicate that encapsulation and release have no adverse effect on the protein structure.

The OVA-loaded AEP-MSNs had the tendency to precipitate and to form large aggregates, probably due to the decreased surface charge upon protein encapsulation ( $-8.1 \pm 1.3$  mV, mean  $\pm$  SD,  $n = 3$ ). In order to increase the colloidal stability, the OVA-loaded AEP-MSNs were therefore stabilized with a lipid bilayer composed of 1,2-dioleoyl-*sn*-glycero-3-phosphocholine (DOPC), 1,2-dioleoyl-*sn*-glycero-3-phospho-L-serine (DOPS) and cholesterol. For this, liposomes and OVA-loaded AEP-MSNs were mixed and equilibrated for 1.5 h and afterwards the excess of lipids was removed by centrifugation. The encapsulation efficiency of OVA in the resulting lipid coated AEP-MSNs (LB-MSNs) was determined to be  $73.83 \pm 0.74\%$ , as compared to  $98.88 \pm 0.52\%$  without lipid (mean  $\pm$  SD,  $n = 3$ ). The obtained LB-MSNs were characterized by dynamic light scattering (DLS), nanoparticle tracking analysis (NTA) and TEM. The mean number-based hydrodynamic diameter ( $176 \pm 11$  nm, mean  $\pm$  SD,  $n = 3$ ) measured by NTA (Figure 3.S2) was close to the Z-average hydrodynamic diameter ( $190.7 \pm 2.7$  nm; PDI =  $0.125 \pm 0.029$ ; mean  $\pm$  SD,  $n = 3$ ) found by DLS (Figure 3.3a). The existence of a lipid layer surrounding the AEP-MSNs was confirmed by cryoTEM (Figure 3.3b,c). The colloidal stability of the formulation was examined by measuring the hydrodynamic diameter and zeta-potential of LB-MSNs for one week (Figure 3.S3). LB-MSNs showed only slight changes in diameter and zeta-potential revealing that the lipid bilayer strongly enhances the colloidal stability. The release of OVA from AEP-MSNs and LB-MSNs was examined in PBS (pH 7.4) for 32 h (Figure 3.2f). The burst release of OVA

from LB-MSNs was less as compared to AEP-MSNs, indicating that the lipid bilayer acts as a barrier retaining the OVA longer inside the AEP-MSNs.

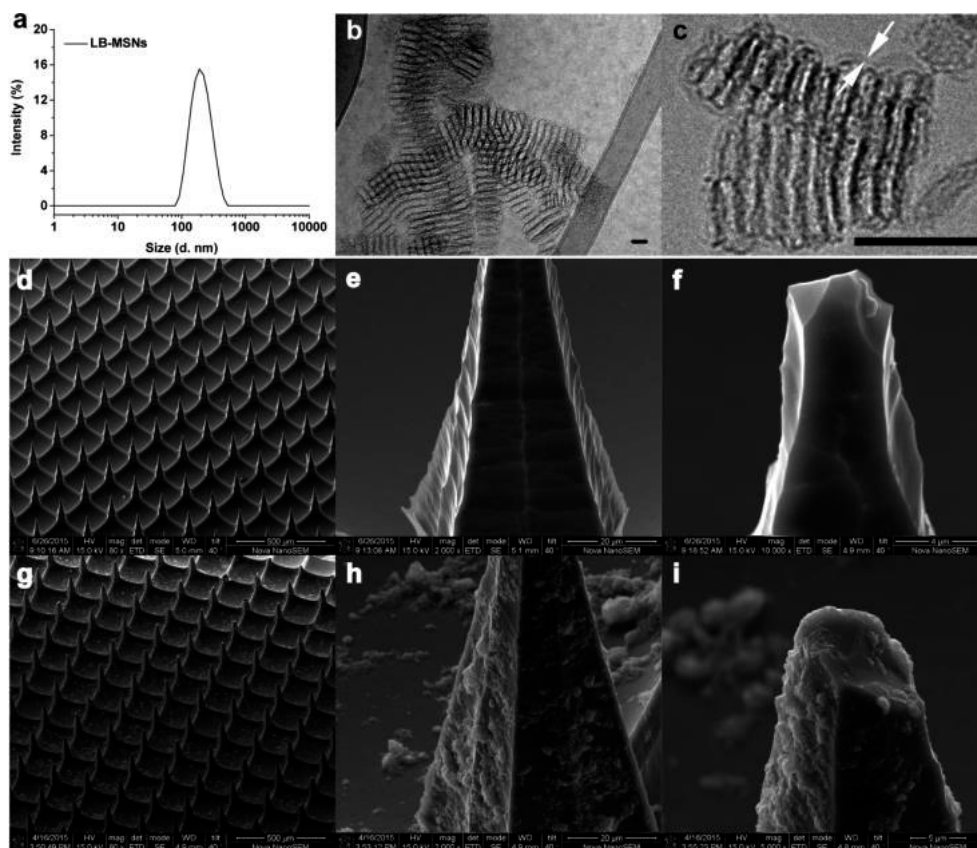


**Figure 3.3** (a) Hydrodynamic diameter of LB-MSNs determined by DLS. (b) Cryogenic TEM image of LB-MSNs, scale bar = 20 nm, (c) revealing a lipid bilayer thickness of  $\sim 4$  nm, scale bar = 100 nm. (d-f) SEM images of pyridine-modified microneedle arrays before the adsorption of LB-MSNs with different magnifications (d: 80  $\times$ ; e: 2000  $\times$ ; f: 5000  $\times$ ). (g-i) SEM images of pyridine-modified microneedle arrays after the adsorption of LB-MSNs with different magnifications (g: 80  $\times$ ; h: 2000  $\times$ ; i: 5000  $\times$ ).

Next, we investigated whether the LB-MSNs could be adsorbed to a silicon microneedle array via physical adsorption. First, the pH-sensitive pyridine-modified microneedle arrays were prepared as described previously.<sup>8</sup> LB-MSNs were coated onto these microneedle arrays at pH 5.8 in an ethylenediaminetetraacetic acid (EDTA) buffer (1 mM). At this pH more than 90% of the pyridine groups are positively charged.<sup>8</sup> Combined with the low ionic strength of the buffer, this allows for the binding of the negatively charged LB-MSNs via electrostatic



interactions. To determine the optimal concentration of LB-MSNs for the coating process, the nanoparticle concentration was varied in the buffered coating solution. Increasing the LB-MSN concentration resulted in increased amounts of LB-MSNs coated onto the microneedle array surfaces. However, the coating efficiency is reduced (Table 3.2). The lowest coating efficiency obtained was  $15.82 \pm 2.67$  % (mean  $\pm$  SD,  $n = 3$ ), corresponding to  $7.91 \pm 1.34$   $\mu\text{g}$  (mean  $\pm$  SD,  $n = 3$ ) and  $1.45 \pm 0.24$   $\mu\text{g}$  (mean  $\pm$  SD,  $n = 3$ ) of LB-MSNs and OVA, respectively coated on the microneedles. Considering the surface area of the microneedles accounts for 40% of the total surface area of microneedle arrays,  $3.16 \pm 0.54$   $\mu\text{g}$  (mean  $\pm$  SD,  $n = 3$ ) of nanoparticles and  $0.58 \pm 0.10$   $\mu\text{g}$  (mean  $\pm$  SD,  $n = 3$ ) of OVA were coated onto the microneedle surface of one array.

**Table 3.2** Coating amount of LB-MSNs and OVA on microneedle arrays

Amount of LB-MSNs <sup>a</sup> ( $\mu\text{g}$ )	Coated LB-MSNs ( $\mu\text{g}$ )	Coated OVA <sup>b</sup> ( $\mu\text{g}$ )	Coating efficiency (%)
5	$1.33 \pm 0.18$	$0.24 \pm 0.03$	$26.58 \pm 2.91$
25	$5.39 \pm 1.70$	$0.99 \pm 0.31$	$21.56 \pm 6.79$
50	$7.91 \pm 1.34$	$1.45 \pm 0.24$	$15.82 \pm 2.67$

<sup>a</sup>The amount of LB-MSNs in coating solution; <sup>b</sup>The amount of coated OVA was calculated from the loading capacity of OVA and the coating amount of LB-MSNs. All the coating amounts are expressed as the amount of AEP-MSNs and are based on one microneedle array which contains 576 needles per array. All the results are based on 3 independent microneedle arrays.

Scanning electron microscopy (SEM) imaging was used to visualize the presence of the LB-MSNs on the pyridine modified microneedle arrays (Figure 3.3d-i). Compared to untreated pyridine-modified arrays (Figure 3.3d-f), a high number of nanoparticles were observed on the surface of the microneedles (Figure 3.3g-i) after coating with LB-MSNs. To determine whether the OVA and nanoparticles colocalized on the microneedles, the LB-MSNs coated microneedles were visualized by confocal laser scanning microscopy (CLSM). For this experiment, we used Alexa Fluor<sup>®</sup>488 labeled ovalbumin (OVA-AF488) and 1,2-dioleoyl-sn-glycero-3-phosphoethanolamine-N-(lissamine rhodamine B sulfonyl) (ammonium salt) (DOPE-LR) enabling the visualization of both the protein and lipids. Imaging revealed that the fluorescent labels were both located at the microneedle surfaces indicative of the integrity of the LB-MSNs upon physical adsorption (Figure 3.4a-c). This showed us that LB-MSNs could be immobilized onto microneedles via electrostatic interaction.

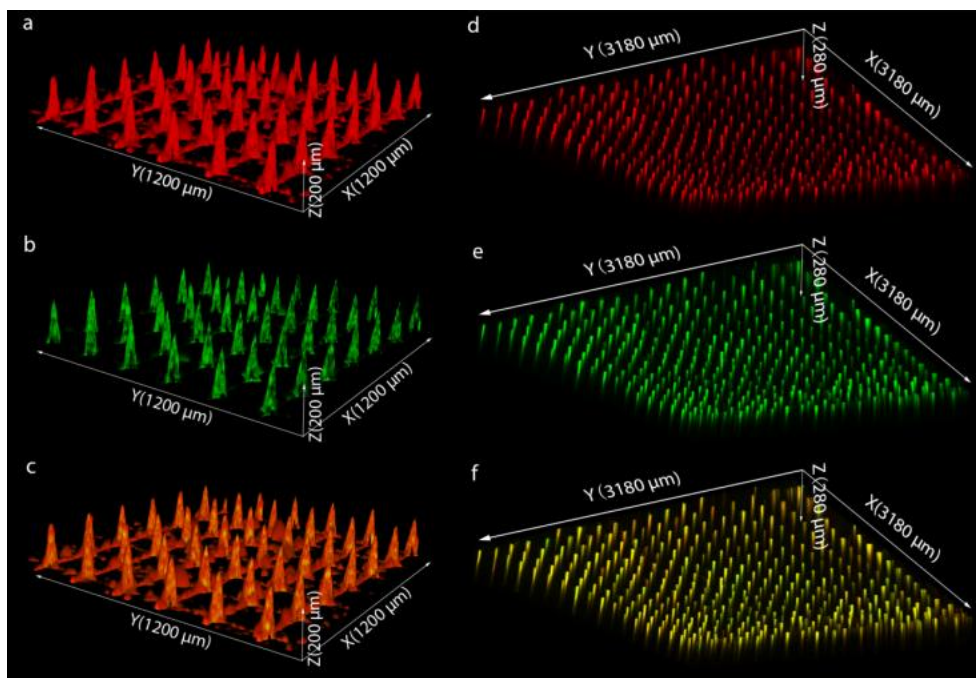


**Figure 3.4** Confocal laser scanning microscopy (CLSM) images of LB-MSN coated microneedles (a-c). Red: DOPE-LR (a); Green: OVA-AF488 (b); Merged (c). The x and y arrows show that the scanning area is  $1200\ \mu\text{m} \times 1200\ \mu\text{m}$  large. The z arrow indicates the scanning depth of  $200\ \mu\text{m}$ . CLSM images after removal of the LB-MSN coated microneedle arrays (d-f). Red: DOPE-LR (d); Green: OVA-AF488 (e); Merged (f). The x and y arrows show that the scanning area is  $3180\ \mu\text{m} \times 3180\ \mu\text{m}$  large. The z arrow indicates the scanning depth of  $280\ \mu\text{m}$ .

Next, the delivery of LB-MSNs from the surface of microneedles into the skin was studied. For this, the nanoparticle-coated microneedle arrays were applied onto human skin *ex vivo* for 30 min and subsequently withdrawn. Next the intradermal delivery was studied, colocalization of the fluorescence from both OVA-AF488 and DOPE-LR was observed inside the skin (Figure 3.4d-f), illustrating that the microneedles penetrated into the skin and successfully delivered the LB-MSNs.

### **3.4 Conclusion**

LB-MSNs based nanoparticles with large (10 nm) pores represent a novel biocompatible carrier for dermal antigen delivery. The large pores enabled the rapid encapsulation of OVA with a high loading capacity. The introduction of lipid bilayers significantly improved the colloidal stability of OVA loaded AEP-MSNs and concomitantly reduced the premature release of OVA. In addition, it enabled the coating of the nanoparticles on the surface of pH-sensitive microneedle arrays. Application of LB-MSNs coated microneedle arrays into human skin (*ex vivo*) resulted in the successful delivery of the OVA loaded nanoparticles into the skin. This is the first example of a microneedle-mediated intradermal delivery system for mesoporous nanoparticles, which could be a promising tool to deliver a wide range of compounds into the skin. The method is not restricted to the delivery of antigens, but can also be used to deliver any compound that can be encapsulated in MSNs like (low-molecular-weight) drugs, RNA/DNA and proteins.<sup>54, 55</sup>

Supporting Information

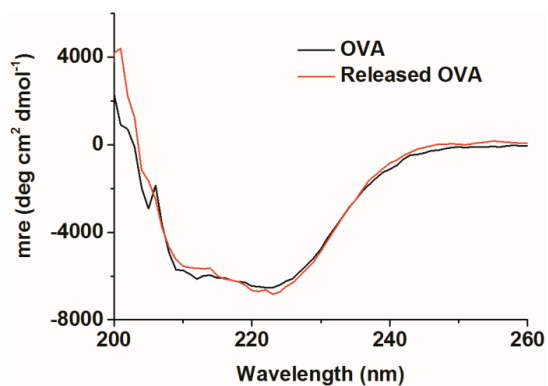


**Figure 3.S1** Far-UV CD spectra of free OVA and OVA released from AEP-MSNs in PBS, pH 7.4, 25 °C.

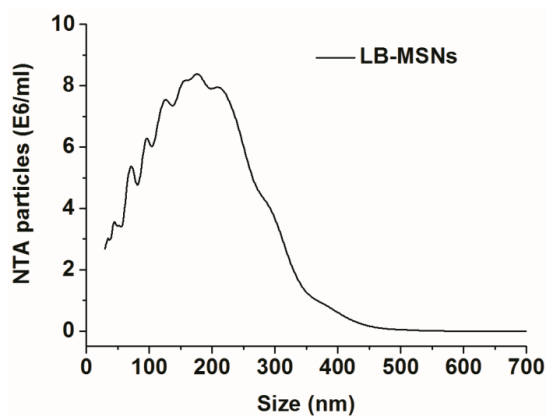


**Figure 3.S2** Size distribution of the LB-MSNs determined by nanoparticle tracking analysis (NTA).

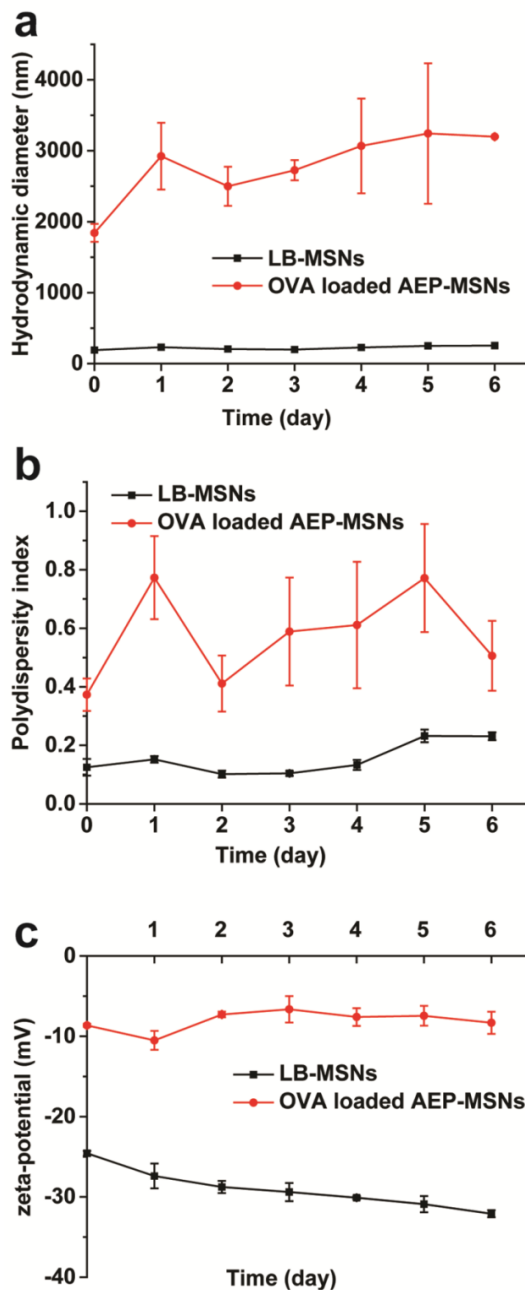


**Figure 3.S3** Colloidal stability of LB-MSNs (black curve) and OVA loaded AEP-MSNs (red curve) as a function of time, measured in 1 mM PB, pH 7.4. (a) Hydrodynamic diameter and (b) polydispersity index (PDI), both determined by DLS (the results of OVA loaded AEP-MSNs do not meet quality criteria), and (c) zeta-potential, determined by laser Doppler electrophoresis.



### 3.5 References

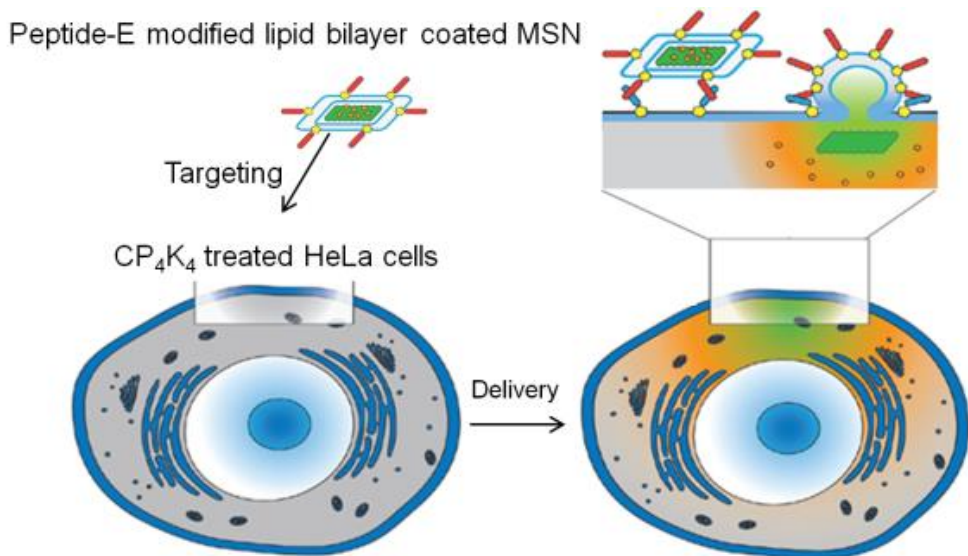
1. Y. B. Deng, R. Mathaes, G. Winter and J. Engert, *Eur. J. Pharm. Sci.*, **2014**, 63, 154-166.
2. K. T. Mody, A. Popat, D. Mahony, A. S. Cavallaro, C. Yu and N. Mitter, *Nanoscale*, **2013**, 5, 5167-5179.
3. C. Wang, Y. Ye, G. M. Hochu, H. Sadeghifar and Z. Gu, *Nano Lett.*, **2016**, 16, 2334-2340.
4. K. van der Maaden, W. Jiskoot and J. Bouwstra, *J. Controlled Release*, **2012**, 161, 645-655.
5. K. van der Maaden, E. Sekerdag, W. Jiskoot and J. Bouwstra, *AAPS J.*, **2014**, 16, 681-684.
6. P. C. Demuth, W. F. Garcia-Beltran, M. L. Ai-Ling, P. T. Hammond and D. J. Irvine, *Adv. Funct. Mater.*, **2013**, 23, 161-172.
7. S. M. Bal, B. Slutter, E. van Riet, A. C. Kruithof, Z. Ding, G. F. A. Kersten, W. Jiskoot and J. A. Bouwstra, *J. Controlled Release*, **2010**, 142, 374-383.
8. K. van der Maaden, H. Yu, K. Sliedregt, R. Zwier, R. Lebox, M. Oguri, A. Kros, W. Jiskoot and J. A. Bouwstra, *J. Mater. Chem. B*, **2013**, 1, 4466-4477.
9. S. H. Lee, H. H. Lee and S. S. Choi, *Korean J. Chem. Eng.*, **2011**, 28, 1913-1917.
10. X. Wang, N. Wang, N. Li, Y. Zhen and T. Wang, *Hum. Vaccines Immunother.*, **2016**, 1-15.
11. K. van der Maaden, K. Sliedregt, A. Kros, W. Jiskoot and J. Bouwstra, *Langmuir*, **2012**, 28, 3403-3411.
12. W. Zhang, J. Gao, Q. G. Zhu, M. Zhang, X. Y. Ding, X. Y. Wang, X. M. Hou, W. Fan, B. Y. Ding, X. Wu, X. Y. Wang and S. Gao, *Int. J. Pharm.*, **2010**, 402, 205-212.
13. P. C. DeMuth, X. F. Su, R. E. Samuel, P. T. Hammond and D. J. Irvine, *Adv. Mater.*, **2010**, 22, 4851-4856.
14. S. A. Coulman, A. Anstey, C. Gateley, A. Morrissey, P. McLoughlin, C. Allender and J. C. Birchall, *Int. J. Pharm.*, **2009**, 366, 190-200.
15. M. Zaric, O. Lyubomska, C. Poux, M. L. Hanna, M. T. McCrudden, B. Malissen, R. J. Ingram, U. F. Power, C. J. Scott, R. F. Donnelly and A. Kissenpfennig, *J. Invest. Dermatol.*, **2015**, 135, 425-434.
16. L. Guo, J. Chen, Y. Qiu, S. Zhang, B. Xu and Y. Gao, *Int. J. Pharm.*, **2013**, 447, 22-30.
17. M. Zaric, O. Lyubomska, O. Touzelet, C. Poux, S. Al-Zahrani, F. Fay, L. Wallace, D. Terhorst, B. Malissen, S. Henri, U. F. Power, C. J. Scott, R. F. Donnelly and A. Kissenpfennig, *ACS Nano*, **2013**, 7, 2042-2055.
18. P. C. DeMuth, J. J. Moon, H. Suh, P. T. Hammond and D. J. Irvine, *ACS Nano*, **2012**, 6, 8041-8051.
19. Y. Zhuang, Y. Ma, C. Wang, L. Hai, C. Yan, Y. Zhang, F. Liu and L. Cai, *J. Controlled Release*, **2012**, 159, 135-142.
20. R. De Rose, A. N. Zelikin, A. P. R. Johnston, A. Sexton, S. F. Chong, C. Cortez, W. Mulholland, F. Caruso and S. J. Kent, *Adv. Mater.*, **2008**, 20, 4698-4703.
21. J. C. Aguilar and E. G. Rodriguez, *Vaccine*, **2007**, 25, 3752-3762.
22. R. A. Rosalia, L. J. Cruz, S. van Duikeren, A. T. Tromp, A. L. Silva, W. Jiskoot, T. de Gruijl, C. Lowik, J. Oostendorp, S. H. van der Burg and F. Ossendorp, *Biomaterials*, **2015**, 40, 88-97.
23. D. Mahony, A. S. Cavallaro, F. Stahr, T. J. Mahony, S. Z. Qiao and N. Mitter, *Small*, **2013**, 9, 3138-3146.
24. A. A. Hwang, J. Lu, F. Tamanoi and J. I. Zink, *Small*, **2015**, 11, 319-328.
25. F. Porta, G. E. M. Lamers, J. Morrhayim, A. Chatzopoulou, M. Schaaf, H. den Dulk, C. Backendorf, J. I. Zink and A. Kros, *Adv. Healthcare Mater.*, **2013**, 2, 281-286.
26. H. Meng, M. Xue, T. Xia, Z. X. Ji, D. Y. Tarn, J. I. Zink and A. E. Nel, *ACS Nano*, **2011**, 5, 4131-4144.
27. S. H. van Rijt, D. A. Bölükbas, C. Argyo, S. Datz, M. Lindner, O. Eickelberg, M. Königshoff, T. Bein and S. Meiners, *ACS Nano*, **2015**, 9, 2377-2389.
28. C. Argyo, V. Weiss, C. Bräuchle and T. Bein, *Chem. Mater.*, **2014**, 26, 435-451.
29. E. Aznar, M. Oroval, L. Pascual, J. R. Murguia, R. Martinez-Manez and F. Sancenon, *Chem. Rev.*, **2016**, 116, 561-718.
30. H. Meng, Y. Zhao, J. Y. Dong, M. Xue, Y. S. Lin, Z. X. Ji, W. X. Mai, H. Y. Zhang, C. H. Chang, C. J. Brinker, J. I. Zink and A. E. Nel, *ACS Nano*, **2013**, 7, 10048-10065.

31. F. Sharif, F. Porta, A. H. Meijer, A. Kros and M. K. Richardson, *Int. J. Nanomed.*, **2012**, 7, 1875-1890.
32. J. Tu, T. Wang, W. Shi, G. Wu, X. Tian, Y. Wang, D. Ge and L. Ren, *Biomaterials*, **2012**, 33, 7903-7914.
33. S. Hudson, J. Cooney and E. Magner, *Angew. Chem., Int. Ed.*, **2008**, 47, 8582-8594.
34. E. C. Dengler, J. W. Liu, A. Kerwin, S. Torres, C. M. Olcott, B. N. Bowman, L. Armijo, K. Gentry, J. Wilkerson, J. Wallace, X. M. Jiang, E. C. Carnes, C. J. Brinker and E. D. Milligan, *J. Controlled Release*, **2013**, 168, 209-224.
35. K. Epler, D. Padilla, G. Phillips, P. Crowder, R. Castillo, D. Wilkinson, B. Wilkinson, C. Burgard, R. Kalinich, J. Townson, B. Chackerian, C. Willman, D. Peabody, W. Wharton, C. J. Brinker, C. Ashley and E. Carnes, *Adv. Healthcare Mater.*, **2012**, 1, 348-353.
36. C. E. Ashley, E. C. Carnes, K. E. Epler, D. P. Padilla, G. K. Phillips, R. E. Castillo, D. C. Wilkinson, B. S. Wilkinson, C. A. Burgard, R. M. Kalinich, J. L. Townson, B. Chackerian, C. L. Willman, D. S. Peabody, W. Wharton and C. J. Brinker, *ACS Nano*, **2012**, 6, 2174-2188.
37. C. E. Ashley, E. C. Carnes, G. K. Phillips, D. Padilla, P. N. Durfee, P. A. Brown, T. N. Hanna, J. Liu, B. Phillips, M. B. Carter, N. J. Carroll, X. Jiang, D. R. Dunphy, C. L. Willman, D. N. Petsev, D. G. Evans, A. N. Parikh, B. Chackerian, W. Wharton, D. S. Peabody and C. J. Brinker, *Nat. Mater.*, **2011**, 10, 389-397.
38. Y. Han and J. Y. Ying, *Angew. Chem., Int. Ed.*, **2005**, 44, 288-292.
39. J. B. Tu, A. L.; Friedrich, H.; Bomans, P. H. H.; Bussmann, J.; Sommerdijk, N. A. J. M.; Wim Jiskoot, W.; Kros, A., **2016**.
40. X. B. Zhao, L. Liu, X. R. Li, J. Zeng, X. Jia and P. Liu, *Langmuir*, **2014**, 30, 10419-10429.
41. S. Brunauer, P. H. Emmett and E. Teller, *J. Am. Chem. Soc.*, **1938**, 60, 309-319.
42. E. P. Barrett, L. G. Joyner and P. P. Halenda, *J. Am. Chem. Soc.*, **1951**, 73, 373-380.
43. H. Friedrich, P. M. Frederik, G. de With and N. A. J. M. Sommerdijk, *Angew. Chem., Int. Ed.*, **2010**, 49, 7850-7858.
44. K. van der Maaden, H. X. Yu, K. Sliedregt, R. Zwier, R. Leboux, M. Oguri, A. Kros, W. Jiskoot and J. A. Bouwstra, *J. Mater.Chem. B*, **2013**, 1, 4466-4477.
45. K. Moller, K. Muller, H. Engelke, C. Brauchle, E. Wagner and T. Bein, *Nanoscale*, **2016**, 8, 4007-4019.
46. N. Z. Knezevic and J.-O. Durand, *Nanoscale*, **2015**, 7, 2199-2209.
47. H. K. Na, M. H. Kim, K. Park, S. R. Ryoo, K. E. Lee, H. Jeon, R. Ryoo, C. Hyeon and D. H. Min, *Small*, **2012**, 8, 1752-1761.
48. X. Du, L. Xiong, S. Dai, F. Kleitz and S. Z. Qiao, *Adv. Funct. Mater.*, **2014**, 24, 7627-7637.
49. S. B. Hartono, N. T. Phuoc, M. H. Yu, Z. F. Jia, M. J. Monteiro, S. H. Qiao and C. Z. Yu, *J. Mater.Chem. B*, **2014**, 2, 718-726.
50. D. S. Lin, Q. Cheng, Q. Jiang, Y. Y. Huang, Z. Yang, S. C. Han, Y. N. Zhao, S. T. Guo, Z. C. Liang and A. J. Dong, *Nanoscale*, **2013**, 5, 4291-4301.
51. B. L. Zhang, Z. Luo, J. J. Liu, X. W. Ding, J. H. Li and K. Y. Cai, *J. Controlled Release*, **2014**, 192, 192-201.
52. J. Sun, H. Zhang, R. Tian, D. Ma, X. Bao, D. S. Su and H. Zou, *Chem. Commun.*, **2006**, 1322-1324.
53. I. I. Slowing, B. G. Trewyn and V. S. Y. Lin, *J. Am. Chem. Soc.*, **2007**, 129, 8845-8849.
54. Q. J. He and J. L. Shi, *Adv. Mater.*, **2014**, 26, 391-411.
55. F. Q. Tang, L. L. Li and D. Chen, *Adv. Mater.*, **2012**, 24, 1504-1534.



## Chapter IV

### Membrane Fusion Mediated Intracellular Delivery of Lipid Bilayer Coated Mesoporous Silica Nanoparticles



Jing Tu, Jian Yang, Gerda E. M. Lamers, René C. L. Olsthoorn and Alexander Kros

**Abstract**

Protein delivery into the cytosol of cells is a challenging topic in the field of nanomedicine, because cellular uptake and endosomal escape are typically inefficient, hampering clinical applications. In this contribution cuboidal mesoporous silica nanoparticles (MSNs) containing disk-shaped cavities with a large average pore diameter (10 nm) were studied as a protein delivery vehicle. Cytochrome c (*cyt. c*) was used as a model membrane-impermeable protein and encapsulated into MSNs (MSNs/*cyt. c*) with fast kinetics and high loading efficiency. To enhance the colloidal stability and to prevent the premature release of *cyt. c* before cellular uptake, the protein loaded MSNs were coated with a fusogenic lipid bilayer. Cellular uptake was enhanced by a complementary pair of coiled-coil forming lipopeptides, which were incorporated into the lipid bilayer of the MSNs particles and the cytoplasmic membrane respectively. Coiled-coil induced membrane fusion led to cytosolic delivery of the *cyt. c* loaded MSNs. Cell uptake inhibition studies with five commonly used inhibitors revealed that indeed endocytosis is not the major pathway of uptake, strongly suggesting that membrane fusion is the dominant uptake mechanism. In contrast, when one of the coiled-coil peptides was omitted the major route of uptake was endocytosis. The release and bioactivity of *cyt. c* inside cells was quantified using a caspase assay. It showed that the cells were driven into apoptosis, confirming the cytosolic delivery. This system is suitable for delivery of any other protein or other high molecular weight compound due to the large pore size of the MSNs and combined with coiled-coil mediated delivery has many potential applications in the field of biomedicine and diagnostics.

**Keywords:** intracellular delivery, lipid bilayers, coiled-coil, apoptosis, nanomedicine, mesoporous silica nanoparticles

## 4.1 Introduction

Intracellular protein delivery holds enormous promise for a range of biomedical applications,<sup>1</sup> such as cancer therapy,<sup>2,3</sup> vaccination and enzyme based therapeutics.<sup>4</sup> However, therapeutic proteins are susceptible to proteolysis and denaturation, limiting their efficacy in the body.<sup>5,6</sup> Thus, a variety of protein delivery systems have been developed in an attempt to solve the delivery problem, such as polymeric nanoparticles,<sup>7</sup> hydrogels,<sup>8,9</sup> and lipid-based nanoparticles.<sup>10,11</sup> Mesoporous silica nanoparticles (MSNs) have shown to be good carriers for a wide variety of biomolecules with varying molecular weight, including anticancer drugs, oligonucleotides and proteins.<sup>2,12-21</sup> However, most MSNs used in drug delivery studies to date have typically pores with diameters up to 4 nm, thereby limiting their use as an efficient carrier for high molecular weight molecules like proteins. As a result, most studies show only low loading capacities and since the MSN pores are generally too small, offer weak proteolytic protection.<sup>22</sup>

Recently our lab developed sub-100nm MSNs with disk-like cavities that have large diameter pores (10 nm) able to encapsulate proteins with a wide molecular weight range and with high capacity and efficiency. While the use of MSNs as a drug delivery carrier has grown exponentially in the last decade, the long-term colloidal stability remains a challenge. Especially in *in vivo* experiments, it is critical that MSNs do not aggregate as this will negatively affect the bio-distribution and concomitant delivery of the drug. To enhance the colloidal stability lipid bilayer on the outer surface of MSNs have been introduced. This lipid bilayer coating also provides protection against enzymatic degradation,<sup>23,24</sup> DNA breakdown<sup>25</sup> and antibody neutralization,<sup>26</sup> resulting in prolonged retention of attached protein activity *in vivo* as long as the proteins remain immobilized within the MSNs carriers. Another advantage of lipid bilayer coated MSNs is the better control over the cargo release.<sup>27,28</sup> For example, Roggers *et al.* showed that the controlled release of a model compound (fluorescein) was dependent on the removal of the lipid bilayer. In this case this was achieved by cleavage of the covalently bound lipids from dipalmitoylated MSNs.<sup>29</sup>

Lipid bilayers typically used to coat MSNs are composed of cationic lipids like DOTAP,<sup>25,30</sup> neutral compounds like DPPC and cholesterol.<sup>31</sup> The pathway of cellular uptake of these lipid bilayer coated MSNs is via by endocytosis or macropinocytosis, which limits the delivery efficiency into the cytosol of cells. To the best of our knowledge, reports about the direct cytosolic delivery of MSNs do not exist yet.

Recently, we developed a new method to deliver anion transporters into the membrane of live cells based on membrane fusion of liposomes with cells.<sup>32,33</sup> Here a complementary pair of coiled-coil lipopeptides was used to trigger fusion between liposomes and control targeted delivery.<sup>34</sup> These peptides, denoted E and K, were conjugated to cholesterol *via* a small polyethylene glycol (PEG) spacer, resulting in CPE and CPK.<sup>35-38</sup> When these lipopeptides were embedded in the lipid bilayer of liposomes and/or cell membranes respectively, triggered membrane fusion with concomitant release of liposome encapsulated cargo was observed.<sup>39,40</sup>

To date, only liposomes with an aqueous core loaded with low molecular weight water soluble drugs, anticancer drugs or hydrophobic ion transporters located in the lipid bilayer of liposomes were fused with live cells.<sup>32</sup> More recently liposomes containing the anticancer drug doxorubicin could target modified HeLa cancer cells in a zebrafish xenograft model, resulting in targeted cell death.<sup>41</sup> Here, we would like to study whether coiled-coil lipopeptide mediated membrane fusion could be used to enhance the delivery of protein loaded MSNs into cells and to circumvent the endocytic pathway (Figure 4.1a). Cytochrome c (*cyt. c*) was chosen as a model protein as its cytosolic delivery activates the intrinsic apoptotic pathway. This allowed us to monitor the efficient uptake and delivery of *cyt. c* loaded MSNs as well as the induction of apoptosis<sup>42</sup> by cytosolic release of *cyt. c*.

## 4.2 Materials and Methods

### 4.2.1 Materials

Cytochrome c from equine heart, pluronic P123 (EO<sub>20</sub>PO<sub>70</sub>EO<sub>20</sub>), tetraethyl orthosilicate (TEOS), HOBT, mesitylene, cholesterol (CHO) and Atto 488 NHS ester were purchased from Sigma-Aldrich and used as received. 1,2-dioleoyl-sn-glycero-3-phosphocholine (DOPC), 1,2-dioleoyl-sn-glycero-3-phosphoethanolamine (DOPE) and 1,2-dioleoyl-sn-glycero-3-phosphoethanolamine-N-(7-nitro-2-1,3-benzoxadiazol-4-yl) (ammonium salt) (DOPE-NBD) were purchased from Avanti Polar Lipids. Fmoc-protected amino acids were purchased from Novabiochem. All other reagents and solvents were obtained at the highest purity available from BioSolve or Sigma-Aldrich and used without further purification. 8-wells slide Lab-tek was purchased from Thermo Scientific. DMEM medium was obtained from Gibco. WST-1 was obtained from Serva. PMS-Ome was obtained from Santa Cruz Biotechnology. Apo-ONE® Homogeneous Caspase-3/7 Assay kit was purchased from Promega. The composition of PBS was K<sub>2</sub>HPO<sub>4</sub> (14.99 mM), KH<sub>2</sub>PO<sub>4</sub> (5 mM), and NaCl (150.07 mM) and PB was composed of Na<sub>2</sub>HPO<sub>4</sub> (1 mM) and NaH<sub>2</sub>PO<sub>4</sub> (1 mM) at a molar ratio of 5:2. The pH was 7.4.

#### 4.2.2 Characterization of MSNs and LB-MSNs

TEM images were collected by using a JEOL 1010 instrument with an accelerating voltage of 70 kV. Nitrogen adsorption-desorption isotherms were obtained with a Micromeritics TriStar II 3020 surface area analyzer. Before each measurement, MSNs were outgassed in the vacuum (below 0.15 mbar) at 300 °C for 16 h. The specific surface areas were calculated from the adsorption data in the low pressure range using the Brunauer-Emmett-Teller (BET) model.<sup>43</sup> The pore size distribution was determined following the Barrett-Joyner-Halenda (BJH) model.<sup>44</sup> The hydrodynamic size distribution and zeta-potential of the samples were measured with a Malvern Nano-zs instrument.

#### 4.2.3 Synthesis of lipopeptides

Peptides E<sub>4</sub> (EIAALEK)<sub>4</sub> and K<sub>4</sub> (KIAALKE)<sub>4</sub> were synthesized on a 250 μmol scale using Fmoc chemistry on a CEM peptide synthesizer. Sieber amide resin with a loading of 0.69 mmol/g was used. Amino acid couplings were performed with 4 eq. of the appropriate amino acid, 4 eq. of the activator HCTU and 8 eq. of the base DIPEA. Fmoc deprotection was performed with piperidine:NMP (4:6 v/v). N<sub>3</sub>-PEG<sub>4</sub>-COOH<sup>36</sup> was coupled to the N-terminus of the peptide using 4 eq. of DIPEA and 3 eq. of HOBT in DMF for 18 hours. The azido group was reduced to NH<sub>2</sub> using 8 eq. of trimethylphosphine (1 M in toluene) in a dioxane/H<sub>2</sub>O mixture (4:1 v/v) for 2 h reaction, this reaction was performed twice. In the final step cholesteryl-4-amino-4-oxobutanoic acid (2 eq.) was coupled to the PEG<sub>4</sub> linker using 5 eq. of DIPEA and 4 eq. of PyBOP in DMF for 72 h. The resulting lipopeptides CP<sub>4</sub>K<sub>4</sub> and CP<sub>4</sub>E<sub>4</sub> were cleaved from the resin with a mixture of TFA/TIS/H<sub>2</sub>O (95:2.5:2.5 v/v) for 1.5 h. The cleavage mixture was precipitated in cold diethyl ether. The precipitate was collected and the crude product was purified by HPLC using a C4 column.<sup>40</sup>

#### 4.2.4 Synthesis of large pore MSNs

0.5 g of surfactant Pluronic P123 and 1.4 g of FC-4 were dissolved in 80 ml of HCl (0.02 M), followed by the addition of 0.48 ml of TMB.<sup>45</sup> After stirring for 6 h, 2.14 ml of TEOS was added dropwise. The resulting mixture was stirred at 30 °C for 24 h and transferred to an autoclave at 120 °C for 2 days. Finally, the solid product was isolated by centrifugation (13000 rpm, 5 min), washed with ethanol and water. The organic template was completely removed by calcination at 550 °C for 5 h in air.

### 4.2.5 Labeling of cytochrome *c* with Atto 488 NHS Ester

Cytochrome *c* (10 mg) was dissolved in 5 ml of sodium carbonate buffer (100 mM, pH 8). Atto 488 NHS ester was dissolved in DMSO (2 mg/ml), and 0.5 ml of this solution was added to the protein solution. The mixture was stirred for 4 h at room temperature. The resulting Atto 488-labeled protein was purified by size exclusion chromatography using a Sephadex-G25 column, PBS as eluent.

### 4.2.6 Liposome preparation

Stock solutions of phospholipids (1 mM) in  $\text{CHCl}_3$  and  $\text{CP}_4\text{E}_4$  (50  $\mu\text{M}$ ) in  $\text{CHCl}_3:\text{CH}_3\text{OH}$  (1:1) were prepared and stored at  $-20^\circ\text{C}$ . The stock solutions were mixed to obtain the desired liposome formulation (DOPC: DOPE: CHO = 2:1:1 molar ratio). Liposomes were prepared by mixing the appropriate amount of lipids and  $\text{CP}_4\text{E}_4$  in a 20 mL glass vial and evaporating the solvents to form a lipid film. The film was rehydrated with 1 ml of phosphate buffer (1 mM PB, pH 7.4). The solution was vortexed for 30 seconds to form a cloudy lipid suspension and sonicated in a water bath at  $50^\circ\text{C}$  for 10 min. The resulting liposomes were stored at  $4^\circ\text{C}$  (final lipid concentration was 1 mM) and the hydrodynamic diameter as determined by DLS was approximately 100 nm. The final concentration of lipids and  $\text{CP}_4\text{E}_4$  in each sample used in the cell experiments was 250  $\mu\text{M}$  and 2.5  $\mu\text{M}$ , respectively.

### 4.2.7 $\text{CP}_4\text{K}_4$ solution

A  $\text{CP}_4\text{K}_4$  stock solution (100  $\mu\text{M}$ ) was prepared in  $\text{CHCl}_3 : \text{CH}_3\text{OH}$  (1:1). An appropriate amount of  $\text{CP}_4\text{K}_4$  stock solution was added in a glass vial and the organic solvent was evaporated under a  $\text{N}_2$  flow. The obtained film was hydrated and diluted by DMEM (+/- FCS, w/o phenol red) and sonicated at  $55^\circ\text{C}$  for 1 min. The final concentration of  $\text{CP}_4\text{K}_4$  was 5  $\mu\text{M}$ .

### 4.2.8 Loading *Cyt. c* into MSNs

Cytochrome *c* (*cyt. c*) solutions with various concentrations (0.25, 0.5, 1, 2 and 4 mg/ml) were prepared in phosphate buffer (1 mM, pH 7.4). MSNs (2 mg/ml) were dispersed in the same buffer by sonication (10 min). In a typical procedure, 0.5 ml of *cyt. c* stock solution was mixed with 0.5 ml of MSNs and incubated and shaken with an Eppendorf ThermoMixer for 5 min (400 rpm,  $25^\circ\text{C}$ ). The *cyt. c*-loaded MSNs were collected by centrifugation (10000 rpm, 5 min) and separated from non-encapsulated *cyt. c*, which remained in the supernatant. The pellet was resuspended in 1 ml of PB (1 mM, pH 7.4) and the zeta-potential was measured. The absorbance of non-encapsulated *cyt. c* was measured in the supernatant using Greiner 96-

well flat-bottom transparent in a plate reader (Tecan infinite M1000). A calibration curve was determined based on the absorbance at 412 nm<sup>46</sup> as a function of *cyt. c* concentration (0-500 µg/ml).

#### 4.2.9 Preparation of MSNs/*cyt. c*@CPE-LBs

A solution of MSNs/*cyt. c* (1 mg/ml; 0.5 ml) was transferred into 1 ml of freshly prepared CPE liposomes (0.5 ml; [lipid]= 0.1 mM containing 1 mol% CP<sub>4</sub>E<sub>4</sub>) and the mixture was shaken with a Eppendorf ThermoMixer (25 °C, 400 rpm) for 90 min. And subsequently centrifuged at 10000 rpm for 3 min. The supernatant was removed and the pellet was washed 3 times with 1 ml of PB and 3 times with DMEM (-FCS, -phenol red). The pellet was resuspended in DMEM at a final concentration of 1 mg/ml based on the MSNs' weight.

#### 4.2.10 *Cyt. c* release profile from MSNs

The *in vitro* release of *cyt. c* from MSNs was determined at 37 °C. *Cyt. c* loaded MSNs with or without a lipid bilayer were suspended in 1 ml of pre-warmed PBS (pH 7.4) or PB (pH 7.4) respectively and incubated at 37 °C on an Eppendorf ThermoMixer (400 rpm). Supernatants were collected thoroughly by a pipette after centrifugation and 1 ml of fresh PBS were added at different time points. The released amount of *cyt. c* from MSNs at the different time points were quantified by measuring the absorption of the Soret band of *cyt. c* at 412 nm.<sup>5</sup> Each experiment was repeated three times.

#### 4.2.11 Cell culture

HeLa cells were grown as a monolayer at 37 °C in 7% CO<sub>2</sub> atmosphere, and were maintained in a continuous logarithmic culture in Dulbecco's Modified Eagle Medium (DMEM) containing phenol red completed with 10% Fetal Calf Serum (FCS), penicillin/streptomycin (100 units/ml, 0.1 mg/ml, respectively), and Glutamax (2 mM). The medium was replaced every 3 days and cells were passaged by trypsinization at 70% confluence.

#### 4.2.12 Cell viability assay

Cells were seeded in a 96 well-plate at a concentration of 1×10<sup>4</sup> cells per well and incubated for 24 h prior to the WST-1 assay. The medium was removed and cells were incubated with 100 µL of a CP<sub>4</sub>K<sub>4</sub> (5 µM) solution in medium (w/o phenol red) for 2 h. The medium containing CP<sub>4</sub>K<sub>4</sub> was removed after 2 h and the cells were washed three times with 250 µl of DMEM medium. Next the cells were incubated with 250 µl (1 mM total lipid) lipid

coated MSNs containing 1 mol% CP<sub>4</sub>E<sub>4</sub> for 1 h. Next, the lipid coated MSNs were removed and fresh medium was added to each well and the plate was incubated at 37 °C to perform a WST-1 assay.<sup>47</sup> The medium containing WST reagent was removed after 24 h and 200 µl of cell proliferation reagent WST-1 in DMEM (w/o phenol red) was added to each well and the cells were incubated for 3 h at 37 °C. Absorption was measured (at 450 nm) at room temperature using a Tecan Infinite M1000 PRO microplate reader, the cells were shaken for 60 s prior to each measurement (2 mm linearly, 654 rpm). The Z-position was 12500 µm, and the gain was optimized according to the amount of fluorophore in the sample. The metabolic activity (cell survival) were normalized with respect to the control (*i.e.* non-treated cells), which was set to 100%. For the control experiments, cells were incubated with MSNs@CPE-LB, only MSNs or MSNs@LB in the absence of lipopeptides.

### 4.2.13 Transmission electron microscopy (TEM)

1×10<sup>6</sup> HeLa cells per well were seeded on 15 mm thermanox coverslips and fixed with 2 v% glutaraldehyde in a sodium cacodylate buffer (0.1 M, pH 7.2) for 2 h at room temperature. Post fixation was performed with 1% w/v osmium tetroxide in distilled water for 1 h at room temperature. The cells were dehydrated through a graded series of ethanol and embedded in Agar 100 resin (Agar Scientific, AGR1043) and the sections were cut with a diamond knife at a Leica Ultramicrotome. Microscopy images were obtained with a JEOL JEM-1010 transmission electron microscope with a maximum output voltage up to 80 KV (Tokyo, Japan) equipped with an Olympus Megaview camera (Tokyo, Japan).

### 4.2.14 Confocal imaging

Cells were grown in an 8-well slide at a density of 2.5×10<sup>4</sup> cells per well and incubated in the DMEM (+FCS, -phenol red) at 37 °C under a 7% CO<sub>2</sub> atmosphere. The medium was removed after 21 h and a CP<sub>4</sub>K<sub>4</sub> solution (5 µM, 300 µl) was added and incubated for 0.5-2 h at 37 °C under a 7% CO<sub>2</sub> atmosphere. The CP<sub>4</sub>K<sub>4</sub> solution was removed and the cells were washed 3 times with 250 µl fresh DMEM (+FCS, -phenol red), and incubated with *cyt. c* or with CPE<sub>4</sub>-decorated lipid bilayers coated MSNs loaded with *cyt. c* (250 µM, 300 µl). After 15 min of incubation, the cells were washed three times and fluorescent images were acquired on Nikon confocal laser scanning microscope. Nikon application suite advanced fluorescence software and Image-J was used for image analysis. The wavelength setting for Atto488 labeled *cyt. c* was Ex/Em: 501/523 nm (Ex laser: 480 nm), for Hoechst 33342 was Ex/Em: 361/497 nm (Ex laser: 420 nm).



#### *4.2.15 Endocytosis inhibition measurements*

HeLa cells were seeded in a 24-well plate at a density of  $1 \times 10^5$  cells per well and incubated in DMEM (+10% FCS, -phenol red) medium at 37 °C. The medium was removed after 21 h and the cells were incubated with 500  $\mu$ L of nocodazole (40  $\mu$ M), wortmannin (0.25  $\mu$ M), chlorpromazine (40  $\mu$ M), genistein (200  $\mu$ M), or sodium azide 0.01% w/v in DMEM (-FCS, -phenol red) medium. After 1 h of pre-incubation, the medium was removed and the cells were treated with 500  $\mu$ l of CP<sub>4</sub>K<sub>4</sub> (5  $\mu$ M) supplemented with the above mentioned inhibitors for 2 h, after removed CP<sub>4</sub>K<sub>4</sub> and washing 3 times with medium, followed by the addition of 100  $\mu$ l of MSNs@cPE-LBs (the concentration of MSNs was 1 mg/ml). After 30 min, liposomes and inhibitors were removed and HeLa cells were washed 3 times by DMEM medium. The cells were incubated at 37 °C for 1 h. Next, the cells were detached using PBS/EDTA (10 mM EDTA) for 15 min, centrifuged and re-suspended in fresh medium at a concentration of  $2 \times 10^5$  cells/ml. The mean fluorescence intensity of Atto 488 of the cells was measured by flow cytometry using a Beckman Coulter Quanta SC machine.

#### *4.2.16 Apoptosis assay*

HeLa cells at the density of  $1 \times 10^4$  per well in 96-well plate were cultured in DMEM (+10% FCS, -phenol red) medium at 37 °C prior to the apoptosis assay. HeLa cells were treated a CP<sub>4</sub>K<sub>4</sub> solution at the concentration of 5  $\mu$ M for 2 h, following CP<sub>4</sub>K<sub>4</sub> was removed, cells were washed 3 time with medium and incubated with MSNs/cyt. c@cPE-LB for 0.5 h. Next, the cells were washed with 100  $\mu$ l medium 3 times and incubated at 37 °C with 7% CO<sub>2</sub> for 30 h or 48 h, finally, 100  $\mu$ l of the Apo-ONE® Homogeneous Caspase-3/7 Assay reagent was added for each well and incubated for 3 h. The caspase activity was measured as a function of the created fluorescent rhodamine 110, which is released upon the cleavage of the non-fluorescent caspase substrate Z-DEVD-R110 (bis-(N-CBZL-aspartyl-L-glutamyl-L-valyl-L-aspartic acid amide) by caspase 3/7 activity.<sup>48</sup> Wavelength settings: Ex/Em: 490/520 nm. Measurements were performed as three independent experiments using Greiner 96-well flat-bottom transparent in a plate reader (Tecan infinite M1000). Statistical analysis was performed to calculate average values and standard deviations.

## 4.3 Results and discussion

We synthesized a new type of cuboidal MSNs featuring a cuboidal-like geometry using a mixture of block copolymers (Pluronic P123), a pore expander (1,3,5-trimethylbenzene, TMB) and fluorocarbons (FC-4) as the structure-directing template. The resulting particles possess an array of disk-shaped mesochannels along the short axis of the rectangular shaped ( $90 \pm 20$  nm by lengths,  $43 \pm 7$  nm by widths) MSNs as shown in the transmission electron micrographs (TEM) (Figure 4.1b). The nitrogen adsorption-desorption isotherms of MSNs exhibited the characteristic type IV isotherms according to International Union of Pure and Applied Chemistry (IUPAC) classification<sup>49</sup> with a BET surface area of  $506 \text{ m}^2/\text{g}$  (Figure 4.1c). The pore size distribution was measured by the BJH method<sup>50</sup> and found to be  $10 \pm 1$  nm for the majority of MSNs.

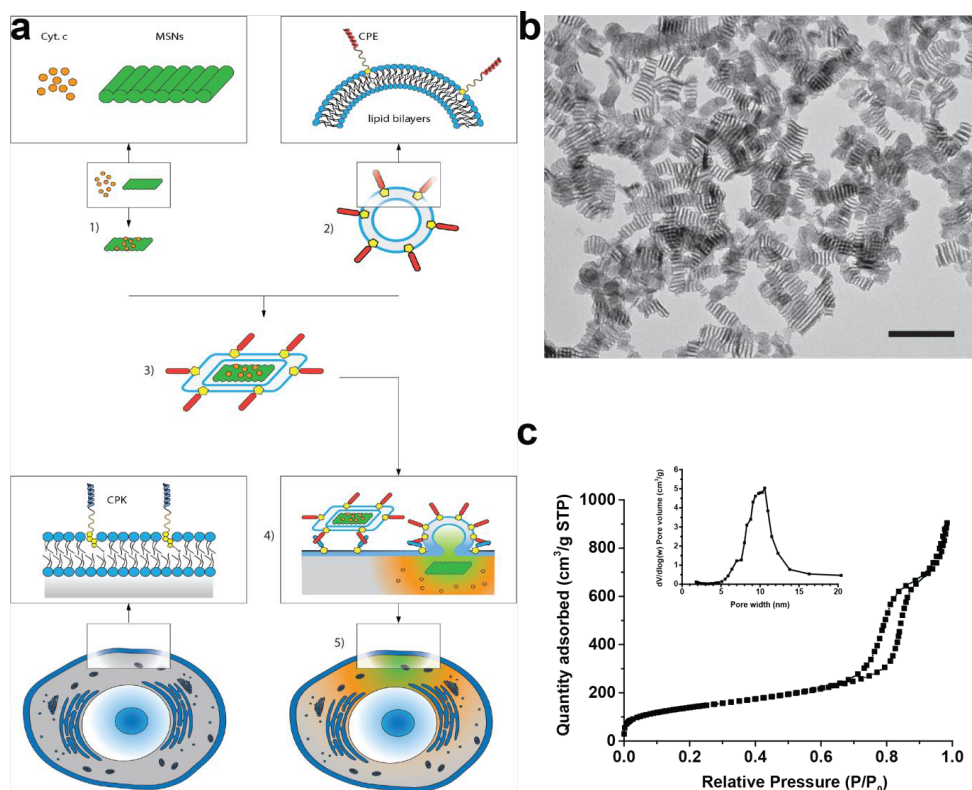


**Figure 4.1** Schematic illustrating the fusion between cells and lipid bilayer coated MSNs driven by coiled-coil formation between  $CP_4K_4$  and  $CP_4E_4$ . (a) Intracellular delivery procedure 1) cyt. c (orange) is encapsulated into MSNs (green); 2) lipid bilayers (light blue) are decorated with lipopeptide CPE (red); 3) combining lipid bilayers (LBs) with MSNs/cyt.

*c*; 4) incorporation of CP<sub>4</sub>K<sub>4</sub> (dark blue) into cellular membrane and addition of CPE-coated MSNs trigger membrane fusion and delivery of *cyt. c* into the cytoplasm and 5) observation of cell membrane labeling and induction of cellular responses (e.g. apoptosis). (b) TEM image of MSNs, scale bar = 200 nm and (c) nitrogen adsorption-desorption isotherms and pore size distribution (insert).

We investigated whether this new type of MSNs could be used to transport proteins into the cytosol of cells. We chose to use cytochrome *c* (*cyt. c*, Mw 12384 Da, geometric size 2.6 × 3.2 × 3.3 nm) as a model protein. *Cyt. c* is a small redox protein that is present in the inner membrane of mitochondrion and induces apoptosis (programmed cell death) when it is released into the cytosol.<sup>51</sup> The pore dimensions of our cuboidal MSNs are sufficiently large to accommodate *cyt. c* and the open disk-shaped mesostructure has a large surface area rendering the encapsulation of *cyt. c* very efficient. Dispersion of as-synthesized MSNs into a *cyt. c* stock solution resulted in a rapid adsorption of the protein inside the disk-like porous structure of the MSNs. The amount of absorbed protein was determined by measuring the difference in absorption of the Soret band (412 nm) in the supernatant before and after the encapsulation (Figure 4.2a).<sup>46</sup> Within 5 min an equilibrium in *cyt. c* adsorption was obtained and 95.49 ± 1.63% of *cyt. c* was encapsulated into the MSNs. The encapsulation capacity of MSNs was further investigated by incubating a fixed amount of MSNs (1 mg) with *cyt. c* at increasing concentrations (0.25-4 mg/ml). The maximum *cyt. c* loading capacity in these cuboidal MSNs was determined to be 470 µg/mg MSN (Figure 4.2a, black curve). The surface charge of *cyt. c* loaded MSNs as a function of initial *cyt. c* concentration was determined by measuring the zeta-potential (Figure 4.2a, red curve). When the protein concentration (0-1 mg/ml) was increased, the zeta-potential of MSNs/*cyt. c* tended to become neutral and remained around 0 mV at higher concentrations of *cyt. c* (1-4 mg/ml). When the weight ratio between *cyt. c* and MSNs was 1:8 or 1:4, the encapsulation efficiency (EE%) of *cyt. c* into MSNs was close to 100%, revealing the excellent protein encapsulation potential of this new type of cuboidal MSNs. As expected, the EE% decreased as the ratio of *cyt. c*/MSNs increased. Compared to native *cyt. c*, the encapsulated *cyt. c* in the MSNs revealed a slight broadening of the adsorption peak in the UV-Visible spectrum, but no blue shift was observed, suggesting that the interaction between the protein and pore surface did not change the structure of *cyt. c*.<sup>52</sup> The absorption maximum of the Soret band remained at 412 nm, showing that *cyt. c* retained its native fold and suffered no conformational change (Figure 4.S1a).<sup>52, 53</sup>

Next, the *in vitro* *cyt. c* release from MSNs was studied at 37 °C by measuring the Soret band (412 nm) of *cyt. c* in the supernatant as a function of time. The *cyt. c* adsorption is mainly driven by electrostatic interaction since *cyt. c* is positively charged at pH 7.4 while MSNs are negatively charged due to the silanol groups on the surface.<sup>46, 54</sup> Therefore, we studied the influence of ionic strength on the release profile. For this, MSNs/*cyt. c* were suspended in phosphate buffered saline (PBS, pH 7.4, ionic strength = 270 mM) and phosphate buffer (PB, pH 7.4, ionic strength = 12 mM), respectively. Next, the protein release as a function of ionic strength was determined over a period of 62 h (Figure 4.S1a). The amount of released *cyt. c* from MSNs was  $70.4 \pm 1.8\%$  in PBS and only  $16.8 \pm 1.8\%$  in 1 mM PB. At higher ionic strength of the buffer, the electrostatic interactions between *cyt. c* and MSNs are weakened resulting in an increased release of the protein. Thus *cyt. c* can be loaded with high efficiency into MSNs at low ionic strength and subsequently released at conditions of high ionic strength, confirming that the electrostatic interaction between *cyt. c* and MSNs contributed highly to the encapsulation and release process.

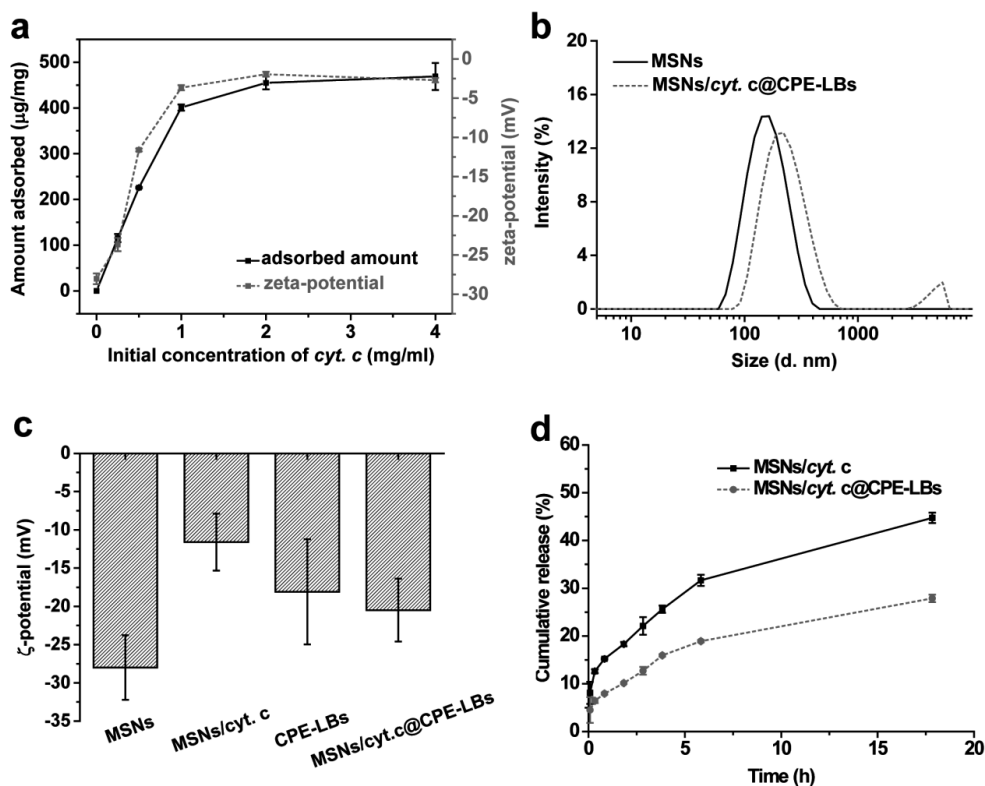


**Figure 4.2** Characterization of MSNs/*cyt. c* (a) Loading capacity and zeta ( $\zeta$ )-potential of MSNs/*cyt. c*, with different initial *cyt. c* concentrations (0.5-4 mg/ml, 1 mM PB, pH 7.4.) (b)

*Dynamic light scattering (DLS) of MSNs and MSNs/cyt. c@CPE-LBs, 1 mM PB, pH 7.4. (c) Zeta-potential of MSNs, MSNs/cyt. c, CPE-LBs and MSNs/cyt. c@CPE-LBs (error bars represented zeta deviation, 1 mM PB, pH 7.4) and (d) in vitro release profiles of MSNs and MSNs/cyt. c@CPE-LBs in PBS, pH 7.4. Error bars show the standard deviation of three independent experiments.*

The repulsive force between MSNs/cyt. c decreased when more protein was loaded into MSNs, as evidenced by the lower zeta-potential. As a result, MSNs/cyt. c tend to form aggregates more readily due to the decreasing surface charge. Indeed, dynamic light scattering (DLS) measurements revealed that after encapsulation, MSNs/cyt. c tended to aggregate as the hydrodynamic diameter increased to >2000 nm. In order to increase the colloidal stability, the MSNs/cyt. c were decorated with a lipid bilayer. After introduction of a lipid bilayer composed of DOPC, DOPE and Cholesterol (2:1:1 molar ratio,<sup>35</sup> the observed diameter by dynamic light scattering of the nanoparticles was reduced from ~2  $\mu\text{m}$  to 229 nm (polydispersity index, PDI = 0.251) (Figure 4.2b). This lipid composition was chosen as it is known to be fusogenic when combined with the complementary lipopeptides CP<sub>4</sub>E<sub>4</sub> and CP<sub>4</sub>K<sub>4</sub>.<sup>40</sup> After loading the MSNs with cyt. c, the zeta-potential shifted from -28.0 to -11.6 mV. Application of the lipid bilayer onto the exterior surface of these particles resulted in a more negative zeta potential (-20.5 mV) (Figure 4.2c). The presence of the lipid bilayer also reduced the burst release of cyt. c by a factor of ~1.6 fold as it acts as a barrier<sup>55</sup> retaining the protein more within the MSNs (Figure 4.2d).

Previously, we reported that the complementary coiled-coil lipopeptides CP<sub>12</sub>E<sub>3</sub> and CP<sub>12</sub>K<sub>3</sub> could be used to dock liposomes at the outer plasma membrane of live cells.<sup>56</sup> Extension of the lipopeptides with one heptad repeat of amino acids (*i.e.* CP<sub>4</sub>E<sub>4</sub>/CP<sub>4</sub>K<sub>4</sub>) resulted in membrane fusion between liposomes and cells using lipopeptides<sup>32, 40</sup> as evidenced by the delivery of low molecular weight dyes, anion transporter and the anticancer drug doxorubicin. To study the scope of this synthetic fusion system, we now were interested to study whether coiled-coil mediated fusion could be used to enhance the intracellular delivery of inorganic MSN. To date, MSNs or lipid bilayer coated MSNs are typically taken up by endocytosis,<sup>14, 29, 55, 57, 58</sup> which can be detrimental to the cargo. By employing coiled-coil mediated delivery using CP<sub>4</sub>E<sub>4</sub> and CP<sub>4</sub>K<sub>4</sub>, the cellular uptake mechanism might be shifted from endocytosis to a direct cytosolic entry *via* membrane fusion. In order to enhance the intracellular delivery of MSNs/cyt. c, a fusogenic lipid bilayer composed of CP<sub>4</sub>E<sub>4</sub> was therefore applied. In order to induce fusion, cells were pretreated with CP<sub>4</sub>K<sub>4</sub>. Next a

suspension containing CP<sub>4</sub>E<sub>4</sub>-lipid bilayer coated MSNs/*cyt. c* was added to the cells and incubated for 30 min. A cell viability assay demonstrated that CP<sub>4</sub>E<sub>4</sub> / CP<sub>4</sub>K<sub>4</sub>, lipid bilayer coated MSNs with or without CP<sub>4</sub>K<sub>4</sub> are well tolerated by HeLa cells after a 24 h post-treatment (Figure 4.S2). Confocal microscopy imaging revealed that the cytosol became fluorescent, indicative of the efficient delivery of Atto488-labeled *cyt. c* inside the cytosol (Figure 4.3a). In contrast, when one or both of the lipopeptides were omitted, and thus coiled-coil mediated fusion cannot occur, only a very limited cellular uptake of *cyt. c* was observed (Figure 4.S3). Furthermore, the incubation of cells with Atto488-labeled *cyt. c* alone did not result in any cellular uptake, revealing that the water-soluble protein cannot enter the cell by transient membrane destabilization or endocytosis. In contrast, by applying the coiled-coil mediated fusion system, *cyt. c* could be efficiently delivered to the cytosolic within 30 min.

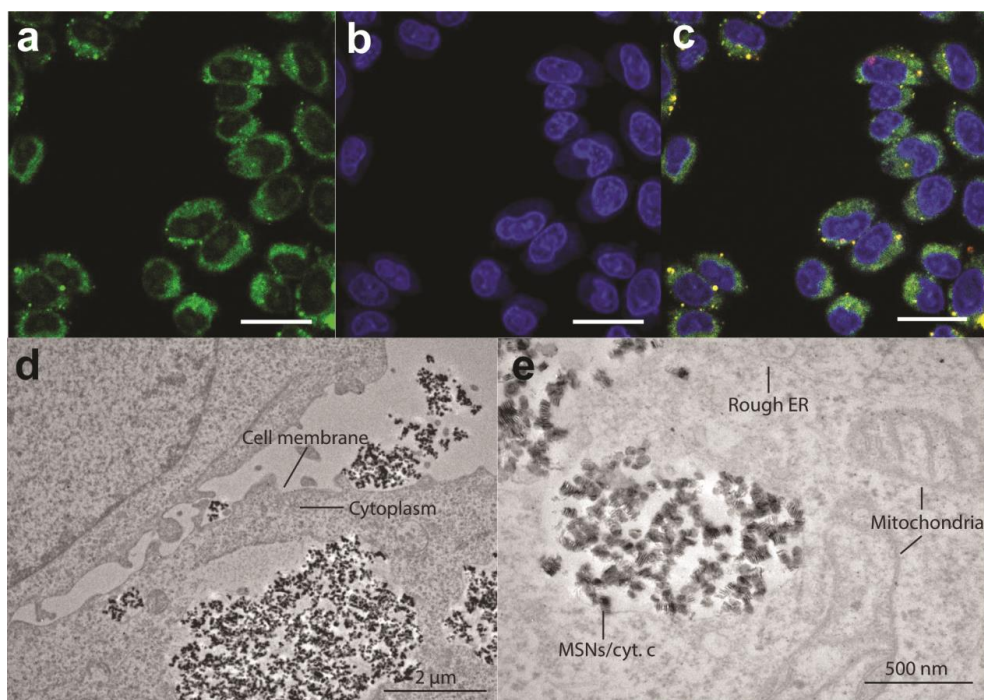


**Figure 4.3** Intracellular delivery of *cyt. c* by MSNs@CPE-LBs. (a-c) Confocal images showing: (a) location of Atto488 labeled *cyt. c*, (b) cell nuclei stained by Hoechst and (c) overlay, scale bar = 25  $\mu\text{m}$ . TEM images of (d) delivered MSNs/*cyt. c*@CPE-LBs into CP<sub>4</sub>K<sub>4</sub> pretreated HeLa cells. Scale bar = 2  $\mu\text{m}$ , (e) magnification showing details of cell organelles' structures, such as rough ER and mitochondria, scale bar = 500 nm.

To obtain more details on the intracellular location of the MSNs upon CP<sub>4</sub>K<sub>4</sub> / CP<sub>4</sub>E<sub>4</sub> mediated delivery, we sectioned the cells. TEM imaging revealed the different stages of the intracellular uptake processes in HeLa cells. A fraction of the MSNs was still outside of the cell, some were entering into the cytoplasm and others had already entered the cytosol (Figure 4.3d). The MSNs were located close to mitochondria and rough ER and seemed to be aggregated (Figure 4.3e). A possible explanation might be that upon the delivery into the cells, the MSNs lose their lipid bilayers and bare MSNs are known for their tendency to aggregate. Strikingly, no membrane was observed around the aggregated MSNs, suggesting that the nanoparticles were not captured in endosomes or lysosomes. In comparison, the cell uptake efficiency of bare MSNs is relatively low (Figure 4.S3c). More importantly, in the control experiment the MSNs were located in early endosomal compartments as evidenced by the presence of a membrane bilayer (Figure 4.S4). These results show that coiled-coil driven membrane fusion enhances the cellular uptake.<sup>14</sup>

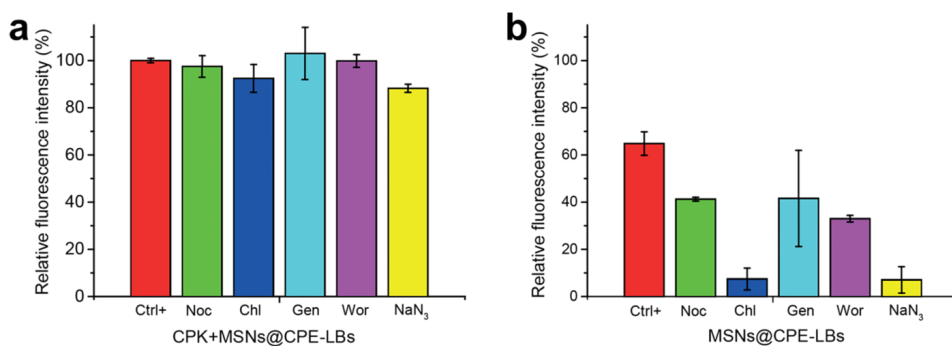


**Figure 4.4** *Mechanistic cellular uptake study. Intracellular uptake of a lipid bilayer coated MSNs in the presence of endocytosis/micropinocytosis inhibitors. (a) Coiled-coil mediated cellular uptake of cyt. c and (b) control experiment in which CP<sub>4</sub>K<sub>4</sub> was omitted, only MSNs@CPE-LBs were tested with endocytosis and micropinocytosis inhibitors. Ctrl+ = HeLa cells incubated with PBS; Noc = Nocodazole; Chl = Chlorpromazine; Gen = Genistein; Wor = Wortmannin; NaN<sub>3</sub> = Sodium azide. Error bars show the standard deviation of three independent experiments.*

To gain insight in the cellular uptake pathways, we repeated the lipid bilayer coated MSNs delivery in the presence of several well-known inhibitors using flow cytometry measurements (FACS) and confocal microscopy imaging. In this study, wortmannin was used as a micropinocytosis inhibitor as it blocks PI3-kinase<sup>59-62</sup> while genistein inhibits tyrosine-

phosphorylation of Cav 1 and caveolin-dependent endocytosis.<sup>63-65</sup> Furthermore, chlorpromazine was used as it blocks clathrin-dependent endocytosis,<sup>66-68</sup> and microtubule formation was inhibited by nocodazole. Uptake studies in the presence of these inhibitors will yield information on the intracellular trafficking and internalization mechanisms involved in the uptake of the lipid bilayer coated MSNs.<sup>61, 62, 68-70</sup> Finally, as endocytosis of nanoparticles is an energy-dependent process, sodium azide was used to deplete the energy demands for endocytosis and thus restrict metabolic activity.<sup>71, 72</sup>

HeLa cells were pre-incubated for 1 h with the above-mentioned inhibitors. After removal of the medium, the cells were treated with CP<sub>4</sub>K<sub>4</sub> (5 μM) for 2 h and subsequently MSNs@CPE-LBs were added in the presence of freshly added inhibitors in the medium. FACS analysis revealed that genistein, wortmannin and nocodazole had no adverse effect on the delivery of fluorescently labeled *cyt. c* (Figure 4.4a), whereas in the presence of chlorpromazine and sodium azide, uptake of nanoparticles containing *cyt. c* was slightly lowered to 90% as compared to *cyt. c* uptake in the absence of inhibitors. To further study the role of coiled-coil formation in the mechanism of cellular uptake, we omitted the CP<sub>4</sub>K<sub>4</sub> pretreatment of HeLa cells in a control experiment and added the MSNs/*cyt.c*@CPE-LBs directly to the cells. In the absence of inhibitors, the *cyt. c* uptake was already lowered to 60%, revealing the importance of coiled-coils for the efficient cellular uptake of the nanoparticles. In the presence of chlorpromazine and sodium azide, the uptake was sharply reduced to 10% (Figure 4.4b), which is in strong contrast with the previous experiments when CP<sub>4</sub>K<sub>4</sub> was present, enabling coiled-coil mediated uptake (Figure 4.4a). This indicates that the nanoparticles are most likely taken up by a clathrin-dependent endocytosis pathway in the control experiment. Combining these inhibition studies indicated the dominant pathway for coiled-coil mediated MSNs delivery is most likely via membrane fusion between lipid bilayer coated MSNs and the cell membrane. In contrast, when coiled-coil formation cannot occur, the dominant but less efficient route of cellular uptake is via endocytosis.



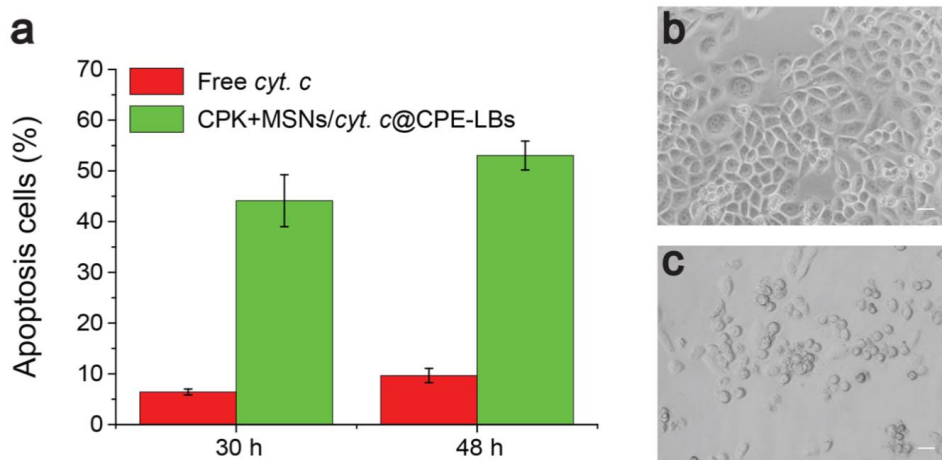


**Figure 4.5** Cytoplasmic *cyt. c* delivery induces apoptosis. (a) Percentage of apoptotic cells as measured by caspase activity, after 30 h and 48 h. Image of HeLa cells treated with (b) *cyt. c* and (c) MSNs/*cyt. c*@CPE-LBs where coiled-coil formation. HeLa cells were incubated with CP<sub>4</sub>K<sub>4</sub> for 1 h, then with MSNs/*cyt. c*@CPE-LBs for 0.5 h. Caspase activity was determined after 30 h and 48 h. Error bars are standard deviation of three independent experiments. Scale bar =25  $\mu$ m.

It is well-known *cyt. c* in the cytosol triggers caspase activation,<sup>73-75</sup> which ultimately results in apoptosis of the cell.<sup>51,76</sup> Coiled-coil mediated delivery and bioactivity of *cyt. c* via MSNs/*cyt. c*@CPE-LBs resulted in 60% of apoptosis after 48 h (Figure 4.5a), while free *cyt. c* induced only minor apoptosis (10%). The morphological changes of apoptotic HeLa cells versus healthy cells upon *cyt. c* delivery were evident (Figure 4.5b,c). In control experiments where one or both of the lipopeptides were omitted only minimal levels of apoptosis (< 10%) were observed, revealing that coiled-coil mediated delivery of MSNs@LBs is more efficient when compared to delivery via endocytic pathways (Figure 4.S5).

#### 4.4 Conclusion

In conclusion we have developed MSNs with a high loading capacity for *cyt. c* due to their large disc-shaped cavities. The introduction of a lipid bilayer at the MSNs outer surface improved the colloidal stability and lowered the initial burst release of *cyt. c*. The cellular uptake of the MSNs resulting in cytosolic delivery of *cyt. c* was significantly enhanced by coiled-coil mediated membrane fusion. As a result, direct cytosolic delivery of *cyt. c* was

achieved while uptake via endocytosis was minimized. The uptake pathway and localization of MSNs/*cyt. c* in HeLa cells were confirmed by TEM and confocal imaging, and release of functional *cyt. c* was demonstrated by its ability to trigger apoptosis. We believe that our coiled-coil based system is suitable for delivery of other proteins or high molecular weight compounds due to the large pore size of the MSNs. This method will also enable the delivery of any other (in)organic nanoparticles as long as it can be encapsulated in a fusogenic lipid bilayer. Therefore it may have applications in the field of biomedicine and diagnostics.

## Supporting Information

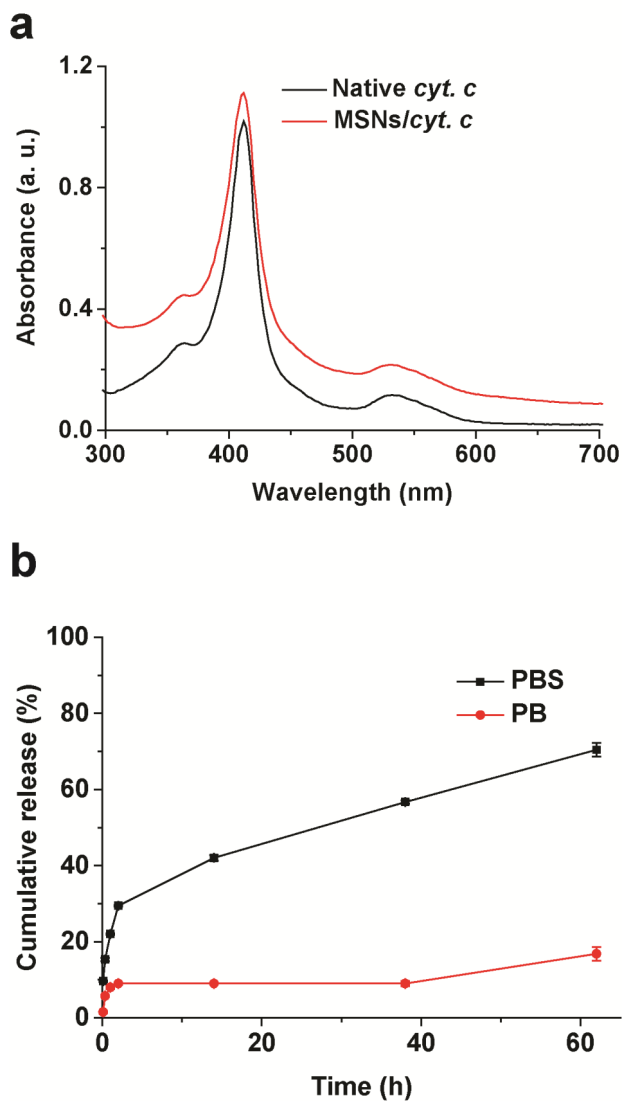


**Figure 4.S1** (a) UV-Visible adsorption spectra of free cyt. c and MSNs/cyt. c in 1 mM, pH 7.4. (b) Release profiles of MSNs/cyt. c in 1 mM PB and PBS, pH 7.4, 37 °C. Error bars show the standard deviation of three independent experiments.

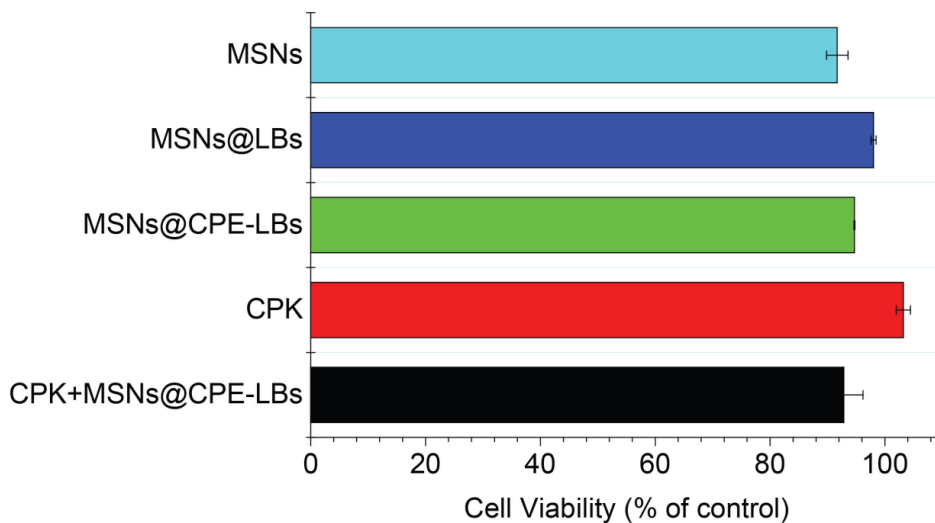


**Figure 4.S2** Cell viability by WST-1 of HeLa cells exposed to MSNs, MSNs@LBs with lipid composition of DOPC:DOPE:CHO (2:1:1), MSNs@CPE-LBs, CP<sub>4</sub>K<sub>4</sub> and combinations thereof. Metabolic activity of untreated cells is 100%. Final concentrations: MSNs: 40  $\mu$ g/ml, total lipids; 0.25 mM; CP<sub>4</sub>K<sub>4</sub>, CPE: 5  $\mu$ M. Error bars show the standard deviation of three independent experiments.

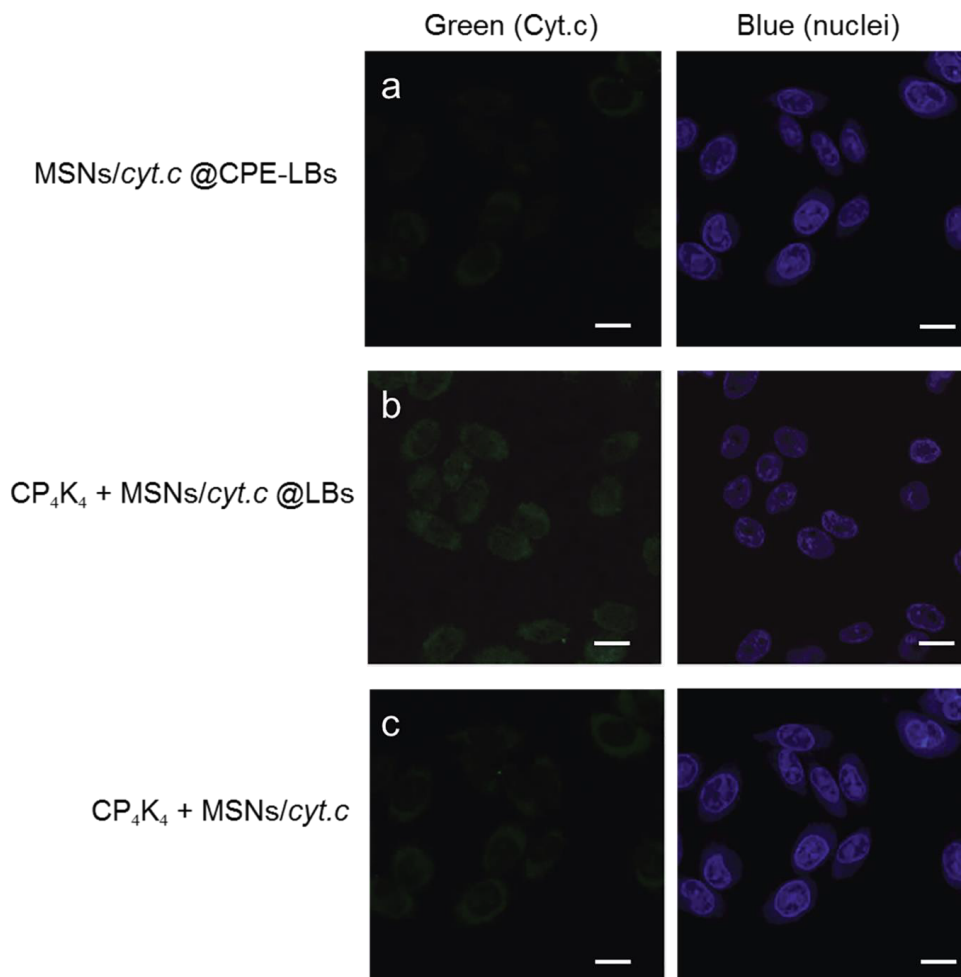


**Figure 4.S3** Delivery of *cyt. c* by *MSNs@LBs* is dependent on coiled-coil formation between *CP<sub>4</sub>K<sub>4</sub>* and *CP<sub>4</sub>E<sub>4</sub>*. Confocal microscopy images of HeLa cells. Cells were pre-incubated with *CP<sub>4</sub>K<sub>4</sub>* (b, c) or medium (a) for 2 h, followed by incubation with *MSNs/cyt. c@LBs* coated with peptide CPE (a) or no lipopeptide coating (b) and LBs coating (c) for 30 min. Images were taken after washing the cells several times with medium. Left panels: Atto 488 labeled *cyt. c*. Right panels: Hoechst staining. The final concentration of *MSNs* was 40  $\mu\text{g/ml}$ . Scale bar = 25  $\mu\text{m}$ .

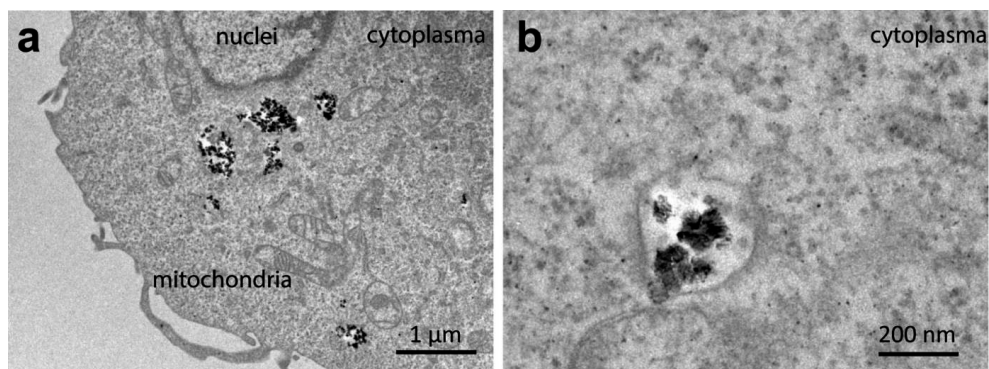


**Figure 4.S4** TEM images of HeLa cells. a) HeLa Cells were treated with bare MSNs for 0.5 h, after 3 times washing by medium, TEM images were taken. b) Magnification showing details of delivery, such as endosomal/lysosomal membrane.

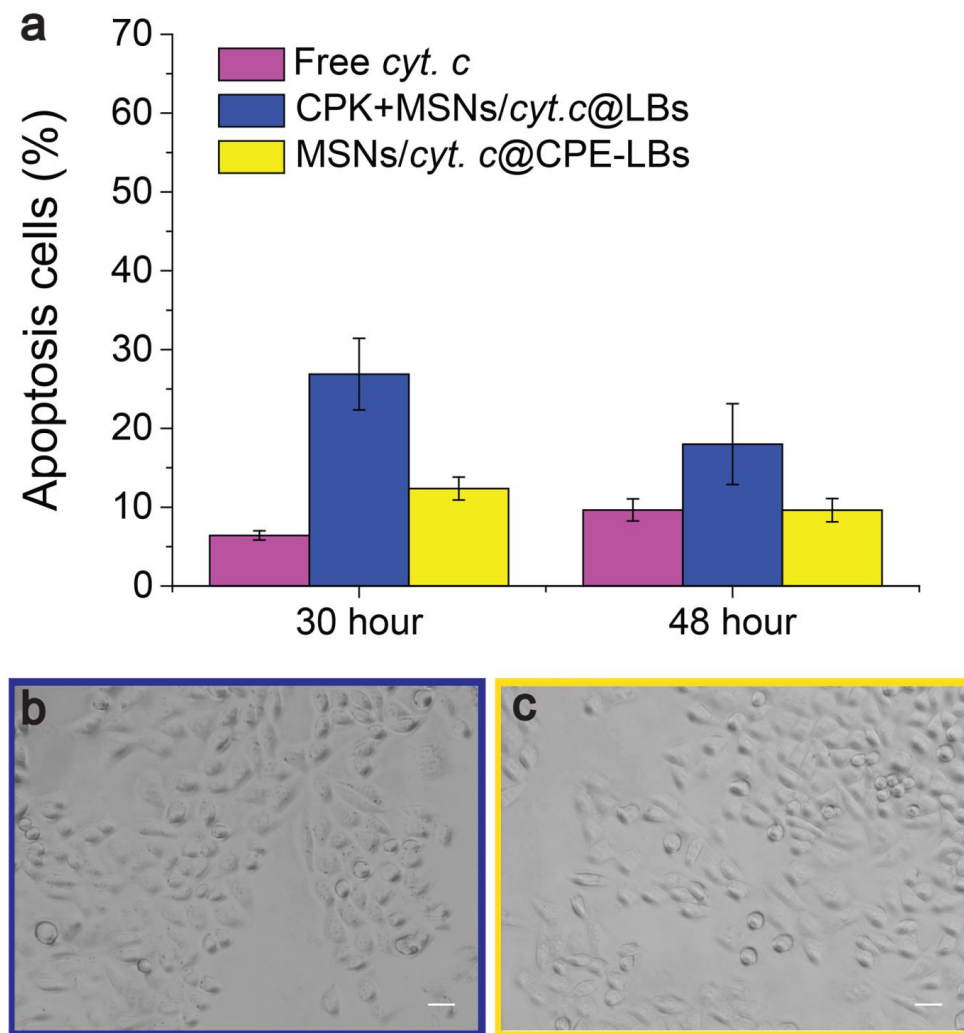


**Figure 4.S5** Apoptosis induced by MSNs/cyt. c@LBs in the absence of coiled-coil formation. a) HeLa cells were incubated with free cyt.c (purple bars), CP<sub>4</sub>K<sub>4</sub> and MSNs/cyt.c @LBs (blue bars), or only MSNs/cyt. c@CPE-LBs (yellow bars). After several washing steps with medium apoptosis was assayed 30 h or 48 h later as described before. b) CP<sub>4</sub>K<sub>4</sub> pre-treated cells incubated with MSNs/cyt.c@LBs. c) HeLa cells incubated with MSNs/cyt.c@CPE-LBs after 30 h treatment. Apoptotic cells are rarely seen in b and c. Error bars show the standard deviation of three independent experiments. Scale bar = 25  $\mu$ m.

#### 4.5 References

1. Z. Gu, A. Biswas, M. Zhao and Y. Tang, *Chem. Soc. Rev.*, **2011**, 40, 3638-3655.
2. J. Ambati, A. M. Lopez, D. Cochran, P. Wattamwar, K. Bean, T. D. Dziubla and S. E. Rankin, *Acta Biomater.*, **2012**, 8, 2096-2103.
3. S. M. Kelly, T. J. Jess and N. C. Price, *Biochim. Biophys. Acta, Proteins Proteomics*, **2005**, 1751, 119-139.
4. F. P. Chang, Y. P. Chen and C. Y. Mou, *Small*, **2014**, 10, 4785-4795.
5. M. C. Manning, D. K. Chou, B. M. Murphy, R. W. Payne and D. S. Katayama, *Int. J. Pharm. Res.*, **2010**, 27, 544-575.
6. Y. Ikada and Y. Tabata, *Adv. Drug Delivery Rev.*, **1998**, 31, 287-301.
7. S. Lee, J. H. Ryu, K. Park, A. Lee, S. Y. Lee, I. C. Youn, C. H. Ahn, S. M. Yoon, S. J. Myung, D. H. Moon, X. Chen, K. Choi, I. C. Kwon and K. Kim, *Nano Lett.*, **2009**, 9, 4412-4416.
8. T. Vermonden, R. Censi and W. E. Hennink, *Chem. Rev.*, **2012**, 112, 2853-2888.
9. R. Censi, P. Di Martino, T. Vermonden and W. E. Hennink, *J. Controlled Release*, **2012**, 161, 680-692.
10. S. Martins, B. Sarmento, D. C. Ferreira and E. B. Souto, *Int. J. Nanomed.*, **2007**, 2, 595-607.
11. B. Chatin, M. Mevel, J. Devalliere, L. Dallet, T. Haudebourg, P. Peuziat, T. Colombani, M. Berchel, O. Lambert, A. Edelman and B. Pitard, *Mol. Ther.--Nucleic Acids*, **2015**, 4, e244.
12. E. Erikci, M. Gursel and I. Gursel, *Biomaterials*, **2011**, 32, 1715-1723.
13. S. P. Hudson, R. F. Padera, R. Langer and D. S. Kohane, *Biomaterials*, **2008**, 29, 4045-4055.
14. J. L. Vivero-Escoto, Slowing, II, B. G. Trewyn and V. S. Lin, *Small*, **2010**, 6, 1952-1967.
15. C. Argyo, V. Weiss, C. Bräuchle and T. Bein, *Chem. Mater.*, **2014**, 26, 435-451.
16. M. Y. Wu, Q. S. Meng, Y. Chen, L. X. Zhang, M. L. Li, X. J. Cai, Y. P. Li, P. C. Yu, L. L. Zhang and J. L. Shi, *Adv. Mater.*, **2016**, 28, 1963-1969.
17. T. L. Liu, H. Y. Liu, C. H. Fu, L. L. Li, D. Chen, Y. Q. Zhang and F. Q. Tang, *J. Colloid Interface Sci.*, **2013**, 400, 168-174.
18. J. Tu, T. X. Wang, W. Shi, G. S. Wu, X. H. Tian, Y. H. Wang, D. T. Ge and L. Ren, *Biomaterials*, **2012**, 33, 7903-7914.
19. S. Heidegger, D. Gossl, A. Schmidt, S. Niedermayer, C. Argyo, S. Endres, T. Bein and C. Bourquin, *Nanoscale*, **2016**, 8, 938-948.
20. S. H. van Rijt, D. A. Bölükbas, C. Argyo, S. Datz, M. Lindner, O. Eickelberg, M. Königshoff, T. Bein and S. Meiners, *ACS Nano*, **2015**, 9, 2377-2389.
21. C. E. Ashley, E. C. Carnes, G. K. Phillips, D. Padilla, P. N. Durfee, P. A. Brown, T. N. Hanna, J. Liu, B. Phillips, M. B. Carter, N. J. Carroll, X. Jiang, D. R. Dunphy, C. L. Willman, D. N. Petsev, D. G. Evans, A. N. Parikh, B. Chackerian, W. Wharton, D. S. Peabody and C. J. Brinker, *Nat. Mater.*, **2011**, 10, 389-397.
22. D. Mahony, A. S. Cavallaro, F. Stahr, T. J. Mahony, S. Z. Qiao and N. Mitter, *Small*, **2013**, 9, 3138-3146.
23. G. E. Francis, D. Fisher, C. Delgado, F. Malik, A. Gardiner and D. Neale, *Int. J. Hematol.*, **1998**, 68, 1-18.
24. A. Coscarella, R. Liddi, M. Di Loreto, S. Bach, A. Faiella, P. H. van der Meide, A. Mele and R. De Santis, *Cytokine*, **1998**, 10, 964-969.



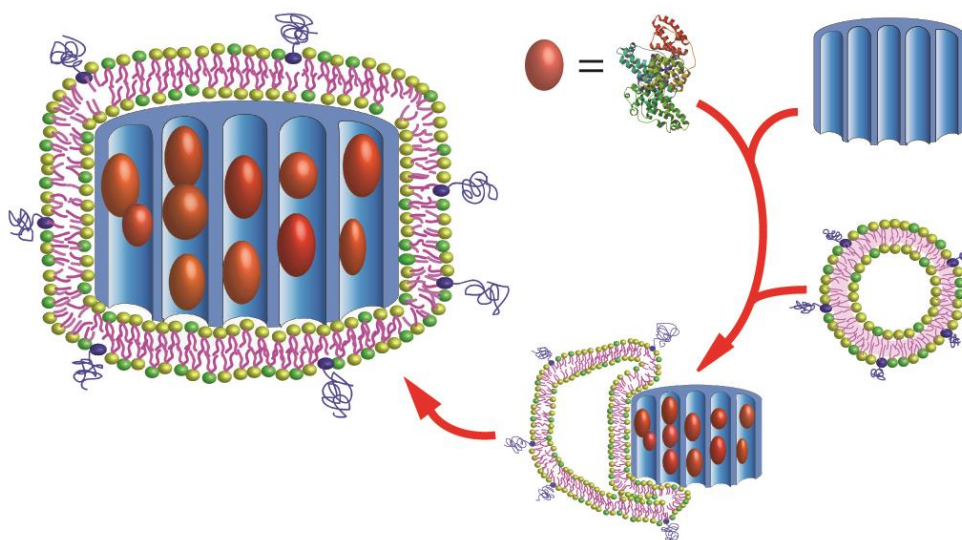
25. E. C. Dengler, J. Liu, A. Kerwin, S. Torres, C. M. Olcott, B. N. Bowman, L. Armijo, K. Gentry, J. Wilkerson, J. Wallace, X. Jiang, E. C. Carnes, C. J. Brinker and E. D. Milligan, *J. Controlled Release*, **2013**, 168, 209-224.
26. J. G. Gribben, S. Devereux, N. S. Thomas, M. Keim, H. M. Jones, A. H. Goldstone and D. C. Linch, *Lancet*, **1990**, 335, 434-437.
27. V. Cauda, H. Engelke, A. Sauer, D. Arcizet, C. Brauchle, J. Radler and T. Bein, *Nano Lett.*, **2010**, 10, 2484-2492.
28. J. Zhang, D. Desai and J. M. Rosenholm, *Adv. Funct. Mater.*, **2014**, 24, 2352-2360.
29. R. A. Roggers, V. S. Lin and B. G. Trewyn, *Mol. Pharm.*, **2012**, 9, 2770-2777.
30. J. W. Liu, A. Stace-Naughton, X. M. Jiang and C. J. Brinker, *J. Am. Chem. Soc.*, **2009**, 131, 1354-1360.
31. H. Meng, M. Wang, H. Liu, X. Liu, A. Situ, B. Wu, Z. Ji, C. H. Chang and A. E. Nel, *ACS Nano*, **2015**, 9, 3540-3557.
32. B. A. Mora N, Valkenier H, Li H, Sharp T, Sheppard D, Davis A and Kros A, *Chem. Sci.*, **2016**, 7, 1768-1772.
33. H. Valkenier, N. Lopez Mora, A. Kros and A. P. Davis, *Angew. Chem., Int. Ed.*, **2015**, 54, 2137-2141.
34. F. Versluis, H. R. Marsden and A. Kros, *Chem. Soc. Rev.*, **2010**, 39, 3434-3444.
35. T. Zheng, J. Voskuhl, F. Versluis, H. R. Zope, I. Tomatsu, H. R. Marsden and A. Kros, *Chem. Commun.*, **2013**, 49, 3649-3651.
36. F. Versluis, J. Voskuhl, B. van Kolck, H. Zope, M. Bremmer, T. Albregtse and A. Kros, *J. Am. Chem. Soc.*, **2013**, 135, 8057-8062.
37. H. R. Marsden, N. A. Elbers, P. H. Bomans, N. A. Sommerdijk and A. Kros, *Angew. Chem., Int. Ed.*, **2009**, 48, 2330-2333.
38. H. R. Marsden, A. V. Korobko, T. Zheng, J. Voskuhl and A. Kros, *Biomater. Sci.*, **2013**, 1, 1046-1054.
39. H. R. Marsden, I. Tomatsu and A. Kros, *Chem. Soc. Rev.*, **2011**, 40, 1572-1585.
40. J. B. Yang, A.; Daudey, G.; Bussmann, J.; Olsthoorn, R.C.L.; Kros, A., *ACS Cent. Sci.*, **2016**, DOI: 10.1021/acscentsci.6b00172.
41. J. Yang, Y. Shimada, R. C. L. Olsthoorn, B. E. Snaar-Jagalska, H. P. Spaink and A. Kros, *ACS Nano*, **2016**, DOI: 10.1021/acsnano.6b01410.
42. J. C. Goldstein, C. Munoz-Pinedo, J. E. Ricci, S. R. Adams, A. Kelekar, M. Schuler, R. Y. Tsien and D. R. Green, *Cell Death Differ.*, **2005**, 12, 453-462.
43. E. P. H. Brunauer S., Teller E., *J. Am. Chem. Soc.*, **1938**, 60, 11.
44. E. P. Barrett, L. G. Joyner and P. P. Halenda, *J. Am. Chem. Soc.*, **1951**, 73, 373-380.
45. Y. Han and J. Y. Ying, *Angew. Chem., Int. Ed.*, **2005**, 44, 288-292.
46. I. I. Slowing, B. G. Trewyn and V. S. Y. Lin, *J. Am. Chem. Soc.*, **2007**, 129, 8845-8849.
47. M. Ishiyama, M. Shiga, K. Sasamoto, M. Mizoguchi and P. G. He, *Chem. Pharm. Bull.*, **1993**, 41, 1118-1122.
48. E. S. Alnemri, D. J. Livingston, D. W. Nicholson, G. Salvesen, N. A. Thornberry, W. W. Wong and J. Yuan, *Cell*, **1996**, 87, 171.
49. B. L. Zhang, Z. Luo, J. J. Liu, X. W. Ding, J. H. Li and K. Y. Cai, *J. Controlled Release*, **2014**, 192, 192-201.
50. E. P. J. Barrett, L. E.; Halenda, P., *J. Am. Chem. Soc.*, **1951**, 73, 373-380.
51. X. Jiang and X. Wang, *Annu. Rev. Biochem.*, **2004**, 73, 87-106.
52. Y. Urabe, T. Shiomi, T. Itoh, A. Kawai, T. Tsunoda, F. Mizukami and K. Sakaguchi, *ChemBioChem*, **2007**, 8, 668-674.
53. C. H. Lee, J. Lang, C. W. Yen, P. C. Shih, T. S. Lin and C. Y. Mou, *J. Phys. Chem. B*, **2005**, 109, 12277-12286.

54. H. S. Park, C. Kim, H. J. Lee, J. H. Choi, S. G. Lee, Y. P. Yun, I. C. Kwon, S. J. Lee, S. Y. Jeong and S. C. Lee, *Nanotechnol.*, **2010**, 21, 225101.
55. J. Liu, X. Jiang, C. Ashley and C. J. Brinker, *J. Am. Chem. Soc.*, **2009**, 131, 7567-7569.
56. H. R. Zope, F. Versluis, A. Ordas, J. Voskuhl, H. P. Spaink and A. Kros, *Angew. Chem., Int. Ed.*, **2013**, 52, 14247-14251.
57. K. Epler, D. Padilla, G. Phillips, P. Crowder, R. Castillo, D. Wilkinson, B. Wilkinson, C. Burgard, R. Kalinich, J. Townson, B. Chackerian, C. Willman, D. Peabody, W. Wharton, C. J. Brinker, C. Ashley and E. Carnes, *Adv. Healthcare Mater.*, **2012**, 1, 348-353.
58. C. E. Ashley, E. C. Carnes, K. E. Epler, D. P. Padilla, G. K. Phillips, R. E. Castillo, D. C. Wilkinson, B. S. Wilkinson, C. A. Burgard, R. M. Kalinich, J. L. Townson, B. Chackerian, C. L. Willman, D. S. Peabody, W. Wharton and C. J. Brinker, *ACS Nano*, **2012**, 6, 2174-2188.
59. A. Arcaro and M. P. Wymann, *Biochem. J.*, **1993**, 296, 297-301.
60. N. Araki, M. T. Johnson and J. A. Swanson, *J. Cell Biol.*, **1996**, 135, 1249-1260.
61. C. K. Payne, S. A. Jones, C. Chen and X. Zhuang, *Traffic*, **2007**, 8, 389-401.
62. S. Coppola, L. C. Estrada, M. A. Digman, D. Pozzi, F. Cardarelli, E. Gratton and G. Caracciolo, *Soft Matter*, **2012**, 8, 7919-7927.
63. N. P. Gabrielson and D. W. Pack, *J. Controlled Release*, **2009**, 136, 54-61.
64. T. Akiyama, J. Ishida, S. Nakagawa, H. Ogawara, S. Watanabe, N. Itoh, M. Shibuya and Y. Fukami, *J. Biol. Chem.*, **1987**, 262, 5592-5595.
65. P. A. Orlandi and P. H. Fishman, *J. Cell Biol.*, **1998**, 141, 905-915.
66. L. H. Wang, K. G. Rothberg and R. G. Anderson, *J. Cell Biol.*, **1993**, 123, 1107-1117.
67. K. von Gersdorff, N. N. Sanders, R. Vandenbroucke, S. C. De Smedt, E. Wagner and M. Ogris, *Mol. Ther.*, **2006**, 14, 745-753.
68. U. S. Huth, R. Schubert and R. Peschka-Suss, *J. Controlled Release*, **2006**, 110, 490-504.
69. J. Rejman, V. Oberle, I. S. Zuhorn and D. Hoekstra, *Biochem. J.*, **2004**, 377, 159-169.
70. C. Goncalves, E. Mennesson, R. Fuchs, J. P. Gorvel, P. Midoux and C. Pichon, *Mol. Ther.*, **2004**, 10, 373-385.
71. S. Simoes, V. Slepushkin, N. Duzgunes and M. C. Pedroso de Lima, *Biochim. Biophys. Acta*, **2001**, 1515, 23-37.
72. H. Gao, Z. Yang, S. Zhang, S. Cao, S. Shen, Z. Pang and X. Jiang, *Sci. Rep.*, **2013**, 3, 2534.
73. X. Liu, C. N. Kim, J. Yang, R. Jemmerson and X. Wang, *Cell*, **1996**, 86, 147-157.
74. R. M. Kluck, E. Bossy-Wetzel, D. R. Green and D. D. Newmeyer, *Science*, **1997**, 275, 1132-1136.
75. Q. Chen, N. Takeyama, G. Brady, A. J. Watson and C. Dive, *Blood*, **1998**, 92, 4545-4553.
76. Q. Chen, B. Gong and A. Almasan, *Cell Death Differ.*, **2000**, 7, 227-233.

# Chapter V

## Lipid Bilayer-Coated Mesoporous Silica Nanoparticles

### Carrying Bovine Hemoglobin as an Erythrocyte Mimic



Jing Tu, Jeroen Bussmann, Guangsheng Du, Yue Gao, Joke A. Bouwstra, Alexander Kros

**Abstract**

Hemoglobin (Hb)-loaded mesoporous silica nanoparticles (MSNs) coated with a lipid bilayer (LB-MSNs) were investigated as an erythrocyte mimic. MSNs with a large average pore size (10 nm) act as a rigid core and provide a protective environment for Hb encapsulated inside the pores. The colloidal stability of Hb-loaded MSNs was enhanced upon the application of a lipid bilayer, through fusion of PEGylated liposomes onto the exterior surface of Hb-loaded MSNs. The morphology and mesostructure of the MSNs were characterized by scanning electron microscopy (SEM), transmission electron microscopy (TEM) and surface area analysis. The Hb loading capacity (LC%) in MSNs was studied by thermogravimetric analysis (TGA). UV-Visible absorption spectroscopy revealed that Hb inside MSNs had an identical, but slightly broadened peak in the Soret region compared to free Hb. Furthermore the encapsulated Hb exhibits similar peroxidase-like activity in catalyzing the oxidation of 2,2'-azino-bis(3-ethylbenzothiazoline-6-sulfonic acid) diammonium salt (ABTS) with hydrogen peroxide. The introduction of a supported lipid bilayer (LB) demonstrated the potential to prevent premature Hb release and increased the colloidal stability of the Hb-loaded MSNs. The *in vivo* systemic circulation and biodistribution of LB-MSNs were studied in optically transparent zebrafish embryos, revealing that LB-MSNs have the potential to act as an erythrocyte mimic.

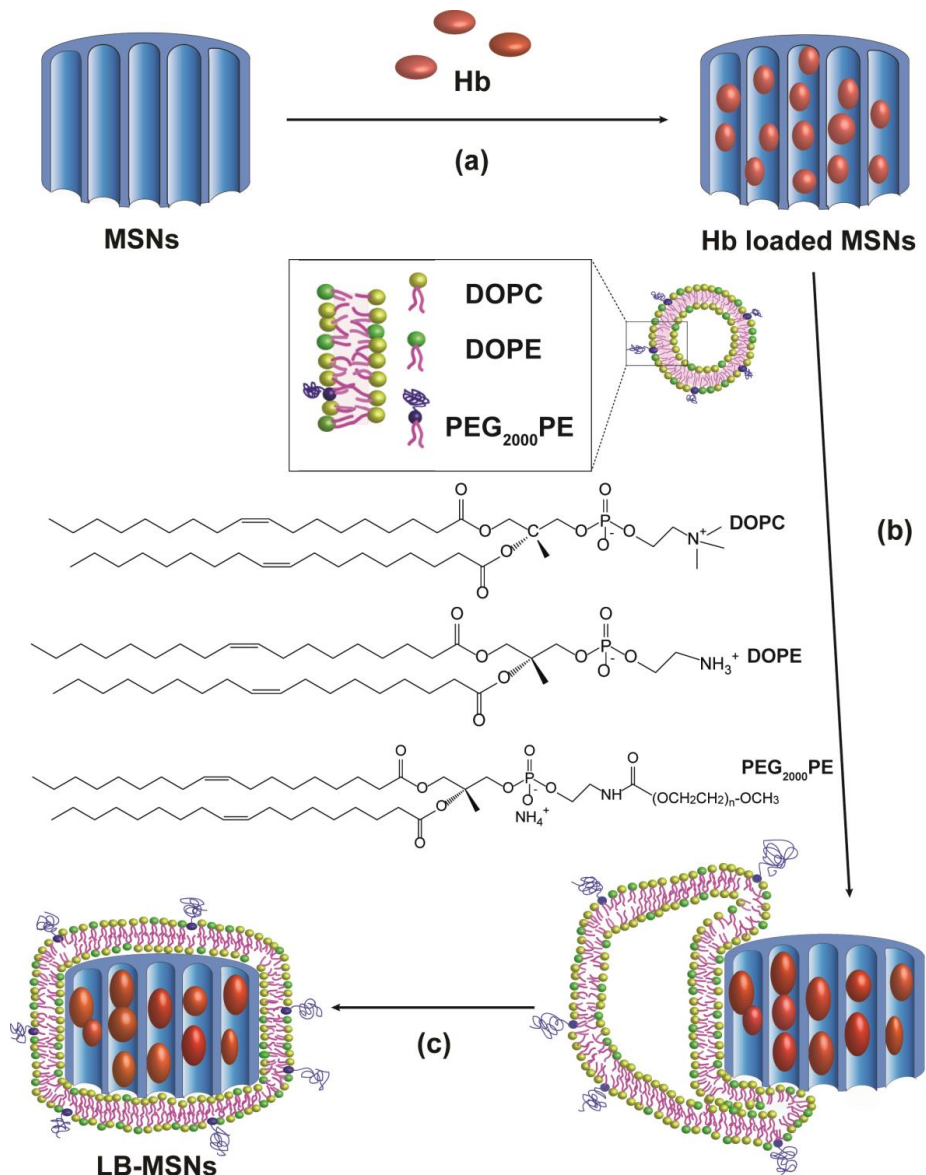
**Keywords:** mesoporous silica nanoparticles, hemoglobin, lipid bilayer, zebrafish embryos, erythrocyte mimic

## 5.1 Introduction

Due to the shortage of blood donations and the risks associated with allogenic donor blood transfusion, such as virus infection, and unmatched blood types, artificial red blood cell (RBC) substitutes have been investigated intensively during the past decades.<sup>1-3</sup> To mimic and fulfil some functions of RBCs, there are two main types of artificial RBC substitute in development.<sup>2, 4</sup> Apart from perfluorocarbon emulsion-based substitutes,<sup>5</sup> hemoglobin (Hb,  $6.5 \times 5.4 \times 5.5$  nm, Mw 64500)-based oxygen carriers (HBOC) have attracted increasing attention.<sup>6</sup> Hb is the essential oxygen carrying protein in erythrocytes.<sup>7</sup> Pioneering work was performed with stroma-free Hb,<sup>2, 8-11</sup> which unfortunately was unsuitable because it induces side effects such as vasoconstriction and renal toxicity in mammals.<sup>12-14</sup> Therefore several approaches have been explored to overcome these challenges, including nanocarriers such as lipid vesicles<sup>14</sup> and biodegradable polymers.<sup>12</sup> The emerged focus on the encapsulation of Hb into nanosized carriers<sup>15</sup> is because nanoparticle-based erythrocyte mimics offer several distinct advantages, including 1) prevention of vasoconstriction, 2) avoidance of renal toxicity, and 3) the protection of Hb from degradation in bodily fluids to prolong the circulation time.<sup>12</sup>

Liposome-based carriers of Hb are one of the most important HBOC formulations and have been widely studied.<sup>14-16</sup> Liposome-encapsulated Hb with a size of 250 nm have been proved its safety and the elimination of vasoconstriction.<sup>15, 17</sup> However, plain liposomes are fragile and easily deform when exposed to fluid shear stresses.<sup>14</sup> Many strategies have been investigated to increase the liposome's mechanical strength, like using solid silica nanoparticle (diameter ~10 nm) as core for a rigid support,<sup>7</sup> introducing an actin matrix inside the aqueous core of submicron liposomes.<sup>7, 14</sup> Mesoporous silica nanoparticles (MSNs) can be used as protein delivery carriers due to their unique properties, namely biocompatibility, chemical inertness, large surface area and controllable pore size.<sup>18-21</sup> Inspired by nature, Brinker and others reported a versatile nanocarrier that synergistically integrates the advantages of liposomes with MSNs, resulting in lipid bilayer (LB) coated MSNs with a so-called "protocell" structure (Scheme 5.1).<sup>18-20, 22-24</sup> The electrostatic interaction of zwitterionic liposomes with the negatively charged MSNs surface, results in vesicle rupture and concomitant bilayer formation. As a result, the MSNs pores are sealed and entrapped the drug of interest inside the MSNs.<sup>18, 19, 22, 25</sup> Furthermore, the lipid bilayer act as an immune-isolative barrier, which can prevent recognition by the reticuloendothelial system and as a result enhance the circulation time.<sup>26</sup> Recently, nanosized-MSNs with large pore diameters (10 nm) and therefore capable of accommodating Hb inside have been developed in our group.

To increase the colloidal stability under physiological conditions and biocompatibility, a lipid bilayer was applied (LB-MSNs).<sup>27</sup> In addition, the charge-neutral highly hydrophilic polymer polyethylene glycol (PEG) was incorporated in the lipid bilayer to induce stealth-like behavior.<sup>14, 28</sup>



**Scheme 5.1** Procedure for the formation of LB-MSNs. (a) Encapsulation of Hb into the MSNs, followed by fusion of (b) liposome (composed of DOPC/DOPE/PEG<sub>2000</sub>PE), resulting in (c) LB-MSNs (i.e. protocell).

Herein, we demonstrate a facile method to prepare liposome encapsulated Hb-loaded MSNs (LB-MSNs) as a potential oxygen carrier. MSNs with a 10 nm channel diameter are used to accommodate Hb. To improve the colloidal stability of these Hb-loaded MSNs, a supported lipid bilayer was introduced to decorate the outer surface of Hb-loaded MSNs resulting in a core-shell structure. The preparation of these nanoparticles is schematically illustrated in Scheme 1. The presence of a lipid bilayer lowers the premature release of Hb. Circulation and distribution studies were performed in zebrafish embryos in order to investigate the *in vivo* behavior of these lipid bilayer coated MSNs.

## 5.2 Experimental Section

### 5.2.1 Materials

Bovine hemoglobin (Hb,  $M_w \sim 64500$ ), Pluronic P123 ( $EO_{20}PO_{70}EO_{20}$ ,  $M_n \sim 5800$ ), tetraethyl orthosilicate (TEOS,  $\geq 98\%$ ), hydrochloric acid (HCl), 1,3,5-trimethylbenzene (TMB), 2',2'-azino-bis (3-ethylbenzothiazoline-6-sulfonic) acid (ABTS) and fluorescein isothiocyanate were purchased from Sigma-Aldrich and used as received. 1,2-dioleoyl-sn-glycero-3-phosphocholine (DOPC), 1,2-dioleoyl-sn-glycero-3-phosphoethanolamine (DOPE), 1,2-dioleoyl-sn-glycero-3-phosphoethanolamine-N-[methoxy(polyethylene glycol)-2000] (ammonium salt) (PEG<sub>2000</sub>PE) and 1,2-dioleoyl-sn-glycero-3-phosphoethanolamine-N-(lissamine rhodamine B sulfonyl) (ammonium salt) (DOPE-LR) were purchased from Avanti Polar Lipids. Fluorocarbon surfactant FC-4 was purchased from Yick-Vic Chemicals & Pharmaceuticals (HK) Ltd. Sephadex G25 was purchased from GE Healthcare Life Sciences. The composition of the phosphate buffered saline (PBS) used was:  $K_2HPO_4$  (14.99 mM),  $KH_2PO_4$  (5 mM), and NaCl (150.07 mM), with an ionic strength of 270 mM. The phosphate buffer (PB) with an ionic strength of 12 mM was prepared by mixing  $Na_2HPO_4$  (1 mM) and  $NaH_2PO_4$  (1 mM) at molar ratio of 5:2. Milli-Q water (18.2 M $\Omega$ /cm, Millipore Co., USA) was used throughout the experiment. All Hb solutions for the experiments are freshly prepared before each experiment.

### 5.2.2 Synthesis of large-pore MSNs

MSNs were synthesized as follows. 0.5 g of surfactant Pluronic P123 and 1.4 g of FC-4 were dissolved in 80 mL of HCl (0.02 M), followed by the introduction of 0.48 mL of TMB. After stirring for 6 h, 2.14 mL of TEOS was added dropwise. The resulting mixture was stirred at 30 °C for 24 h and transferred to an autoclave at 120 °C for 2 days. Finally, the solid

product was isolated by centrifugation, and washed with ethanol and water. The organic template was completely removed by calcination at 550 °C for 5 h.

### 5.2.3 Preparation of liposome

Liposomes were prepared by dispensing stock solutions of DOPC (80 µl, 25 mg/mL), DOPE (40 µl, 25 mg/mL), and PEG<sub>2000</sub>-PE (30 µl, 25 mg/mL) into scintillation vials. All lipids were dissolved in chloroform. A lipid film was formed by slow evaporation of chloroform in the vial under a nitrogen flow and kept under vacuum overnight. The lipid film was rehydrated by the addition of phosphate buffer (2 mL, 1 mM, pH 7.4) and the mixture was vortexed to form a cloudy lipid suspension. The obtained suspension was sonicated in a water bath (50 °C) for 10 min. If necessary, fluorescent lipids (DOPE-LR) were incorporated into the lipid mixture at 1 wt% to make fluorescent liposomes. The resulting liposomes were stored at 4 °C (final lipid concentration was 1.875 mg/mL).

### 5.2.4 Loading Hb into MSNs

MSNs were dispersed in phosphate buffer (PB, 1 mM, pH 7.4) at a concentration of 2 mg/mL and sonicated for 10 min. 0.5 mL of MSNs were mixed with a series of Hb with relatively low concentrations (0-700 µg/mL, 0.5 mL) and shaken using an Eppendorf mixer (400 rpm, 25 °C) for 10 min. Hb-loaded MSNs were collected by centrifugation (14000 rpm, 5 min) for further physical characterization and the amount of non-encapsulated Hb in the supernatant was quantified using a Tecan M1000 plate reader. A calibration curve was determined based on the absorbance at 405 nm as a function of Hb concentration (0-350 µg/mL).

The maximum loading capacity (LC%) of Hb in MSNs can be obtained by thermogravimetric analysis (TGA),<sup>2</sup> the same loading procedure was repeated by mixing MSNs suspensions and Hb with higher initial concentrations (0, 0.25, 0.5, 1, 1.5, 2, 3 and 4 mg/mL). Before thermogravimetric analysis (TGA), Hb-loaded MSNs were freeze-dried until the weight was constant. The loading capacity (LC%) was calculated according to equation 5.1:<sup>29</sup>

$$LC \% = \frac{\text{Loading}_{\text{Hb}}}{\text{Loading}_{\text{Hb}} + \text{MSNs}} \times 100 \% \quad (5.1)$$

Where  $\text{Loading}_{\text{Hb}}$  represents the amount of Hb absorbed in the MSNs.



### *5.2.5 Preparation of LB-MSNs*

To prepare LB-MSNs, 0.5 mL of Hb (0.5 mg/mL, PB) was transferred into a 2-mL Eppendorf tube, followed by the addition of a MSNs suspension (0.5 mL, 2 mg/mL). After shaking for 10 min, Hb-loaded MSNs were isolated by centrifugation. A dispersion (0.5 mL) of Hb-loaded MSNs (1 mg/mL) in PB (1 mM, pH 7.4) liposomes (composed of DOPC, DOPE, PEG<sub>2000</sub>PE). The mixture was for 1.5 h (400 rpm, 25 °C). LB-MSNs were separated by centrifugation (13000 rpm, 5 min) from the excess of liposomes in the supernatant and then washed 3 times with PB. The hydrodynamic diameter and zeta-potential as a function of time were determined in 1 mM PB (pH 7.4) using a Malvern Nano-zs instrument. Hb-loaded MSNs (1:4 w/w) were used as control.

### *5.2.6 Characterization of MSNs, Hb-loaded MSNs and LB-MSNs*

The morphology and mesostructure of the MSNs were characterized with scanning electron microscopy (SEM) and transmission electron microscopy (TEM). SEM imaging was conducted using a NovaSem microscope with an accelerating voltage of 15 kV and TEM imaging was conducted on a JEOL 1010 instrument with an accelerating voltage of 70 kV. Nitrogen adsorption-desorption isotherms were obtained with a Micromeritics TrisStar II 3020 surface area analyzer. Before the measurements, MSNs (at 300 °C) and Hb-loaded MSNs (at 25 °C) were outgassed in the instrument for 16 h under vacuum (< 0.15 mbar). The specific surface areas were calculated from the adsorption data in the low pressure range using the Brunauer-Emmett-Teller (BET) model.<sup>30</sup> The pore size distribution was determined following the Barrett-Joyner-Halenda (BJH) model.<sup>31</sup> The hydrodynamic size distribution and zeta-potential were measured with a Malvern Nano-zs instrument. Thermogravimetric analysis (TGA) was conducted with a Perkin Elmer TGA7. All the samples were tested under an air atmosphere from 25 °C to 800 °C at a heating rate of 10 °C/min. UV-Visible absorbance spectra were measured using 96-well plates with a Tecan M1000 plate reader. LB-MSNs were imaged by fluorescence microscopy (Zeiss Axio imager D2 fluorescence microscope, magnification 100×).

### *5.2.7 Peroxidase-like activity of Hb-loaded MSNs and Hb*

The peroxidase-like activity of Hb after encapsulation by MSNs was measured using 2,2'-azino-bis(3-ethylbenzothiazoline-6-sulfonic acid) diammonium salt (ABTS).<sup>6, 32</sup>

An ABTS solution was prepared by dissolving 15 mg of ABTS in 1 mL MilliQ water and 9 mL acetic acid.<sup>33</sup> Hydrogen peroxide (1 mL, 30% w/w in water) was diluted into 30 mL of MilliQ water. Hb (0.05 and 0.1 mg/mL, 5  $\mu$ l) and Hb-loaded MSNs (0.05 and 0.1 mg/mL, 5  $\mu$ l) were mixed with hydrogen peroxide (150  $\mu$ L) in 96-well plate followed by the immediate addition of the ABTS solution (45  $\mu$ L). The absorbance at 418 nm of the oxidized blue-green ABTS<sup>+</sup> was monitored every 20 sec for 20 min using a plate reader (Tecan infinite M1000). The control experiment was performed by using enzyme-free PBS and plain MSNs (0.05 and 0.1 mg/mL) in PBS. All experiments were performed in triplicate.

### 5.2.8 Labeling of Hb with Fluorescein isothiocyanate

Hb (10 mg) was dissolved in 5 mL of sodium carbonate buffer (100 mM, pH 9). Fluorescein isothiocyanate (FITC) was dissolved in DMSO at 1 mg/mL, and 0.25 mL of the FITC solution was added to the protein solution. The mixture was stirred overnight at 4 °C. The resulting FITC-labelled Hb was purified by size exclusion chromatography using a Sephadex-G25 column and PBS as the eluent.

### 5.2.9 Release profiles of Hb from MSNs and LB-MSNs

The *in vitro* release profiles of Hb from MSNs and LB-MSNs were investigated by suspending Hb-loaded MSNs or LB-MSNs in PBS (warmed to 37 °C, pH 7.4) at a concentration of 1 mg/mL. The solution was incubated at 37 °C using an Eppendorf mixer (400 rpm). At various time points, the solution was centrifuged and the supernatants were replaced with fresh PBS. The released amount of Hb in the supernatant was determined with a Tecan M1000 plate reader. All analyses were performed in triplicate.

### 5.2.10 Zebrafish husbandry

Transgenic zebrafish of the Tg (kdrl:GFP) strain, which has a GFP reporter gene expressed specifically in the endothelial cells,<sup>34-36</sup> resulting in a green fluorescent vasculature. Zebrafish were handled in compliance with the local animal welfare regulations and maintained according to standard protocols (zfin.org). Embryos were raised in egg water (0.21 gm Instant Ocean sea salts in 1 liter of demi water) at 28.5 °C. For the duration of bacterial injections, embryos were kept under anesthesia in egg water containing 0.02% buffered 3-aminobenzoic acid ethyl ester (Tricaine). The

breeding of adult fish was approved by the local animal welfare committee (DEC) of the University of Leiden. All protocols adhered to the international guidelines specified by the EU Animal Protection Directive 2010/63/EU.

#### *5.2.11 Zebrafish injection of LB-MSNs*

A stock solution of LB-MSNs (5 mg/mL) and injected (5  $\mu$ L) into the duct of cuvier. PBS injections were used as a control experiment. Injections were performed using a FemtoJet microinjector (Eppendorf) and a micromanipulator with pulled microcapillary pipettes.

#### *5.2.12 Confocal microscopy imaging*

Embryos were imaged after injection, embedded in 1% low melting point agarose and transferred to a Leica DMIRBE inverted microscope with a Leica SP1 confocal scan head for imaging with 40 or 63 $\times$  lenses. For quantification purposes acquisition settings and area of imaging (in the caudal vein region) were kept the same across the groups.

### **5.3 Results and discussion**

The morphology and mesoporous structure of the MSNs was analyzed by scanning electron microscopy (SEM) and transmission electron microscopy (TEM). From the SEM images, it became apparent that particles were non-spherical, the diameter of the as-prepared MSNs was found to be < 100 nm (Figure 5.1a). The TEM images more clearly visualized that the particles were  $90 \pm 20$  nm long, with an average widths of  $43 \pm 7$  nm (average of 150 nm particles). TEM imaging also revealed that the particles possessed an array of disc-shaped mesochannels that run parallel to the short axis of the MSNs (Figure 5.1b).

To characterize the channels within the cuboidal MSNs and to prove encapsulation of Hb molecules within the channels is possible, nitrogen sorption measurements were performed. Both MSNs and Hb-loaded MSNs, exhibited characteristic type IV isotherms with type H<sub>1</sub> hysteresis loops, showed that these nanoparticles have disc-like mesopores according to International Union of Pure and Applied Chemistry (IUPAC) classification.<sup>37</sup> The presence of encapsulated Hb does reduce the surface area from 506 m<sup>2</sup>/g to 275 m<sup>2</sup>/g. This is in agreement with the reduced average channel diameter from 10 nm (MSNs) to 7 nm (Hb-loaded MSNs), which was confirmed from the desorption branch of the isotherm using the Barrett-

Joyner-Halenda (BJH) method (Figure 5.1c,d). Upon Hb encapsulation, both surface area and pore diameter of the MSNs decreased, indicating that hemoglobin was indeed encapsulated within the channels of the MSNs.

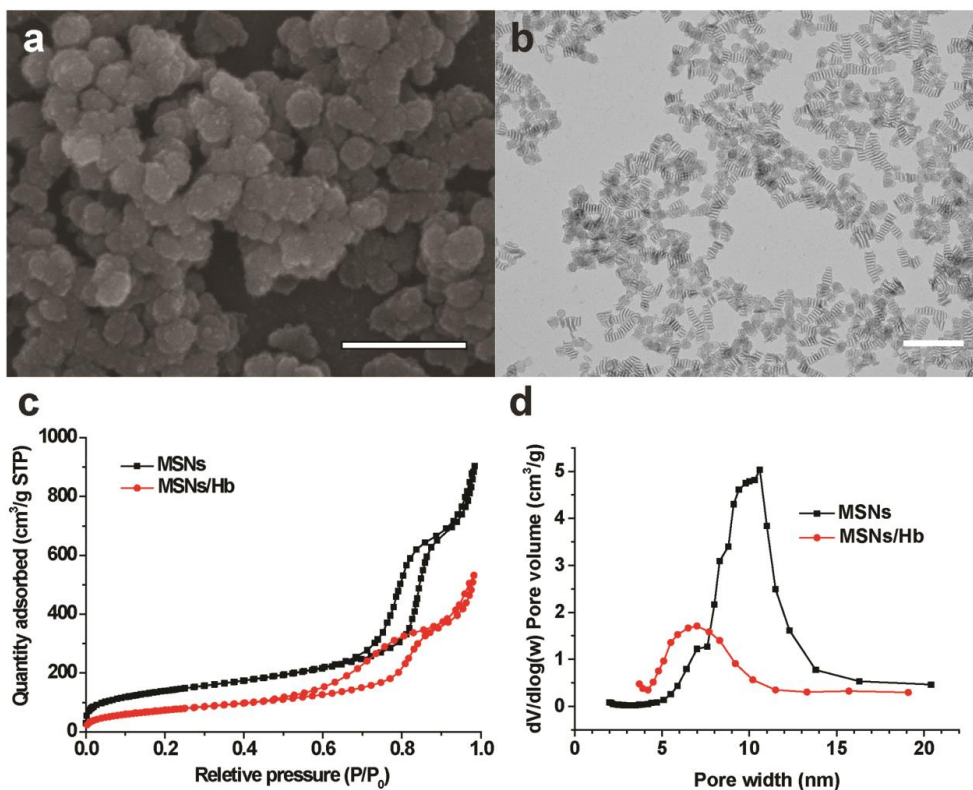


**Figure 5.1** (a and b) SEM and TEM images of MSNs. Scale bar = 250 nm. (c) Nitrogen adsorption-desorption isotherms and (d) plots of pore diameter vs. pore volume, calculated from the desorption isotherms using the BJH model, show that the MSNs and Hb loaded MSNs (146 mg/g) have an average pore diameter of  $10 \pm 1$  nm and  $7.5 \pm 1.5$  nm, respectively.

Thermogravimetric analysis (TGA) is one of most commonly use methods to detect the drug loading efficiency.<sup>2, 37, 38</sup> A half-life of cell-free Hb is relatively short (0.5-1.5 h), because of the dissociation of the Hb tetramer ( $\alpha_2\beta_2$ ) into dimers ( $2\alpha\beta$ ).<sup>10</sup> To reduce the errors, the percentage of Hb loaded within the MSNs was determined by TGA.<sup>2</sup> We observed that the weight loss upon heating the sample corresponding to the amount of Hb inside the MSNs for Hb correlated with the initial Hb concentration. Upon heating, both MSNs (as control) and MSNs/Hb (initial concentration, 4 mg/mL) underwent a total weight loss of 3.8% (H<sub>1</sub>) and 42.1% (H<sub>2</sub>) when measured up to

800 °C (Figure 5.2a). The initial weight loss up to 100 °C was caused by the removal of thermo-desorbed water corresponding to 1.5% ( $L_1$ ) and 3.4% ( $L_2$ ) of the total weight loss. The weight loss ( $W$ ) corresponding to Hb was calculated according to the following equation 5.2:<sup>39</sup>

$$\frac{H_1 - L_1}{100 - H_1} = \frac{H_2 - W - L_2}{100 - H_2}$$

$$W = H_2 - L_2 - \frac{(H_1 - L_1)(100 - H_2)}{100 - H_1} \quad (5.2)$$

$L$ : the initial weight loss until 100 °C was caused by the presence of thermo-desorbed water;  $H$ : the total weight loss up to 800 °C; Plain MSNs were used as control,  $L_1$  (100 °C) and  $H_1$  (800 °C).

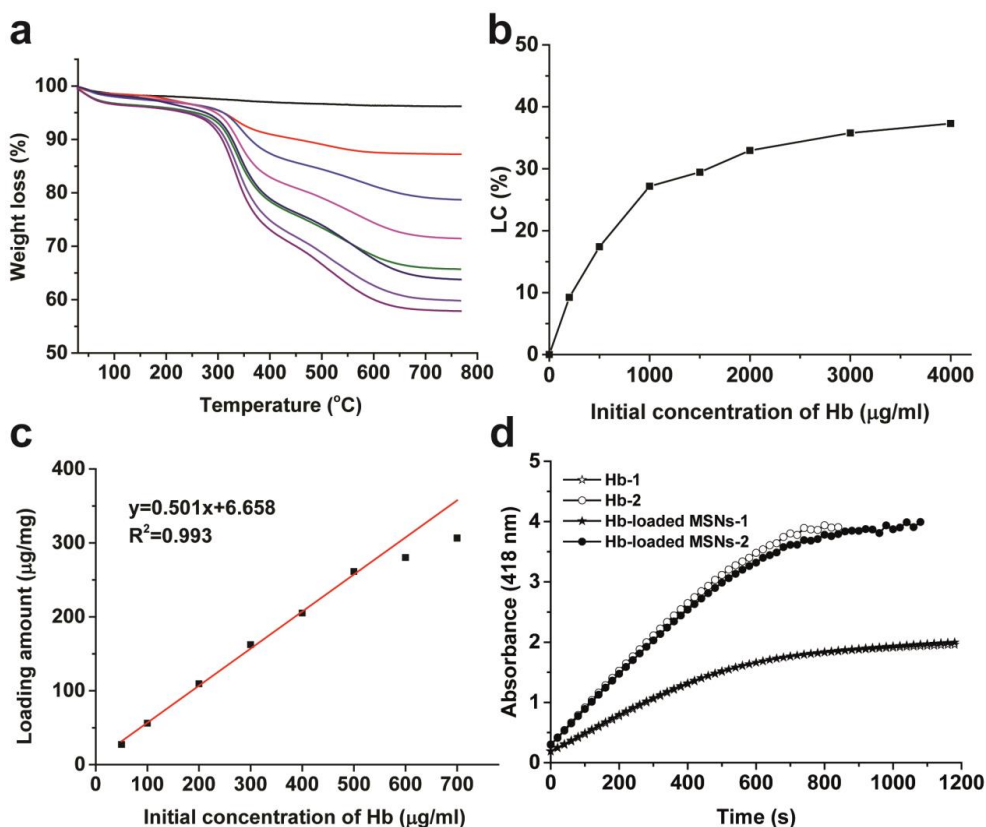


**Figure 5.2** (a) TGA curves of Hb-loaded MSNs with different initial concentrations of Hb (0, 0.25, 0.5, 1, 1.5, 2, 3 and 4 mg/mL, from top to bottom) and its corresponding (b) LC% of Hb into MSNs calculated by TGA; (c) Loading amount of Hb into MSNs at low loading concentrations by a Tecan M1000 plate reader, absorbance at 405 nm, 0-700 µg/mL; (d)

*ABTS catalyzed by native Hb (white) and MSNs/Hb (black). Hb<sub>1</sub> and Hb-loaded MSNs<sub>1</sub> represent the initial concentration of Hb were 50 µg/mL and Hb<sub>2</sub> and Hb-loaded MSNs<sub>2</sub> were 100 µg/mL. The enzymatic activity of Hb was measured at 418 nm by examining the catalytic conversion of the oxidation of ABTS.*

When the initial concentration of Hb used to load the MSNs was 4 mg/mL, the maximum loading capacity (37.3%) was obtained (Figure 5.2b). To investigate the encapsulation procedure in more detail, MSNs (2 mg/mL) were loaded with Hb using concentration range of this protein (0-700 µg/mL). This revealed that Hb loading in MSNs is a linearly correlated ( $R^2 = 0.993$ ) with the initial Hb concentration (0-700 µg/mL, Figure 5.2c). At higher initial concentration of Hb this correlation is lost, because concentrated Hb competing for the encapsulation, leading the blockage of pores (Figure 5.2b,c).

Hemoglobin can act as a peroxidase-like protein as its heme center catalyses the reduction of hydrogen peroxide. Compared to inorganic catalysts, proteins (Hb) have a high substrate specificity and reactive efficiency under normal conditions.<sup>6</sup> To examine the enzymatic activity of encapsulated Hb, the oxidation of ABTS by hydrogen peroxide was used as an indicator.<sup>6</sup> The catalytic reactivity of MSNs/Hb was analyzed and compared with native Hb in solution (Hb concentrations, 0.025 and 0.5 mg/mL). As shown in Figure 5.3b,c, the kinetics of the two enzyme-catalyzed reactions are essentially identical, indicating that the encapsulated Hb in MSNs exhibit high peroxidase-like activity as native Hb in aqueous solution.<sup>32</sup> As expected, a higher concentration of Hb resulting a faster conversion of H<sub>2</sub>O<sub>2</sub>. This result indicated that after encapsulation, Hb remained its peroxidase-like activity of Hb was not altered.

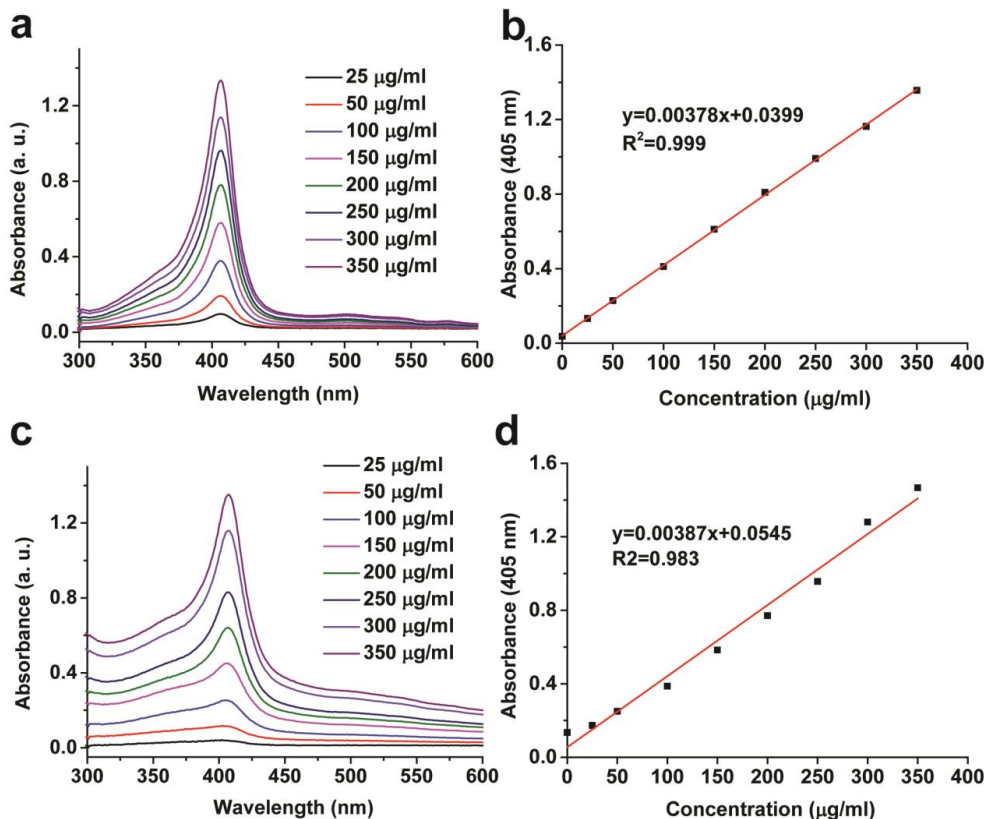


**Figure 5.3** (a) UV-VIS absorption spectra of Hb at varying concentrations (25-350 µg/mL); (b) standard curve of Hb absorbance (405 nm); (c) UV-Visible absorption spectra of Hb-loaded MSNs with varying concentration (based on Hb, 25-350 µg/mL); (d) standard curve of Hb-loaded MSNs (405 nm).

Helpful information on the heme protein folding can be obtained. From the Soret band in the UV-Visible absorption spectrum of hemoglobin as it is sensitive to the microenvironment, substructure, and oxidation state.<sup>40</sup> The spectral characteristics of MSNs/Hb (Hb concentration: 25-350 µg/mL) showed absorption curves that closely resembled those of native Hb as in all cases the maximum absorption was centered at 405 nm and no blue-shift was observed, suggesting no occurrence of protein unfolding.<sup>41</sup> The only noticeable difference is that MSNs/Hb showed some slight peak broadening, probably caused by the light scattering of MSNs (Figure 5.3a,c). A good linear relationship ( $R^2 = 0.983$ ) between the absorbance (405 nm) and MSNs/Hb concentration was obtained, similar to native Hb (Figure 5.3b,d,  $R^2 = 0.999$ ).

This confirms that Hb retains its higher-order structure in the mesopores of MSNs and does not undergo significant denaturation after encapsulation inside the silica pores.<sup>6, 40</sup>

Efficient encapsulation of Hb into MSNs occurs when the physicochemical properties of the Hb surface and the MSNs are complementary.<sup>42</sup> As the isoelectric point (pI) of Hb is 6.8-7.0 and 2-3 for the MSNs,<sup>15, 42</sup> both MSNs and Hb are negatively charged at physiological pH (7.4). The amount of Hb encapsulated in the MSNs was dependent on its initial concentration, indicating that the adsorption process was probably driven by capillary action.<sup>43</sup> Hb was encapsulated into the mesoporous channels (Figure 5.1c,d), but also the encapsulation process on the outer surface of the MSNs (Figure 5.S1). At higher Hb concentrations, the hydrodynamic diameter of Hb-loaded MSNs increased dramatically due to aggregation (Figure 5.S1a). Therefore a lipid bilayer was introduced to coat the Hb-loaded MSNs and form a physical barrier preventing colloidal aggregation (Figure 5.4a). The long-term colloidal stability of LB-MSNs is an important criteria for future biomedical applications. The hydrodynamic diameter and the zeta-potential of LB-MSNs were therefore measured for one week. The hydrodynamic diameter and the zeta-potential remained stable within this period (~250 nm, ~-23 mV) for at least one week (Figure 5.4b,c). Next, the cumulative release of Hb from MSNs and LB-MSNs was studied *in vitro* (Figure 5.4d). Hb-loaded MSNs (1:4 w/w) showed a burst release during the first hour with a release amount of  $25.50 \pm 0.33\%$ , while for LB-MSNs this was decreased to  $6.73 \pm 0.83\%$ . After 180 h, the cumulative release percentage of Hb-loaded MSNs and LB-MSNs was  $42.27 \pm 0.60\%$  and  $27.49 \pm 0.29\%$ , respectively. This shows that the lipid bilayer physically lowers the amount of Hb leaching out from the MSNs (Figure 5.4d).



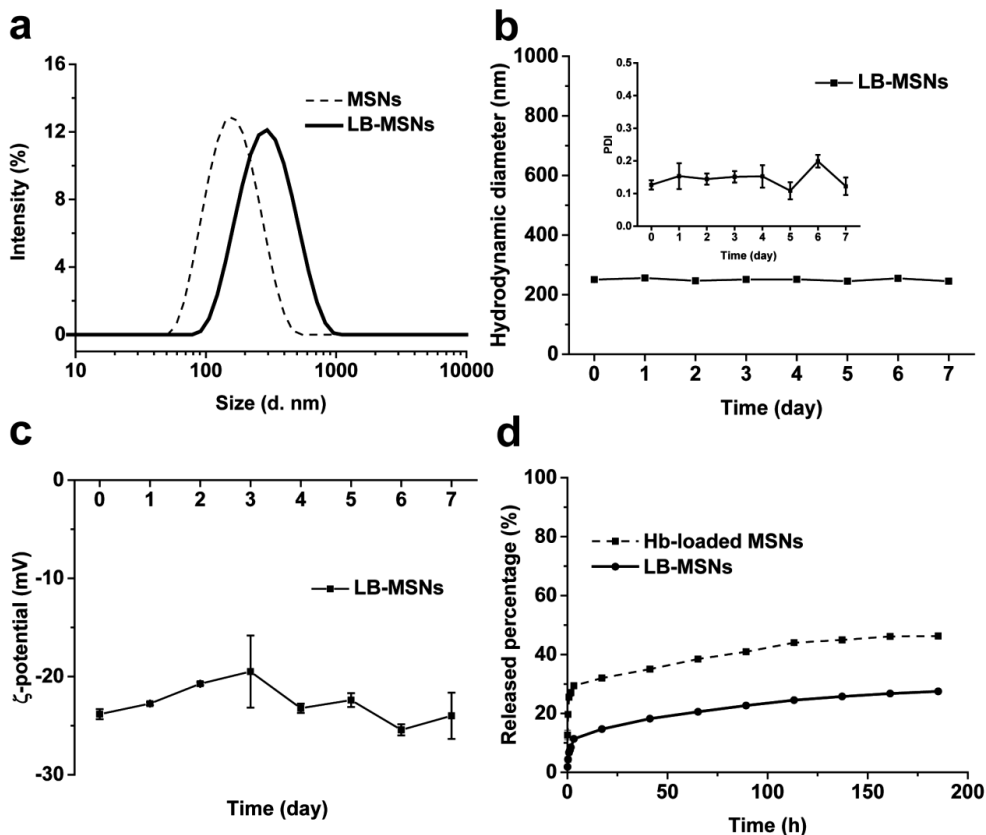


**Figure 5.4** Colloidal stability of LB-MSNs. (a) Hydrodynamic diameter of MSNs and LB-MSNs according to DLS (1 mM PB, pH 7.4); (b) size stability (insert: PDI values) and (c) zeta-potential of LB-MSNs were measured as a function of time (1 mM PB, pH 7.4); (d) release profiles of Hb-loaded MSNs and LB-MSNs in PBS (37 °C, pH 7.4).

Fluorescence microscopy imaging was used to visualize and confirm the localization of Hb within the nanoparticles using fluorescent microscopy. For this, Hb was labelled with fluorescein isothiocyanate (FITC) while DOPE-LR was used to visualize the lipid bilayer on the Hb-loaded MSNs (Figure 5.S2). Due to the low magnification (100 $\times$ ) of the microscope and the small particle size ( $\sim$ 250 nm, Figure 5.4a,b), it was not possible to observe single particle with great detail. Still the overlap of both dyes is a clear indication of the co-localization of Hb and the lipid bilayer at the same particle. Furthermore, the uniform distribution of LB-MSNs on the silicon slide proved the LB-MSNs were well-dispersed.

Zebrafish (*Danio rerio*) embryos have emerged as an important transparent vertebrate model and are useful *in vivo* model for real-time imaging technique of a wide activity of biological processes and to study the distribution and circulation of nanoparticles.<sup>34, 44, 45</sup> To study the *in vivo* behaviour of Hb loaded LB-MSNs in circulation, we injected fluorescent labelled LB-MSNs into the blood circulation system. After injection, the nanoparticles moved with the blood flow and readily distributed throughout the circulation of the bloodstream as evidenced by confocal imaging<sup>35</sup> (Figure 5).

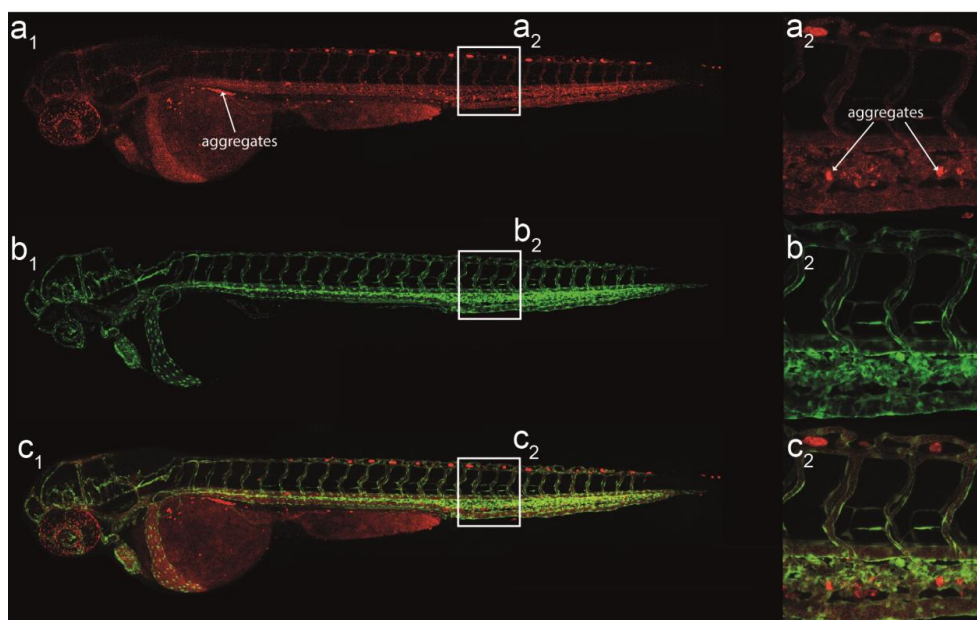


**Figure 5.5** Confocal fluorescence images of (a) lissamine rhodamine labeled LB-MSNs), with a few regular red dots attributed to autofluorescence, (b) GFP expressed blood vessels of a zebrafish embryo, (c) overlay images show the localization of the LB-MSNs in the blood vessels.

Imaging revealed that LB-MSNs could systemic circulate and are evenly distributed in the blood vessels, with only little aggregation in the caudal hematopoietic tissue and the dorsal region of the yolk sac (Figure 5.5). The large majority of the nanoparticles however did not interact with endothelium, only a few adhered to the endothelium lining of the blood vessel and were trapped as expected. PEGylation of nanoparticle has shown to be an effective method to lower the binding affinity of the

particles for endothelial cells *in vivo*.<sup>35</sup> However, further optimization of the lipid bilayer composition and the amount of PEGylation are planned.

#### **5.4 Conclusion**

In summary, lipid bilayer coated MSNs were used as a carrier for Hb. The large disc-like pores of the MSNs enabled the rapid encapsulation of Hb into the mesopores with a high loading capacity. Encapsulated Hb remained active and exhibited similar enzymatic activity to non-encapsulated Hb. The introduction of a supported lipid bilayer prevented premature Hb release from LB-MSNs and improved the colloidal stability *in vitro*. These Hb loaded LB-MSNs could be considered as an artificial erythrocyte mimic. Only the circulation and distribution of the LB-MSNs was tested in zebrafish embryos. Unfortunately, convective blood flow is not essential to supply oxygen to the tissues during the early larval development of zebrafish.<sup>46</sup> Therefore Hb oxygen transport had no effect on oxygen-dependent processes<sup>47</sup> as even mutant zebrafish lacking erythrocytes survive for about 2 weeks after fertilization.<sup>46, 48</sup> Further testing using other animal models (*e.g.* mice) are therefore required to test these Hb-loaded MSNs as a mimic for red-blood cells.

## Supporting information

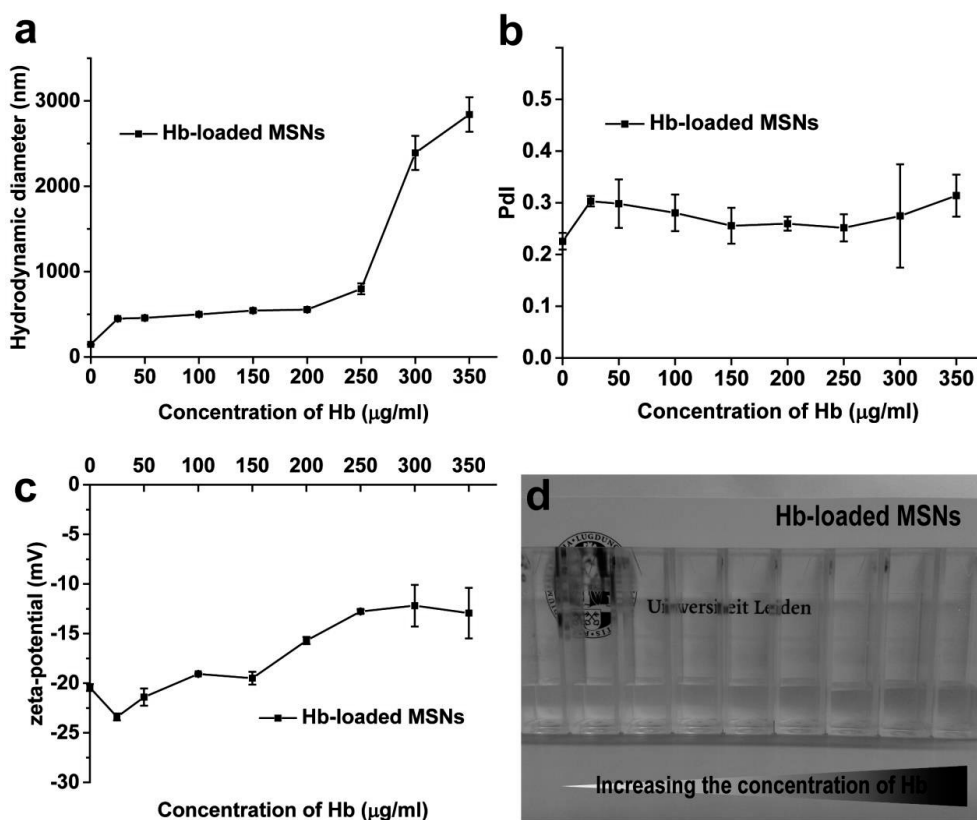


**Figure 5.S1** (a) Hydrodynamic diameter of Hb-loaded MSNs with varying concentrations (0-350  $\mu\text{g/mL}$ ) and the corresponding (b) PDI values, (c) zeta-potential in 1 mM PB (pH 7.4); (d) digital photograph of Hb-loaded MSNs with increasing concentration of Hb from the left to the right.

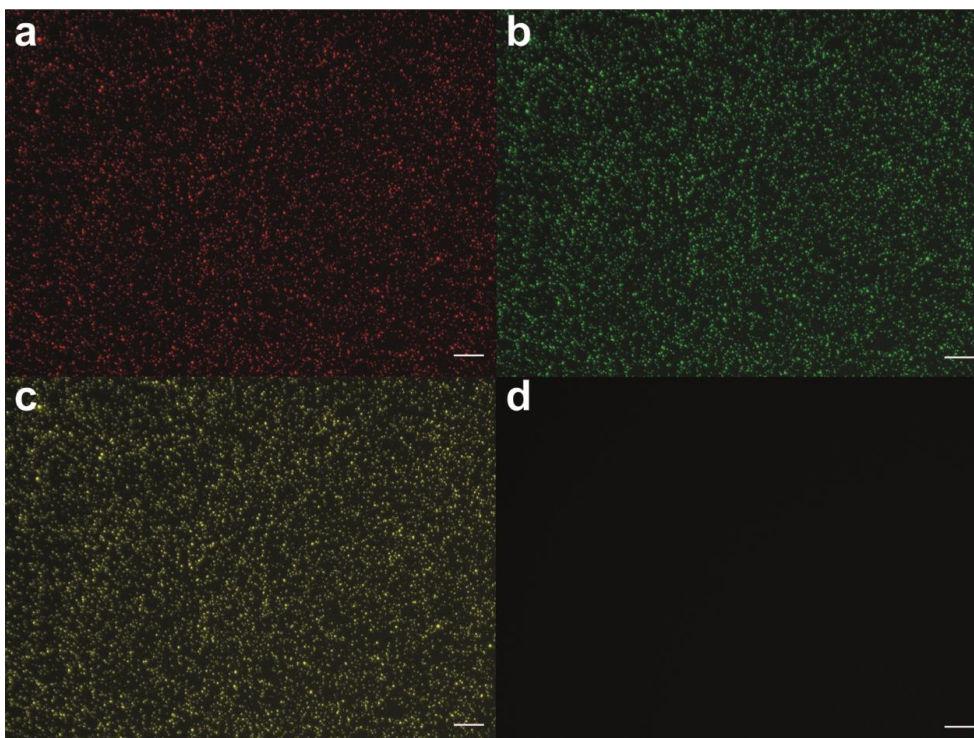


**Figure 5.S2** (a) Fluorescence images of LB-MSNs on silicon slides, the scale bar represents 100  $\mu\text{m}$ . (a) liposomes labelled with 1wt% DOPE-LR, (excitation wavelength = 546 nm); (b) FITC-labelled Hb (excitation wavelength = 488 nm); (c) overlay image, (d) control, empty silicon slide (magnification 100 $\times$ ).

## 5.5 References

1. W. Q. Wang, S. Liu, Y. B. Huang, X. B. Jing and Z. G. Xie, *J. Mater. Chem. B*, 2015, 3, 5753-5759.
2. L. Duan, X. H. Yan, A. H. Wang, Y. Jia and J. B. Li, *ACS Nano*, 2012, 6, 6897-6904.
3. H. G. Klein, D. R. Spahn and J. L. Carson, *Lancet*, 2007, 370, 415-426.
4. T. Henkel-Honke and M. Oleck, *AANA J.*, 2007, 75, 205-211.
5. D. R. Spahn, *Crit. Care*, 1999, 3, R93-R97.
6. Y. Urabe, T. Shiomi, T. Itoh, A. Kawai, T. Tsunoda, F. Mizukami and K. Sakaguchi, *Chembiochem*, 2007, 8, 668-674.
7. M. X. Liu, L. H. Gan, L. H. Chen, D. Z. Zhu, Z. J. Xu, Z. X. Hao and L. W. Chen, *Int. J. Pharm.*, 2012, 427, 354-357.
8. K. Chen, T. J. Merkel, A. Pandya, M. E. Napier, J. C. Luft, W. Daniel, S. Sheiko and J. M. DeSimone, *Biomacromolecules*, 2012, 13, 2748-2759.
9. T. M. S. Chang, *Artif. Cells, Blood Substitutes, Biotechnol.*, 2012, 40, 197-199.
10. E. Tsuchida, K. Sou, A. Nakagawa, H. Sakai, T. Komatsu and K. Kobayashi, *Bioconjugate Chem.*, 2009, 20, 1419-1440.
11. T. M. S. Chang, *Artif. Organs*, 2004, 28, 789-794.
12. J. Zhao, C. S. Liu, Y. Yuan, X. Y. Tao, X. Q. Shan, Y. Sheng and F. Wu, *Biomaterials*, 2007, 28, 1414-1422.
13. Y. Xiong, A. Steffen, K. Andreas, S. Muller, N. Sternberg, R. Georgieva and H. Baumler, *Biomacromolecules*, 2012, 13, 3292-3300.
14. S. L. Li, J. Nickels and A. F. Palmer, *Biomaterials*, 2005, 26, 3759-3769.
15. W. Gao, B. Y. Sha, W. Zou, X. Liang, X. Z. Meng, H. Xu, J. Tang, D. C. Wu, L. X. Xu and H. Zhang, *Biomaterials*, 2011, 32, 9425-9433.
16. H. Sakai, K. Tomiyama, K. Sou, S. Takeoka and E. Tsuchida, *Bioconjugate Chem.*, 2000, 11, 425-432.
17. H. Sakai, H. Horinouchi, Y. Masada, S. Takeoka, E. Ikeda, M. Takaori, K. Kobayashi and E. Tsuchida, *Biomaterials*, 2004, 25, 4317-4325.
18. J. Liu, X. Jiang, C. Ashley and C. J. Brinker, *J. Am. Chem. Soc.*, 2009, 131, 7567-7569.
19. J. W. Liu, A. Stace-Naughton, X. M. Jiang and C. J. Brinker, *J. Am. Chem. Soc.*, 2009, 131, 1354-1355.
20. J. W. Liu, A. Stace-Naughton and C. J. Brinker, *Chem. Commun.*, 2009, 5100-5102.
21. I. I. Slowing, C. W. Wu, J. L. Vivero-Escoto and V. S. Y. Lin, *Small*, 2009, 5, 57-62.
22. H. Meng, M. Wang, H. Liu, X. Liu, A. Situ, B. Wu, Z. Ji, C. H. Chang and A. E. Nel, *ACS Nano*, 2015, 3540-3557.
23. C. E. Ashley, E. C. Carnes, G. K. Phillips, D. Padilla, P. N. Durfee, P. A. Brown, T. N. Hanna, J. Liu, B. Phillips, M. B. Carter, N. J. Carroll, X. Jiang, D. R. Dunphy, C. L. Willman, D. N. Petsev, D. G. Evans, A. N. Parikh, B. Chackerian, W. Wharton, D. S. Peabody and C. J. Brinker, *Nat. Mater.*, 2011, 10, 389-397.
24. P. N. Durfee, Y. S. Lin, D. R. Dunphy, A. J. Muniz, K. S. Butler, K. R. Humphrey, A. J. Lokke, J. O. Agola, S. S. Chou, I. M. Chen, W. Wharton, J. L. Townson, C. L. Willman and C. J. Brinker, *ACS Nano*, 2016, 8325-8345.
25. S. Mornet, O. Lambert, E. Duguet and A. Brisson, *Nano Lett.*, 2005, 5, 281-285.
26. D. R. Arifin and A. F. Palmer, *Biotechnol. Prog.*, 2003, 19, 1798-1811.
27. M. Bouchoucha, R. C-Gaudreault, M. A. Fortin and F. Kleitz, *Adv. Funct. Mater.*, 2014, 24, 5911-5923.
28. G. Y. Tonga, K. Saha and V. M. Rotello, *Adv. Mater.*, 2014, 26, 359-370.

29. X. X. Zhang, F. F. Li, S. Y. Guo, X. Chen, X. L. Wang, J. Li and Y. Gan, *Biomaterials*, 2014, 35, 3650-3665.
30. E. P. H. Brunauer S. , Teller E., *J. Am. Chem. Soc.*, 1938, 60, 309-319.
31. E. P. Barrett, L. G. Joyner and P. P. Halenda, *J. Am. Chem. Soc.*, 1951, 73, 373-380.
32. I. I. Slowing, B. G. Trewyn and V. S. Y. Lin, *J. Am. Chem. Soc.*, 2007, 129, 8845-8849.
33. M. Takayanagi and T. Yashiro, *Clin. Chem.*, 1984, 30, 357-359.
34. L. Evensen, P. L. Johansen, G. Koster, K. Zhu, L. Herfindal, M. Speth, F. Fenaroli, J. Hildahl, S. Bagherifam, C. Tulotta, L. Prasmickaite, G. M. Maelandsmo, E. Snaar-Jagalska and G. Griffiths, *Nanoscale*, 2016, 8, 862-877.
35. P. L. Johansen, F. Fenaroli, L. Evensen, G. Griffiths and G. Koster, *Nat. Commun.*, 2016, 7.
36. J. Choi, L. Dong, J. Ahn, D. Dao, M. Hammerschmidt and J. N. Chen, *Dev. Biol.*, 2007, 304, 735-744.
37. B. L. Zhang, Z. Luo, J. J. Liu, X. W. Ding, J. H. Li and K. Y. Cai, *J. Controlled Release*, 2014, 192, 192-201.
38. Y. Zhang, Z. Zhi, T. Jiang, J. Zhang, Z. Wang and S. Wang, *J. Controlled Release*, 2010, 145, 257-263.
39. M. Xie, H. Shi, Z. Li, H. J. Shen, K. Ma, B. Li, S. Shen and Y. Jin, *Colloids Surf., B*, 2013, 110, 138-147.
40. Y. Xian, Y. Xian, L. Zhou, F. Wu, Y. Ling and L. Jin, *Electrochem. Commun.*, 2007, 9, 142-148.
41. J. Wu, X. Li, Y. Yan, Y. Hu, Y. Zhang and Y. Tang, *J. Colloid Interface Sci.*, 2013, 406, 130-138.
42. S. Hudson, J. Cooney and E. Magner, *Angew. Chem., Int. Ed.*, 2008, 47, 8582-8594.
43. X. Liu, L. Zhu, T. Zhao, J. Lan, W. Yan and H. Zhang, *Microporous Mesoporous Mater.*, 2011, 142, 614-620.
44. F. Sharif, F. Porta, A. H. Meijer, A. Kros and M. K. Richardson, *Int. J. Nanomed.*, 2012, 7, 1875-1890.
45. R. M. White, A. Sessa, C. Burke, T. Bowman, J. LeBlanc, C. Ceol, C. Bourque, M. Dovey, W. Goessling, C. E. Burns and L. I. Zon, *Cell Stem Cell*, 2008, 2, 183-189.
46. S. Grillitsch, N. Medgyesy, T. Schwerte and B. Pelster, *J. Exp. Biol.*, 2005, 208, 309-316.
47. B. Pelster and W. W. Burggren, *Circ. Res.*, 1996, 79, 358-362.
48. B. M. Weinstein, A. F. Schier, S. Abdelilah, J. Malicki, L. SolnicaKrezel, D. L. Stemple, D. Y. R. Stainier, F. Zwartkruis, W. Driever and M. C. Fishman, *Development*, 1996, 123, 303-309.
49. J. Tamayo, *Nat. Nanotechnol.*, 2015, 10, 738-739.
50. T. E. Angel, U. K. Aryal, S. M. Hengel, E. S. Baker, R. T. Kelly, E. W. Robinson and R. D. Smith, *Chem. Soc. Rev.*, 2012, 41, 3912-3928.
51. J. Shang and X. H. Gao, *Chem. Soc. Rev.*, 2014, 43, 7267-7278.
52. R. P. Carney, J. Y. Kim, H. F. Qian, R. C. Jin, H. Mehenni, F. Stellacci and O. M. Bakr, *Nat. Commun.*, 2011, 2.
53. S. Bruckenstein and M. Shay, *Electrochim. Acta*, 1985, 30, 1295-1300.
54. D. A. Buttry and M. D. Ward, *Chem. Rev.*, 1992, 92, 1355-1379.
55. M. Rodahl, F. Hook, A. Krozer, P. Brzezinski and B. Kasemo, *Rev. Sci. Instrum.*, 1995, 66, 3924-3930.
56. A. Janshoff, H. J. Galla and C. Steinem, *Angew. Chem., Int. Ed.*, 2000, 39, 4004-4032.
57. T. P. Burg, M. Godin, S. M. Knudsen, W. Shen, G. Carlson, J. S. Foster, K. Babcock and S. R. Manalis, *Nature*, 2007, 446, 1066-1069.

58. M. Fakruddin, Z. Hossain and H. Afroz, *J. Nanobiotechnol.*, 2012, 10.
59. J. Chaste, A. Eichler, J. Moser, G. Ceballos, R. Rurali and A. Bachtold, *Nat. Nanotechnol.*, 2012, 7, 300-303.
60. M. S. Hanay, S. Kelber, A. K. Naik, D. Chi, S. Hentz, E. C. Bullard, E. Colinet, L. Duraffourg and M. L. Roukes, *Nat. Nanotechnol.*, 2012, 7, 602-608.
61. M. Godin, A. K. Bryan, T. P. Burg, K. Babcock and S. R. Manalis, *Appl. Phys. Lett.*, 2007, 91.
62. W. H. Grover, A. K. Bryan, M. Diez-Silva, S. Suresh, J. M. Higgins and S. R. Manalis, *Proc. Natl. Acad. Sci. U. S. A.*, 2011, 108, 10992-10996.
63. Y. T. Yang, C. Callegari, X. L. Feng, K. L. Ekinici and M. L. Roukes, *Nano Lett.*, 2006, 6, 583-586.
64. A. Malloy, *Mater. Today*, 2011, 14, 170-173.
65. V. Filipe, A. Hawe and W. Jiskoot, *Pharm. Res.*, 2010, 27, 796-810.
66. T. Ito, L. Sun, M. A. Bevan and R. M. Crooks, *Langmuir*, 2004, 20, 6940-6945.
67. Z. Gu, A. Biswas, M. Zhao and Y. Tang, *Chem. Soc. Rev.*, 2011, 40, 3638-3655.
68. F. P. Chang, Y. P. Chen and C. Y. Mou, *Small*, 2014, 10, 4785-4795.
69. Z. Gao and I. Zharov, *Chem. Mater.*, 2014, 26, 2030-2037.
70. C.-H. Lee, T.-S. Lin and C.-Y. Mou, *Nano Today*, 2009, 4, 165-179.
71. J. Sun, H. Zhang, R. Tian, D. Ma, X. Bao, D. S. Su and H. Zou, *Chem. Comm.*, 2006, 1322-1324.
72. D. Y. Zhao, J. L. Feng, Q. S. Huo, N. Melosh, G. H. Fredrickson, B. F. Chmelka and G. D. Stucky, *Science*, 1998, 279, 548-552.
73. J. Gu, K. Huang, X. Zhu, Y. Li, J. Wei, W. Zhao, C. Liu and J. Shi, *J. Colloid Interface Sci.*, 2013, 407, 236-242.
74. N. Z. Knezevic and J. O. Durand, *Nanoscale*, 2015, 7, 2199-2209.
75. H. K. Na, M. H. Kim, K. Park, S. R. Ryoo, K. E. Lee, H. Jeon, R. Ryoo, C. Hyeon and D. H. Min, *Small*, 2012, 8, 1752-1761.
76. X. Du, L. Xiong, S. Dai, F. Kleitz and S. Z. Qiao, *Adv. Funct. Mater.*, 2014, 24, 7627-7637.
77. S. B. Hartono, N. T. Phuoc, M. H. Yu, Z. F. Jia, M. J. Monteiro, S. H. Qiao and C. Z. Yu, *J. Mater. Chem. B*, 2014, 2, 718-726.
78. M. Y. Wu, Q. S. Meng, Y. Chen, Y. Y. Du, L. X. Zhang, Y. P. Li, L. L. Zhang and J. L. Shi, *Adv. Mater.*, 2015, 27, 215-222.
79. F. Gao, P. Botella, A. Corma, J. Blesa and L. Dong, *J. Phys. Chem. B*, 2009, 113, 1796-1804.
80. Y. Han and J. Y. Ying, *Angew. Chem., Int. Ed.*, 2005, 44, 288-292.
81. H. Zhang, J. M. Sun, D. Ma, X. H. Bao, A. Klein-Hoffmann, G. Weinberg, D. S. Su and R. Schlögl, *J. Am. Chem. Soc.*, 2004, 126, 7440-7441.
82. J. Fan, J. Lei, L. Wang, C. Yu, B. Tu and D. Zhao, *Chem. Comm.*, 2003, 2140-2141.
83. M. Zaric, O. Lyubomska, O. Touzelet, C. Poux, S. Al-Zahrani, F. Fay, L. Wallace, D. Terhorst, B. Malissen, S. Henri, U. F. Power, C. J. Scott, R. F. Donnelly and A. Kissenpfennig, *ACS Nano*, 2013, 7, 2042-2055.
84. S. A. Coulman, A. Anstey, C. Gateley, A. Morrissey, P. McLoughlin, C. Allender and J. C. Birchall, *Int. J. Pharm.*, 2009, 366, 190-200.
85. P. C. DeMuth, X. F. Su, R. E. Samuel, P. T. Hammond and D. J. Irvine, *Adv. Mater.*, 2010, 22, 4851-4856.
86. K. van der Maaden, W. Jiskoot and J. Bouwstra, *J. Controlled Release*, 2012, 161, 645-655.
87. S. S. Wang, F. Yuan, K. Chen, G. J. Chen, K. H. Tu, H. J. Wang and L. Q. Wang, *Biomacromolecules*, 2015, 16, 2693-2700.

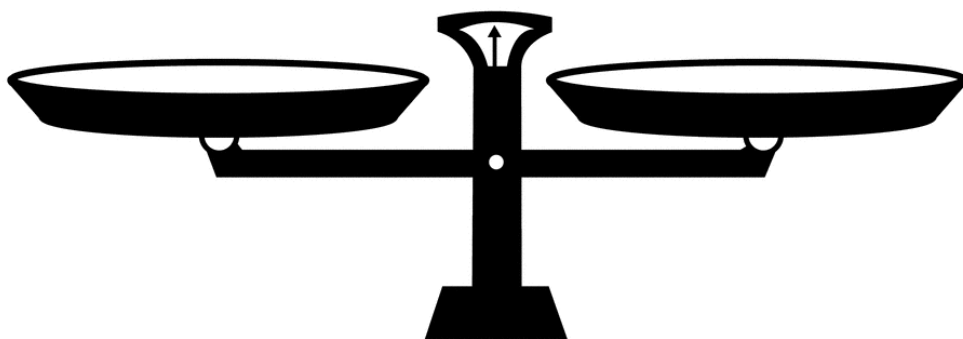


88. Y. Wang, Y. A. Nor, H. Song, Y. N. Yang, C. Xu, M. H. Yu and C. Z. Yu, *J. Mater. Chem. B*, 2016, 4, 2646-2653.
89. K. Lee, E. A. Silva and D. J. Mooney, *J. R. Soc., Interface*, 2011, 8, 153-170.
90. M. Cross and T. M. Dexter, *Cell*, 1991, 64, 271-280.
91. T. P. Richardson, M. C. Peters, A. B. Ennett and D. J. Mooney, *Nat. Biotechnol.*, 2001, 19, 1029-1034.
92. F. M. Chen, M. Zhang and Z. F. Wu, *Biomaterials*, 2010, 31, 6279-6308.
93. K. Y. Lee and S. H. Yuk, *Prog. Polym. Sci.*, 2007, 32, 669-697.
94. B. Chatin, M. Mevel, J. Devalliere, L. Dallet, T. Haudebourg, P. Peuziat, T. Colombani, M. Berchel, O. Lambert, A. Edelman and B. Pitard, *Mol. Ther.--Nucleic Acids*, 2015, 4, e244.
95. T. D. Dziubla, V. V. Shuvaev, N. K. Hong, B. J. Hawkins, M. Madesh, H. Takano, E. Simone, M. T. Nakada, A. Fisher, S. M. Albelda and V. R. Muzykantov, *Biomaterials*, 2008, 29, 215-227.
96. L. Schoonen and J. C. M. van Hest, *Adv. Mater.*, 2015, 1109-1128.
97. V. Nadihe and Y. H. Bae, *Tissue Eng., Part A*, 2011, 17, 2453-2462.
98. X. Li, Y. J. Chen, M. Q. Wang, Y. J. Ma, W. L. Xia and H. C. Gu, *Biomaterials*, 2013, 34, 1391-1401.
99. A. Fire, S. Q. Xu, M. K. Montgomery, S. A. Kostas, S. E. Driver and C. C. Mello, *Nature*, 1998, 391, 806-811.
100. J. Conde, A. Ambrosone, Y. Hernandez, F. Tian, M. McCully, C. C. Berry, P. V. Baptista, C. Tortiglione and J. M. de la Fuente, *Nano Today*, 2015, 10, 421-450.
101. X. Xu, J. Wu, Y. Liu, M. Yu, L. Zhao, X. Zhu, S. Bhasin, Q. Li, E. Ha, J. Shi and O. C. Farokhzad, *Angew. Chem., Int. Ed.*, 2016, 55, 7091-7094.
102. C.-f. Xu and J. Wang, *Asian J. Pharm. Sci.*, 2015, 10, 1-12.
103. Y. Jiang, R. Tang, B. Duncan, Z. Jiang, B. Yan, R. Mout and V. M. Rotello, *Angew. Chem., Int. Ed.*, 2015, 54, 506-510.
104. J. Tu, T. Wang, W. Shi, G. Wu, X. Tian, Y. Wang, D. Ge and L. Ren, *Biomaterials*, 2012, 33, 7903-7914.



## **Chapter VI (Appendix)**

### **Weight Estimation of a Single Mesoporous Silica Nanoparticle**



Jing Tu, Wim Jiskoot, Alexander Kros

## 6.1 Introduction

Characterization of building blocks of cell's like proteins by their mass is essential for the discovery of disease biomarkers and the development of early disease diagnostic tools.<sup>49,</sup>  
<sup>50</sup> In (bio)nanotechnology, individual nanoparticles are as unique as people's fingerprints,<sup>51</sup> therefore it becomes imperative to find methods for the full characterization of nanoparticles. In the field of nanomedicine,<sup>52</sup> knowing the mass of nanoparticles could result in more precise *in vivo* administration.<sup>51</sup> One of the most widely used mass-sensing methods is the quartz crystal microbalance,<sup>53-56</sup> with a total mass resolution of  $\sim 1$  ng.<sup>51, 57</sup> However, rapid developments of nanotechnology in biology require a more sensitive technique, with a mass detection limit preferably at the level of nano-sized objects.<sup>49, 58</sup> In the last decade, mechanical resonator based nanomechanical mass sensors have been developed and used to weigh cells, biomolecules, bacteria and viruses.<sup>49, 57, 59, 60</sup> Burg<sup>57</sup> demonstrated that suspended microchannel resonators (SMR) can be used to weigh single particles or cells in water with sub-femtogram resolution; such as gold nanoparticles ( $100 \pm 8$  nm, 10 fg), *Escherichia coli* ( $110 \pm 30$  fg) and *Bacillus subtilis* ( $150 \pm 40$  fg). In principle, added mass from a sample of interest induces a downshift of the resonance frequency that is proportional to the ratio between the added mass and the resonator's mass.<sup>49, 60</sup> However, this technique isn't suitable for measuring the weight the particle size with small diameter ( $< 50$  nm).<sup>61</sup> In recent years, with the development of nanomechanical devices, the ultimate mass detection limit rapidly shifted from pictograms ( $10^{-12}$  g)<sup>57, 62</sup> to yoctograms ( $10^{-24}$  g).<sup>59</sup> However, most of these techniques require complex high-vacuum conditions and are therefore, not suitable for analyzing biomolecules or nanoparticles in solution.<sup>49, 57, 59, 63</sup>

Here, a simple and non-destructive method to estimate the weight of a single particle in solution using Nanoparticle tracking analysis (NTA) is described. Nanosight, a laser-illuminated light scattering microscopy,<sup>51</sup> is capable of directly sizing and visualizing nanoscale particles in liquids with high-resolution, providing the size, total number of particles and the concentration of the measured samples.<sup>51, 64</sup> The NTA software can identify and track individual nanoparticles moving under Brownian motion and relates the movement to a particle size according to the formula derived from the Stokes-Einstein equation.<sup>65</sup> Taking the advantages of this technique and combined with a gravimetric measurement yields a simple and complementary method to determine the colloidal stability and estimate a single nanoparticle's weight of the sample of interest in solution such as the MSNs described in Chapter 2, 3, 4 and 5.

## **6.2 Materials and method**

### *6.2.1 Materials*

Pluronic P123 (EO<sub>20</sub>PO<sub>70</sub>EO<sub>20</sub>, M<sub>n</sub>~5800 g/mol), tetraethyl orthosilicate (TEOS, ≥98%), hydrochloric acid (HCl), 1,3,5-trimethylbenzene (TMB) were purchased from Sigma-Aldrich and used as received. Fluorocarbon surfactant FC-4 was purchased from Yick-Vic Chemicals & Pharmaceuticals (HK) Ltd, China. Milli-Q water (18.2 MΩ/cm, Millipore Co., USA) was used throughout the experiments.

### *6.2.2 Preparation of large-pore MSNs*

MSNs were synthesized as follows. 0.5 g of surfactant Pluronic P123 and 1.4 g of FC-4 were dissolved in 80 mL of HCl (0.02 M), followed by the introduction of 0.48 mL of TMB. After stirring for 6 h, 2.14 mL of TEOS was added dropwise. The resulting mixture was stirred at 30 °C for 24 h and transferred to an autoclave at 120 °C for 2 days. Finally, the solid product was isolated by centrifugation, and washed with ethanol and water. The organic template was completely removed by calcination at 550 °C for 5 h.

To determine the colloidal stability and concentration in particles (1 × 10<sup>8</sup>/mL), MSNs (1 mg/mL) were sonicated (10 min) and dispersed in MilliQ. The sample was diluted with MilliQ to final concentrations ranging from 1 to 10 µg/mL. All the suspensions were sonicated for 10 min (Branson 1510 ultrasonic cleaner) before the measurements. The mean size, standard deviation (SD), and total concentration values were measured using a NanoSight LM20. Four measurements were taken from each sample and averaged. The weight of a single particle was determined using the following equations.

$$m (\text{single MSN weight}) = \frac{M}{N} \quad (6.1)$$

When the volume of the MSNs suspension is 1 mL,

$$m (\text{weight of a single MSN}) = \frac{\text{particle concentration by weight}}{\text{particle concentration by counts}} \quad (6.2)$$

M: Weight of MSNs (mg) as determined by micro balance (Sartorius),

N: Number of MSN particles as determined by NTA.

### *6.2.3 Particle analysis*

The porous structure of the as-prepared MSNs was characterized using transmission

electron microscopy (TEM) operated at 70 kV (TEM, JEOL 1010, USA). The hydrodynamic diameter of the MSNs was measured with a Malvern Nano-ZS instrument. Nanoparticle tracking analysis (NTA) measurement was performed by using a NanoSight LM20 (NanoSight, Amesbury, United Kingdom). The software used for capturing and analyzing the data was the NTA 2.0 Build 127. Data analysis was performed using NTA 2.0 Build 127. All the samples were measured for 40 s at room temperature.

### 6.3 Results and discussion

The morphology and mesoporous structure of the MSNs was visualized by TEM (Figure 6.1a). Analysis of the TEM images revealed the MSNs had lengths of  $90 \pm 20$  nm and widths of  $43 \pm 7$  nm, giving them an elongated cuboidal-like geometry. Dynamic light scattering (DLS) measurements revealed MSNs with a unimodal distribution that possessed an average hydrodynamic diameter of 146 nm (Figure 6.1b). These sizes were slightly larger than those determined by DLS, since TEM provides the size distribution of dehydrated particles while DLS measurements yield an average hydrodynamic diameter of the particles in solution.<sup>66</sup> Nanoparticle tracking analysis (NTA) enables the determination of the hydrodynamic diameter distribution of the particles and in addition counts the number of individual nanoparticles.<sup>51, 65</sup> Therefore, the colloidal stability of the MSNs as a function of concentration was determined using NTA (Figure 6.1c and d). A dilution series of MSNs (1-10  $\mu\text{g/mL}$ ) was prepared and the concentration of MSN was determined to be  $4.6 \times 10^8$  -  $2.9 \times 10^9$  particles/mL were determined by NTA (Figure 6.1d, red dots curve). The mean size, standard deviation (SD), and molarity (n/v) as a function of MSN concentration (w/v) were also measured by NTA (Figure 6.1c, d, table 6.1). Surprisingly, an increase in MSN concentration, resulted in a decrease in the observed mean size of the MSN from 148 to 87 nm, which fits with both the transmission electron microscopy (TEM) and the dynamic light scattering (DLS) data results (Figure 6.1a, b). Since the mean size and SD values obtained by NTA correspond to the arithmetic values calculated with all the particles analyzed, the decrease in mean size may be due to a more accurate calculation at higher particle concentrations.<sup>65</sup>

**Table 6.1** Mean size, size distribution and concentration in particles of MSNs from NTA measurements

Particle <i>conc.</i> ( $\mu\text{g/mL}$ )	Mean (nm)	SD (nm) <sup>a</sup>	Particle <i>conc.</i> ( $1 \times 10^8/\text{mL}$ ) <sup>b</sup>
1	$146.8 \pm 4.3$	$63.8 \pm 1.9$	$4.6 \pm 0.7$
2	$131.5 \pm 5.2$	$58.5 \pm 1.0$	$8.5 \pm 0.2$
3	$138.3 \pm 5.7$	$63.0 \pm 6.8$	$9.4 \pm 0.7$
4	$131.3 \pm 6.7$	$68.5 \pm 2.4$	$13.6 \pm 1.2$
5	$122.5 \pm 4.0$	$69.5 \pm 1.0$	$15.4 \pm 1.3$
6	$118.8 \pm 2.1$	$68.0 \pm 1.6$	$18.0 \pm 2.1$
7	$106.5 \pm 5.8$	$64.5 \pm 4.2$	$19.5 \pm 0.8$
8	$107.0 \pm 1.2$	$70.3 \pm 0.5$	$22.2 \pm 1.8$
9	$106.5 \pm 7.5$	$72.3 \pm 8.4$	$26.0 \pm 2.1$
10	$86.5 \pm 6.1$	$64.8 \pm 3.8$	$29.4 \pm 3.4$

<sup>a</sup>SD standard deviation calculated by the NTA software; <sup>b</sup>Conc. Concentration in particles  $10^8/\text{mL}$  as measured by NTA. Numbers represent average values  $\pm$  standard deviation (n = 4 measurements).

Figure 6.1d (red curve) shows, the linear ( $R^2 = 0.99$ ) relationship between particle concentration by weight and by count rate ( $y = 2.61x + 2.315$ ). The calculated weight of a single particle using equation 6.2 (red dots) increased steadily until they reached a plateau (Table 6.1). The weight of a single particle was calculated according to equation 6.3.

$$m (\text{single MSNs' weight}) = \frac{x}{2.61x + 2.315} \quad (6.3)$$

The slope reflects the weight of a single MSN. When a higher particle concentration is used for the NTA measurements, the value of a single MSN weight is closer to the real weight. When  $x$  goes to  $\infty$ , the weight of a single MSN is the reciprocal of the slope and thus the weight was calculated to be 3.8 fg. As no aggregation was observed over the used particle concentration range during all the measurements, the MSNs showed good colloidal stability.

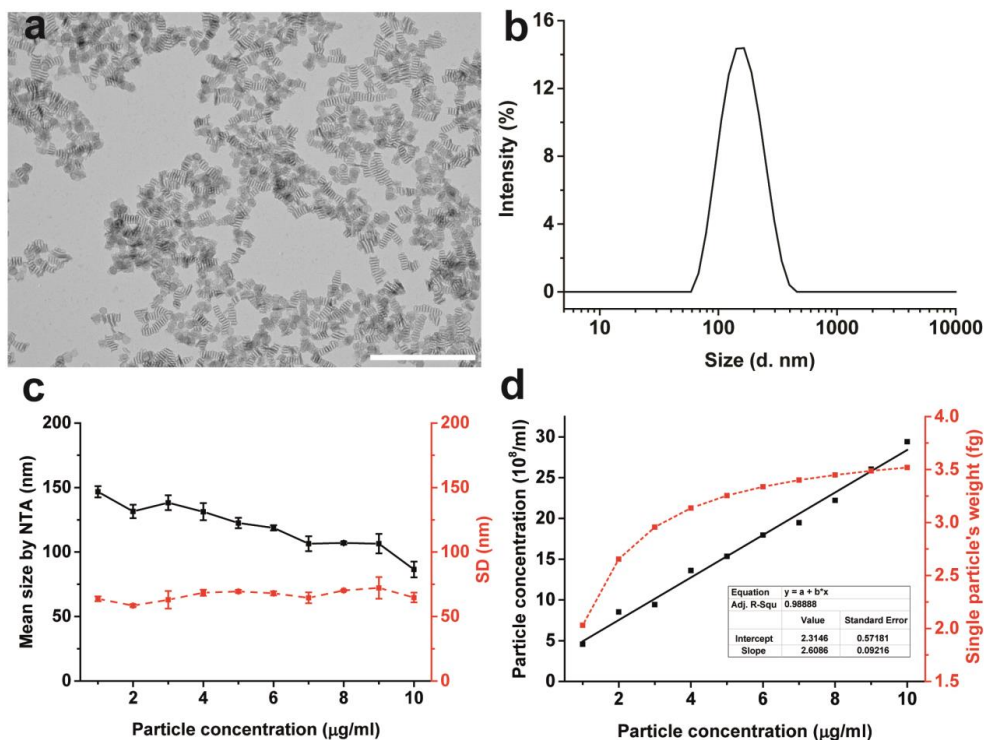


**Figure 6.1** (a) TEM image of MSNs, scale bar = 500 nm; (b) hydrodynamic diameter by DLS; (c) mean MSN size and standard deviation (SD) calculated by the NTA software; (d) NTA particle concentration ( $10^8$  particles/mL) as a function of particle concentration (weight/volume, 1-10  $\mu\text{g/mL}$ ) from NTA measurements and estimation of singular particle weight. Concentration in particle number ( $10^8$  particles/mL) as measured by NTA. Numbers represent average values based on 4 measurements.

## 6.4 Conclusion

In conclusion, we developed a simple method to measure the colloidal stability of MSNs and estimate the weight of a single MSN at the same time. The detection limit for the nanoparticle size is determined by the sensitivity of the camera of NTA and the accuracy of the micro balance. This complementary and non-invasive method uses the advantage of NTA and provides a new and easy method for determining the weight of single nanoparticles and biomolecules in solution with a femtogram resolution.



## 6.5 References

1. J. Tamayo, *Nat. Nanotechnol.*, **2015**, 10, 738-739.
2. T. E. Angel, U. K. Aryal, S. M. Hengel, E. S. Baker, R. T. Kelly, E. W. Robinson and R. D. Smith, *Chem. Soc. Rev.*, **2012**, 41, 3912-3928.
3. J. Shang and X. H. Gao, *Chem. Soc. Rev.*, **2014**, 43, 7267-7278.
4. R. P. Carney, J. Y. Kim, H. F. Qian, R. C. Jin, H. Mehenni, F. Stellacci and O. M. Bakr, *Nat. Commun.*, **2011**, 2.
5. S. Bruckenstein and M. Shay, *Electrochim. Acta*, **1985**, 30, 1295-1300.
6. D. A. Buttry and M. D. Ward, *Chem. Rev.*, **1992**, 92, 1355-1379.
7. M. Rodahl, F. Hook, A. Krozer, P. Brzezinski and B. Kasemo, *Rev. Sci. Instrum.*, **1995**, 66, 3924-3930.
8. A. Janshoff, H. J. Galla and C. Steinem, *Angew. Chem., Int. Ed.*, **2000**, 39, 4004-4032.
9. T. P. Burg, M. Godin, S. M. Knudsen, W. Shen, G. Carlson, J. S. Foster, K. Babcock and S. R. Manalis, *Nature*, **2007**, 446, 1066-1069.
10. M. Fakruddin, Z. Hossain and H. Afroz, *J. Nanobiotechnol.*, **2012**, 10.
11. J. Chaste, A. Eichler, J. Moser, G. Ceballos, R. Rurali and A. Bachtold, *Nat. Nanotechnol.*, **2012**, 7, 300-303.
12. M. S. Hanay, S. Kelber, A. K. Naik, D. Chi, S. Hentz, E. C. Bullard, E. Colinet, L. Duraffourg and M. L. Roukes, *Nat. Nanotechnol.*, **2012**, 7, 602-608.
13. M. Godin, A. K. Bryan, T. P. Burg, K. Babcock and S. R. Manalis, *Appl. Phys. Lett.*, **2007**, 91.
14. W. H. Grover, A. K. Bryan, M. Diez-Silva, S. Suresh, J. M. Higgins and S. R. Manalis, *Proc. Natl. Acad. Sci. U. S. A.*, **2011**, 108, 10992-10996.
15. Y. T. Yang, C. Callegari, X. L. Feng, K. L. Ekinci and M. L. Roukes, *Nano Lett.*, **2006**, 6, 583-586.
16. A. Malloy, *Mater. Today*, **2011**, 14, 170-173.
17. V. Filipe, A. Hawe and W. Jiskoot, *Pharm. Res.*, **2010**, 27, 796-810.
18. T. Ito, L. Sun, M. A. Bevan and R. M. Crooks, *Langmuir*, **2004**, 20, 6940-6945.



# **Chapter VII**

## **Summary and Perspectives**

## 7.1 Summary and Perspectives

Proteins play a crucial role in life, taking part in all vital process in the body,<sup>67</sup> and are therefore used as therapeutic agents in a diverse range of biomedical applications. When administrated into bodily fluids, most native proteins are prone to degradation or inactivation process. The challenges of protein delivery are overcoming poor stability, low permeability toward cell membrane.<sup>68</sup> Among all existing materials for protein delivery, mesoporous silica nanoparticles (MSNs) are one of the most promising intracellular nanocarriers due to its key properties: biocompatible, straightforward synthesis, and surface modification. For various biomedical applications, monodisperse MSNs with a particle size in the 50-200 nm range,<sup>69</sup> controllable surface chemistry,<sup>70</sup> and a large pore size (> 5 nm) are desired.<sup>71-77</sup>

This thesis presents a new method to synthesize large disc-like pore ( $10 \pm 1$  nm) containing MSNs with an elongated cuboidal-like geometry ( $90 \times 43$  nm). Building upon previous reports, we designed a facile synthetic route to a new type of MSNs which effectively encapsulate and release proteins. To obtain the desired large pores in a sub-200 nm particle, a double-surfactant system consisting of a high molecular weight block copolymer (Pluronic P123)<sup>72, 78</sup> and fluorocarbons,<sup>79, 80</sup> was employed as the structure-directing template. The swelling agent 1,3,5-trimethylbenzene (TMB) was added to expand the diameter of the pores.<sup>72</sup> These MSNs were synthesized as stable colloidal suspensions with a narrow size distribution and channels aligned parallel to the short axis. This mesostructure favors efficient mass transfer,<sup>81</sup> as it possesses a high density of entrances enabling rapid and efficient encapsulation of proteins.<sup>82</sup> The encapsulation and release behavior for seven model proteins ( $\alpha$ -lactalbumin, ovalbumin, bovine serum albumin, catalase, hemoglobin, lysozyme and cytochrome c) in these MSNs was investigated in **Chapter II**. These MSNs with their large surface area and optimal dimensions, provide a scaffold with a high encapsulation efficiency and controllable release profiles for a variety of proteins, enabling potential applications in fields such as drug delivery and protein therapy.

Next, a new intradermal delivery system, which synergistically integrated the advantages of nanoparticles and microneedles was described in **Chapter III**. Microneedle-mediated intradermal vaccine is a minimally invasive and effective method for reducing mortality and improving human health.<sup>83-86</sup> To further improve the immunogenicity of vaccine, nanoparticle-based vaccines have been utilized to improve the antigen stability *in vivo* and ensure sustained delivery to the vaccine site.<sup>83</sup> For this, pH-sensitive microneedles were coated with antigen-loaded, lipid bilayer-cover. Negatively charged ovalbumin (OVA, at pH

7.4) was chosen as a model antigen vaccine. Positively charged AEP-MSNs with large pores (10 nm) facilitated the rapid encapsulation of OVA with a high loading capacity. The introduction of lipid bilayer significantly improved the colloidal stability of OVA loaded-AEP-MSNs and reduced the premature release of OVA. In addition, it enabled the coating of the nanoparticles on the surface of pH-sensitive microneedle arrays. Application of LB-MSNs coated microneedle arrays into human skin (*ex vivo*) resulted in the successful delivery of the OVA loaded nanoparticles into the skin in a pH dependent manner.

Protein delivery into cytosol of cells is still a challenging topic, since the inefficient cellular uptake and escape from the endosome to the cytosol hampers clinical applications. In **Chapter IV**, we studied the intracellular delivery of protein loaded MSNs via lipopeptide mediated membrane fusion. Positively charged cytochrome c (*cyt. c*, at pH 7.4) was selected as a typical membrane impermeable protein cargo and encapsulated into MSNs (MSNs/*cyt. c*) with fast kinetics and high loading capacity. In order to enhance the colloidal stability and prevent the premature release of *cyt. c*, MSNs/*cyt. c* were coated with a fusogenic lipid bilayer. To realize direct cytosolic delivery, a complementary pair of coiled-coil lipopeptides (CP<sub>4</sub>E<sub>4</sub> and CP<sub>4</sub>K<sub>4</sub>) was introduced to trigger the targeted delivery of MSNs/*cyt. c*. For this, MSNs/*cyt. c* were coated with a lipid bilayer containing CP<sub>4</sub>E<sub>4</sub>, and these particles were added to CP<sub>4</sub>K<sub>4</sub> pre-treated HeLa cells. The complementary coiled-coil forming lipopeptides enhanced the intracellular delivery of MSNs/*cyt. c*. The subsequent cytosolic release of *cyt. c* from LB-MSNs resulted in the activation of the apoptosis pathway and eventually leading to cell death.

Apart from intracellular protein delivery for potential vaccine (OVA) and cancer therapy (*cyt. c*), we also applied our MSN-based protein delivery system for other clinic applications, like an erythrocyte mimic. Hemoglobin (Hb), the most abundant protein in blood, is responsible for oxygen transport around the body.<sup>2, 8, 87</sup> Cell-free Hb is cleared quickly and is too toxic to serve as a blood substitute.<sup>2, 8</sup> In the past decades, a variety of nanoparticles have been used for physical encapsulation or chemical conjugation of Hb in order to develop an universal blood substitute.<sup>2, 8, 13, 15, 87</sup> In **Chapter V**, Hb-based oxygen carriers were fabricated simply by using MSNs as rigid core to encapsulate Hb and which were covered with a lipid bilayer (named LB-MSNs) to increase the colloidal stability. This bilayer is composed of phospholipids (DOPC, DOPE) and a PEG-modified lipid (PEG<sub>2000</sub>PE) to provide a steric coating on the surface of MSNs/Hb in order to prolong the circulating plasma half-life. The bio-distribution and circulation of LB-MSNs were monitored in zebrafish (*Danio rerio*) embryos for real-time imaging. Upon injection, the nanoparticles moved with the blood flow and readily distributed throughout the circulation of the bloodstream.

In addition to load therapeutic proteins for vaccine purposes, cancer therapy and artificial cells (**Chapter III, IV, V**), MSNs described in this thesis can also be employed as a nanocarrier to load a wide range of proteins for other biomedical applications. For example, lysozyme, a naturally occurring antimicrobial enzyme, is abundant in nature.<sup>88</sup> However, its antimicrobial effectiveness is limited by its poor stability and low uptake by bacteria. MSNs, as a delivery vesicle for a series of antimicrobial proteins, could improve the antimicrobial effect by enhancing the loading capacity and increasing the bacteria uptake. Another example is the tissue engineering field where growth factors and soluble-secreted signaling polypeptides capable of instructing specific cellular responses in a biological environment are required to promote tissue formation.<sup>89-92</sup> However, many of them are inherently unstable in the blood stream and have a short half-life after administration.<sup>93</sup> MSNs with their excellent biocompatibility<sup>88</sup> and tunable structure are suitable for loading and releasing a wide range of these growth factors.

Proteins typically need to be transport intracellularly to exert their therapeutic effect,<sup>94</sup> which requires custom-designed nanocarriers for each specific problem. Almost all protein cargos need endolysosomal escape in order to reach the various subcellular compartments of interest.<sup>67</sup> However, there are some exceptions. Catalase is active in acidic environments found in endosomes and ischemic pathological foci (pH 4-6) and decomposes the highly permeable small oxidant H<sub>2</sub>O<sub>2</sub> and therefore could be used for the treatment of vascular oxidative stress.<sup>95</sup>

In biology, compartmentalization is a dominant feature to tightly regulate multiple reactive species in a crowded cellular environment.<sup>68</sup> Inspired by this compartmentalized structure, co-encapsulation of multiple enzymes inside the MSNs can be a promising approach to construct a synthetic cell.<sup>96</sup> For example, based on the result of **Chapter V**, antioxidant enzymes (superoxide dismutase and catalase) can be added into hemoglobin-based oxygen carrier (LB-MSNs) to increase the level of complexity in both structure and functions, protecting this erythrocyte mimic from severe hypoxia.<sup>97</sup>

Small interfering (siRNA), can be also loaded into this new type of MSNs and further delivered into the targeted cells. Since the first report of gene silencing within mammalian cells in 1998,<sup>98-100</sup> RNA interference (RNAi) is widely regarded as a promising technology for disease treatment, yet one major obstacle for its clinical application is the lack of efficient *in vivo* siRNA delivery vehicles.<sup>98, 101-103</sup> siRNA can be used as a drug because it does not require genome integration and at least 22 RNAi-based drugs have entered clinical trials.<sup>102</sup> Similar to proteins, the intracellular delivery of siRNA needs to overcome the same barrier, as

siRNA is membrane impermeable and prone to degradation in the bodily fluids. Efforts have been made to employ a variety of nanoparticle platforms to transport siRNA into cells.<sup>98, 100, 103</sup> Existing literature describes positively charged MSNs as a non-viral vector for siRNA delivery, where siRNA is bound through electrostatic interactions. These siRNAs with a 21-23 base-pair length (~13 kDa) and possesses multiple negative charges have some similarity to the properties of  $\alpha$ -lactalbumin (14.2 kDa, pI 4.5). Based on previous studies, the surface of the MSNs described in this thesis can also be easily modified with PEI to obtain PEI-MSNs.<sup>104</sup> Next siRNA can be encapsulated and are covered with a lipid bilayer, that can be labeled with a fluorescent dye and targeting molecules<sup>23</sup> for imaging and enhanced targeting. These follow-up studies will further show the potential applications of this new type of MSNs and LB-MSNs as a generic biomacromolecule delivery system.

## 7.2 References

1. Z. Gu, A. Biswas, M. Zhao and Y. Tang, *Chem. Soc. Rev.*, **2011**, 40, 3638-3655.
2. F. P. Chang, Y. P. Chen and C. Y. Mou, *Small*, **2014**, 10, 4785-4795.
3. Z. Gao and I. Zharov, *Chem. Mater.*, **2014**, 26, 2030-2037.
4. C.-H. Lee, T.-S. Lin and C.-Y. Mou, *Nano Today*, **2009**, 4, 165-179.
5. J. Sun, H. Zhang, R. Tian, D. Ma, X. Bao, D. S. Su and H. Zou, *Chem. Comm.*, **2006**, 1322-1324.
6. D. Y. Zhao, J. L. Feng, Q. S. Huo, N. Melosh, G. H. Fredrickson, B. F. Chmelka and G. D. Stucky, *Science*, **1998**, 279, 548-552.
7. J. Gu, K. Huang, X. Zhu, Y. Li, J. Wei, W. Zhao, C. Liu and J. Shi, *J. Colloid Interface Sci.*, **2013**, 407, 236-242.
8. N. Z. Knezevic and J. O. Durand, *Nanoscale*, **2015**, 7, 2199-2209.
9. H. K. Na, M. H. Kim, K. Park, S. R. Ryoo, K. E. Lee, H. Jeon, R. Ryoo, C. Hyeon and D. H. Min, *Small*, **2012**, 8, 1752-1761.
10. X. Du, L. Xiong, S. Dai, F. Kleitz and S. Z. Qiao, *Adv. Funct. Mater.*, **2014**, 24, 7627-7637.
11. S. B. Hartono, N. T. Phuoc, M. H. Yu, Z. F. Jia, M. J. Monteiro, S. H. Qiao and C. Z. Yu, *J. Mater. Chem. B*, **2014**, 2, 718-726.
12. M. Y. Wu, Q. S. Meng, Y. Chen, Y. Y. Du, L. X. Zhang, Y. P. Li, L. L. Zhang and J. L. Shi, *Adv. Mater.*, **2015**, 27, 215-222.
13. F. Gao, P. Botella, A. Corma, J. Blesa and L. Dong, *J. Phys. Chem. B*, **2009**, 113, 1796-1804.
14. Y. Han and J. Y. Ying, *Angew. Chem., Int. Ed.*, **2005**, 44, 288-292.
15. H. Zhang, J. M. Sun, D. Ma, X. H. Bao, A. Klein-Hoffmann, G. Weinberg, D. S. Su and R. Schlogl, *J. Am. Chem. Soc.*, **2004**, 126, 7440-7441.
16. J. Fan, J. Lei, L. Wang, C. Yu, B. Tu and D. Zhao, *Chem. Comm.*, **2003**, 2140-2141.
17. M. Zaric, O. Lyubomska, O. Touzelet, C. Poux, S. Al-Zahrani, F. Fay, L. Wallace, D. Terhorst, B. Malissen, S. Henri, U. F. Power, C. J. Scott, R. F. Donnelly and A. Kissenpfennig, *ACS Nano*, **2013**, 7, 2042-2055.
18. S. A. Coulman, A. Anstey, C. Gateley, A. Morrissey, P. McLoughlin, C. Allender and J. C. Birchall, *Int. J. Pharm.*, **2009**, 366, 190-200.
19. P. C. DeMuth, X. F. Su, R. E. Samuel, P. T. Hammond and D. J. Irvine, *Adv. Mater.*, **2010**, 22, 4851-4856.
20. K. van der Maaden, W. Jiskoot and J. Bouwstra, *J. Controlled Release*, **2012**, 161, 645-655.
21. S. S. Wang, F. Yuan, K. Chen, G. J. Chen, K. H. Tu, H. J. Wang and L. Q. Wang, *Biomacromolecules*, **2015**, 16, 2693-2700.
22. L. Duan, X. H. Yan, A. H. Wang, Y. Jia and J. B. Li, *ACS Nano*, **2012**, 6, 6897-6904.
23. K. Chen, T. J. Merkel, A. Pandya, M. E. Napier, J. C. Luft, W. Daniel, S. Sheiko and J. M. DeSimone, *Biomacromolecules*, **2012**, 13, 2748-2759.
24. Y. Xiong, A. Steffen, K. Andreas, S. Muller, N. Sternberg, R. Georgieva and H. Baumler, *Biomacromolecules*, **2012**, 13, 3292-3300.
25. W. Gao, B. Y. Sha, W. Zou, X. Liang, X. Z. Meng, H. Xu, J. Tang, D. C. Wu, L. X. Xu and H. Zhang, *Biomaterials*, **2011**, 32, 9425-9433.
26. Y. Wang, Y. A. Nor, H. Song, Y. N. Yang, C. Xu, M. H. Yu and C. Z. Yu, *J. Mater. Chem. B*, **2016**, 4, 2646-2653.
27. K. Lee, E. A. Silva and D. J. Mooney, *J. R. Soc., Interface*, **2011**, 8, 153-170.
28. M. Cross and T. M. Dexter, *Cell*, **1991**, 64, 271-280.



29. T. P. Richardson, M. C. Peters, A. B. Ennett and D. J. Mooney, *Nat. Biotechnol.*, **2001**, 19, 1029-1034.
30. F. M. Chen, M. Zhang and Z. F. Wu, *Biomaterials*, **2010**, 31, 6279-6308.
31. K. Y. Lee and S. H. Yuk, *Prog. Polym. Sci.*, **2007**, 32, 669-697.
32. B. Chatin, M. Mevel, J. Devalliere, L. Dallet, T. Haudebourg, P. Peuziat, T. Colombani, M. Berchel, O. Lambert, A. Edelman and B. Pitard, *Mol. Ther.--Nucleic Acids*, **2015**, 4, e244.
33. T. D. Dziubla, V. V. Shuvaev, N. K. Hong, B. J. Hawkins, M. Madesh, H. Takano, E. Simone, M. T. Nakada, A. Fisher, S. M. Albelda and V. R. Muzykantov, *Biomaterials*, **2008**, 29, 215-227.
34. L. Schoonen and J. C. M. van Hest, *Adv. Mater.*, **2015**, 1109-1128.
35. V. Nadithe and Y. H. Bae, *Tissue Eng., Part A*, **2011**, 17, 2453-2462.
36. X. Li, Y. J. Chen, M. Q. Wang, Y. J. Ma, W. L. Xia and H. C. Gu, *Biomaterials*, **2013**, 34, 1391-1401.
37. A. Fire, S. Q. Xu, M. K. Montgomery, S. A. Kostas, S. E. Driver and C. C. Mello, *Nature*, **1998**, 391, 806-811.
38. J. Conde, A. Ambrosone, Y. Hernandez, F. Tian, M. McCully, C. C. Berry, P. V. Baptista, C. Tortiglione and J. M. de la Fuente, *Nano Today*, **2015**, 10, 421-450.
39. X. Xu, J. Wu, Y. Liu, M. Yu, L. Zhao, X. Zhu, S. Bhasin, Q. Li, E. Ha, J. Shi and O. C. Farokhzad, *Angew. Chem., Int. Ed.*, **2016**, 55, 7091-7094.
40. C.-f. Xu and J. Wang, *Asian J. Pharm. Sci.*, **2015**, 10, 1-12.
41. Y. Jiang, R. Tang, B. Duncan, Z. Jiang, B. Yan, R. Mout and V. M. Rotello, *Angew. Chem., Int. Ed.*, **2015**, 54, 506-510.
42. J. Tu, T. Wang, W. Shi, G. Wu, X. Tian, Y. Wang, D. Ge and L. Ren, *Biomaterials*, **2012**, 33, 7903-7914.
43. C. E. Ashley, E. C. Carnes, G. K. Phillips, D. Padilla, P. N. Durfee, P. A. Brown, T. N. Hanna, J. Liu, B. Phillips, M. B. Carter, N. J. Carroll, X. Jiang, D. R. Dunphy, C. L. Willman, D. N. Petsev, D. G. Evans, A. N. Parikh, B. Chackerian, W. Wharton, D. S. Peabody and C. J. Brinker, *Nat. Mater.*, **2011**, 10, 389-397.



# Nederlandse Samenvatting en Perspectieven

Eiwitten spelen een cruciale rol in het leven en zijn betrokken bij alle vitale processen in het lichaam. Eiwitten worden daarom gebruikt als therapeutica voor diverse biomedische doeleinden. Echter bij toediening in het menselijk lichaam worden de meeste eiwitten afgebroken of geïnactiveerd. Voor een succesrijke eiwit-therapie zullen dan ook problemen rond stabiliteit en membraan-penetratie moeten worden opgelost. Van de huidige materialen die gebruikt worden voor het afleveren van eiwitten zijn mesoporous silica nanodeeltjes een van de meest veel belovende nano-voertuigen onder andere vanwege hun a) goede biocompatibiliteit, b) beschikbaarheid van veel protocollen voor hun synthese, c) gemakkelijke modificatie van hun oppervlak zodat de lading naar believen kan worden aangepast. Voor menige biomedische toepassing zijn monodisperse MSNs met een deeltjesgrootte van 50-200 nm, een chemisch-modificeerbare oppervlakte, en grote poriën (> 5 nm) gewenst.

In dit proefschrift is een nieuwe methode geïntroduceerd om MSNs met een kubusachtige geometrie ( $90 \times 43$  nm) te synthetiseren die bovendien grote schijfvormige poriën ( $10 \pm 1$  nm) bevatten. Voortbordurend op eerder onderzoek hebben we een eenvoudige synthetische route ontworpen voor een nieuw type MSNs met goede opname en afgifte eigenschappen. Om de gewenste porie-grootte te verkrijgen in een sub-200 nm deeltje werd als structuur-matrijs een dubbel-surfactant systeem gebruikt bestaande uit een hoog-moleculair gewicht block-copolymeer en fluorocarbons. 1,3,5-trimethylbenzene (TMB) werd toegevoegd om de porie-diameter te vergroten. Deze MSNs werden gesynthetiseerd als stabiele colloïdale suspensies met een smalle grootte-verdeling en kanalen die parallel lopen aan de korte as. Een dergelijke “mesostructuur” bevordert een efficiënte overdracht van massa vanwege de hoge dichtheid aan openingen die zorgen voor snelle en efficiënte inkapseling van eiwitten. De inkapseling en afgifte van een zevental modeleiwitten ( $\alpha$ -lactalbumine, ovalbumine, bovine serum albumine, catalase, hemoglobine, lysozym en cytochroom c) door deze MSNs werd bestudeerd in **Hoofdstuk II**. De hoge inkapselingsefficiëntie en controleerbare afgifte profiel voor een verscheidenheid aan eiwitten maken deze MSNs geschikt voor toepassingen in het veld van medicijnafgifte en eiwit-therapieën.

In **Hoofdstuk III** werd een nieuw intradermaal (onderhuids) afgifte systeem beschreven dat de voordelen van nano-deeltjes en micronealden combineert door pH-gevoelige micronealden te voorzien van lipiden-gecoate MSNs die een antigeen bevatten. Het negatief-geladen ovalbumine (OVA) werd gekozen als model-antigeen voor dit vaccinonderzoek.

Intradermale vaccinatie met micronealden is een pijnloze en effectieve methode van vaccineren. Om de immunogeniciteit van vaccins te verbeteren worden vaccins gebruikt die gebaseerd zijn op nanodeeltjes omdat deze zorgen voor een verhoogde antigen-stabiliteit in vivo en een langdurige afgifte op de plek van vaccinatie. Positief geladen silica nanodeeltjes (AEP-MSNs) met een porie-grootte van 10 nm zorgden voor een snelle inkapseling van ovalbumine (OVA) met een hoge ladingscapaciteit. De introductie van een lipide bilaag resulteerde in een verbeterde colloïdale stabiliteit van OVA-geladen-MSNs en voorkwam voortijdige afgifte van OVA. Bovendien faciliteerde de lipide bilaag de coating van de pH-gevoelige micronealden met deze nanodeeltjes. Toepassing van deze gecoate nanodeeltjes leidde tot de succesvolle afgifte van OVA-geladen nanodeeltjes in de menselijke huid (ex vivo) in een pH-afhankelijke manier.

Eiwit-afgifte in het cytosol van cellen is nog steeds een uitdagende opgave vanwege de inefficiënte cellulaire opname en ontsnapping van eiwitten uit endosomen naar het cytosol, hierdoor worden mogelijke klinische toepassingen beperkt. In **Hoofdstuk IV** bestudeerden we de intracellulaire afgifte van eiwit-bevattende MSNs door middel van lipopeptide geïnduceerde membraanfusie. Het positief geladen eiwit cytochroom c (CytC) dat van zichzelf niet door membranen heen kan werd in deze studie als model-eiwit gebruikt. CytC kon snel en in hoge hoeveelheden ingekapseld worden in MSNs. Om de colloïdale stabiliteit te verhogen en voortijdige afgifte van CytC te voorkomen werden ook deze nanodeeltjes voorzien van een lipide bilaag. Om directe afgifte in het cytosol te bewerkstelligen werd gebruikt gemaakt een complementair paar van *coiled-coil* peptides (CP<sub>4</sub>E<sub>4</sub> en CP<sub>4</sub>K<sub>4</sub>) die via een cholesterol-anker in de lipide membraan van respectievelijk de nanodeeltjes en HeLa cellen werden aangebracht. De *coiled-coil* vormende lipopeptides zorgden voor de intracellulaire opname van CytC-geladen MSN deeltjes door middel van membraan-fusie van de lipide bilaag van de nanodeeltjes met het plasmamembraan van HeLa cellen. Vervolgens leidde de afgifte van CytC in het cytosol tot de activatie van apoptotische processen resulterend in celdood.

Naast de intracellulaire afgifte van eiwitten voor potentiële vaccinatie (OVA) en kankertherapie (CytC) gebruikten we ons MSN-gebaseerde eiwit-afgifte systeem ook voor andere klinische toepassingen zoals een erythrocyten-*mimic*. Hemoglobine (Hb), het meest voorkomende eiwit in bloed, is verantwoordelijk voor zuurstof-transport in het lichaam. Celvrije Hb wordt echter snel afgebroken en is te giftig om als bloedvervanger te dienen. In de afgelopen decennia zijn daarom diverse nanodeeltjes getest voor de inkapseling of chemische conjugatie van Hb als een mogelijk universele bloedvervanger. In **Hoofdstuk V**

werden Hb-gebaseerde zuurstof dragers gefabriceerd door MSNs te gebruiken om Hb in te kapselen en vervolgens af te dekken met een lipide-bilaag om de colloïdale stabiliteit te verhogen. De lipide-bilaag bestond uit fosfolipiden (DOPC, DOPE) en PEG-gemodificeerde lipiden (PEG<sub>2000</sub>PE) die dienden om de circulatietijd in de bloedcirculatie te verlengen. De bio-distributie en circulatie van deze nanodeeltjes getest in zebrawis embryo's als een alternatief in vivo proefdiermodel voor real-time beeldweergave. Na injectie verspreidden de nanodeeltjes zich snel in de bloedbaan.

De MSNs die beschreven werden in dit proefschrift kunnen naast belading met therapeutische eiwitten voor vaccinatie, kankertherapie en kunstmatig bloed (**Hoofdstukken III, IV en V**) ook ingezet worden als nanotransporter voor een wijd scala aan eiwitten voor andere biomedische toepassingen. Bijvoorbeeld lysozyme, dat van nature een antimicrobieël enzym is komt veelvuldig voor in de natuur. Echter de antimicrobiële effectiviteit is beperkt door de lage stabiliteit en matige opname door bacteriën. MSNs zouden, als transportmiddel voor allerlei antimicrobiële eiwitten, de effectiviteit van deze eiwitten kunnen verbeteren door verhoging van hun stabiliteit en opname door bacteriën. Andere toepassingen zijn mogelijk op het gebied van weefsel-engineering, waarbij groeifactoren gebruikt worden om de groei van bepaalde weefsel te stimuleren. Echter veel van deze groeifactoren hebben inherent lage stabiliteit in de bloedbaan en dus een korte levensduur na toediening. MSNs met hun excellente biocompatibiliteit en aanpasbare structuur zijn mogelijk geschikt voor het laden en gecontroleerd lossen van een reeks van deze groeifactoren.

Talrijke eiwitten moeten intracellulair vervoerd worden om hun therapeutisch effect te bereiken, dit vereist custom-designed nanocarriers voor ieder probleem. Bijna elk eiwit vereist endolysosomale ontsnapping om de gewenste subcellulaire compartimenten te bereiken. Een van de weinige uitzonderingen is catalase, dat actief is in het zure milieu van endosomen en ischemisch pathologische foci (pH4-6) en waterstofperoxide onschadelijk maakt bij behandeling van vasculaire oxidatieve stress.

Compartimentalizing is in de biologie een belangrijke methode om reactieve moleculen te scheiden in een cel.<sup>68</sup> Geïnspireerd door deze compartimenten in cellen kan co-encapsulatie van meerdere enzymen in MSN een veelbelovende methode zijn om een synthetische cel te creëren. Bijvoorbeeld, gebaseerd op de resultaten van **hoofdstuk V** kunnen anti-oxidatie enzymen (superoxide dismutase en catalase) toegevoegd worden aan hemoglobine-bevattende zuurstofdragers (LB-MSNs) om de complexiteit in structuur en functie te verhogen en deze erythrocyten-*mimic* te beschermen tegen ernstige hypoxia.

Behalve eiwitten kunnen ook andere functionele biomoleculen zoals siRNAs worden geladen in dit nieuwe type MSN en vervolgens afgeleverd worden in cellen. Sinds de eerste publicatie over *gene silencing* in dierlijke cellen in 1998 wordt RNA interferentie (RNAi) wereldwijd gezien als een veelbelovende technologie voor behandeling van ziektes. Echter een belangrijk obstakel voor klinische toepassing is het gebrek aan geschikte transporters om *short interfering* (si) RNAs af te leveren. siRNAs zijn geschikt als medicijn omdat ze niet hoeven te integreren in het genoom en omdat ze eenvoudig te synthetiseren zijn. Niet minder dan 22 RNAi-gebaseerde drugs hebben hun weg gevonden tot klinische trials. Zoals ook met eiwitten het geval is, zal voor de afgifte aflevering van siRNA in cellen een aantal hordes genomen moeten worden aangezien siRNAs niet membraan-permeabel zijn en gevoelig voor afbraak door lichaamsvloeistoffen. Om siRNAs in het cytoplasma te krijgen wordt een verscheidenheid aan nanodeeltjes toegepast. De bestaande literatuur beschrijft MSNs als niet-virale vector voor siRNA afgifte. Deze MSNs beschikken over het kationische polyethyleenimine (PEI) aan het oppervlak en kunnen door middel van electrostatische interacties siRNAs binden. Bekend is dat siRNAs met een lengte van 21 tot 23 basenparen (~13 kDa) meerdere negatieve ladingen bevatten en zodoende vergelijkbaar zijn met het negatief geladen  $\alpha$ -lactalbumine (14.2 kDa, pI 4.5). Encapsulatie van siRNAs door PEI-gemodificeerde MSNs kan worden gevolgd door bedekking met een lipide bilaag die voorzien kan worden van fluorescerende kleurstoffen, of *targeting* moleculen voor *imaging* en *targeting*. Toekomstige studies zullen de potentiële toepassingen van dit nieuwe type MSNs met of zonder lipide laag als delivery systeem voor biomacromoleculen moeten aantonen.

## Curriculum vitae

Jing Tu was born on 11<sup>th</sup> October 1985 in Wuhan, Hubei, China. After completing her secondary education, she started her academic study in Faculty of Materials Science and Chemistry, China University of Geosciences (Wuhan), in 2004. After 4 years study, she obtained a bachelor degree of Materials and Chemistry. Thereafter, she studied at Xiamen University as a master student in the field of biomedical engineering, with the thesis “Mesoporous silica nanoparticle as a drug carrier for photodynamic therapy: synthesis, characterization and properties”.



From September 2012 to December 2016, she studied in the group of Supramolecular & Biomaterials Chemistry in Leiden University as a PhD student under supervision of Prof. Dr. Alexander Kros. She conducted research in the field of protein delivery with a scholarship from the Chinese Scholarship Counsel (CSC). During her PhD studies, she collaborated with Prof. Dr. Wim Jiskoot (Leiden University), Prof. Dr. Joke A. Bouwstra (Leiden University), Dr. Heiner Friedrich (Eindhoven University of Technology) and Prof. Dr. Nico A. J. M. Sommerdijk (Eindhoven University of Technology). Furthermore, she participated in the PhD training courses as well as COST training school “Supramolecular chemistry in water”, Padova, 2014. She presented the 14<sup>th</sup> European Symposium on Controlled Drug Delivery, with a poster presentation named “Coiled-coil Forming Peptides Enhance Intracellular Delivery by Lipid Bilayers Coated Mesoporous Silica Nanoparticles”, the Netherlands, 2016. She attended the 43<sup>rd</sup> Annual Meeting & Exposition of the Controlled Release Society, with a poster presentation “Mesoporous silica nanoparticles with large pores for the encapsulation and release of proteins”, USA, 2016.

## List of publications

1. J. Tu, A.L. Boyle, H. Friedrich, P.H.H. Bomans, J. Bussmann, Nico A.J.M. Sommerdijk, Wim Jiskoot\*, Alexander Kros\*, Mesoporous Silica Nanoparticles with Large Pores for the Encapsulation and Release of Proteins. *ACS Appl. Mater. Interfaces*, **2016**, DOI: 10.1021/acsami.6b11324
2. J. Tu, G. Du, R. Nejadnik, J. Mönkäre, K. van der Maaden, P.H.H. Bomans, Nico A. J. M. Sommerdijk, Wim Jiskoot\*, Joke A. Bouwstra\*, Alexander Kros\*, Lipid Bilayer Coated Mesoporous Silica Nanoparticles for the Dermal Delivery of Ovalbumin. (Submitted).
3. J. Tu, J. Yang, G.E.M. Lamers, P.H.H. Bomans, Nico A.J.M. Sommerdijk, R.C.L. Olsthoorn, Alexander Kros\*, Membrane Fusion Mediated Intracellular Delivery by Lipid Bilayers Coated Mesoporous Silica Nanoparticles. (Submitted)
4. J. Tu, J. Bussmann, G. Du, Y. Gao, Joke A. Bouwstra, Alexander Kros\*, Lipid Bilayers Coated Mesoporous Silica Nanoparticles Highly Encapsulated Bovine Hemoglobin. (In preparation)
5. S.A. van den Berg, J. Tu, K.M. Sliedregt, A. Kros, T. Wennekes, H.C. Zuilhof Mesoporous Silica via Functionalization with 1, $\omega$ -Alkenes. *Adv. Mater. Interfaces*, **2014**, 1.

## Other publications

1. J. Tu, T. Wang, W. Shi, G. Wu, X. Tian, Y. Wang, Multifunctional ZnPc-loaded mesoporous silica nanoparticles for enhancement of photodynamic therapy efficacy by endolysosomal escape. *Biomaterials*, **2012**, 33: 7903-7914.
2. C. Song, W. Shi, H. Jiang, J. Tu, D. Ge. pH-sensitive characteristics of poly(acrylic acid)-functionalized anodic aluminum oxide (AAO) membranes. *J. Membrane Sci.*, **2011**, 372: 340-345.
3. W. Shi, Y. Ma, C. Song, H. Jiang, X. Ru, J. Tu, Affinity electromembrane: Electrically facilitated adsorption. *J. Membrane Sci.*, **2010**, 354: 86-92.
4. W. Shi, H. Cao, C. Song, H. Jiang, J. Wang, S. Jiang, J. Tu, D. Ge, Poly(pyrrole-3-carboxylic acid)-alumina composite membrane for affinity adsorption of bilirubin. *J. Membrane Sci.*, **2010**, 353: 151-158.
5. D. Ge, X. Ru, S. Hong, S. Jiang, J. Tu, J. Wang, Coating metals on cellulose-polypyrrole composites: A new route to self-powered drug delivery system. *Electrochem. Commun.*, **2010**, 12: 1367-1370.